

DISS. ETH NO. 25383

***Development of a biomimetic surface for
blood-contacting devices via electrospinning
technologies***

A thesis submitted to attain the degree of
DOCTOR OF SCIENCES of ETH ZURICH
(Dr. sc. ETH Zurich)

presented by

Lukas Weidenbacher

MSc Materials Science and Engineering, FAU Erlangen-Nürnberg

born on 19.01.1989

citizen of Germany

accepted on the recommendation of

Prof. Dr. Stephen J Ferguson, examiner

Dr. Giuseppino Fortunato, co-examiner

Prof. Dr. Katharina Maniura, co-examiner

Prof. Dr. René M Rossi, co-examiner

2018

“If you cannot do great things, do small things in a great way.” – Napoleon Hill

Summary

2 500 000 000 – the average number of heartbeats in the lifespan of a healthy 70 year old human being. The heart is an incredible organ engineered by nature and, up to date, impossible to recreate by humans. Despite, or perhaps because of this incredible performance, the heart is susceptible to failure or disease. The consequences are in most cases fatal.

Since decades, physicians, biologists and engineers try to develop solutions to assist, repair or replace the human heart. Up to date most patients suffering from end stage heart failure have to rely on donor organs, which is a major concern due to donor organ shortage or non-eligibility of certain patients. As an alternative treatment, ventricular assist devices (VAD's) – artificial pumps that assist the heart to maintain the blood flow within the human body – were introduced as bridge to transplant and recovery or destination therapy. However, one major drawback of such devices is the relatively high risk of thrombosis within the pump, since the artificial surfaces of the VAD are in permanent contact with blood at high shear stresses, triggering blood clot formation.

The goal of this thesis was to design and develop a novel biomimetic approach, to be applied on the surface of such a VAD that enables prolonging the pump lifetime as well as reduces the risk of thrombosis. Blood vessels in the human body are composed of multiple layers of smooth muscle cells (SMC) that are embedded in an extracellular matrix. On top of this, an interconnected monolayer of endothelial cells (EC) is adhering to regulate the anti-thrombotic function of the vessel. For this approach, a biomimetic electrospun matrix interface that consists of both, SMCs and ECs, as found in native blood vessels was therefore envisioned. Three main tasks had to be addressed within the presented study, namely the development of viable cell-infiltrated porous sub-micron scaled fiber scaffolds, tailoring of the raw scaffold membrane material in terms of mechanical response and hemocompatibility, and finally analysis of the endothelial cell response to the newly designed surfaces.

To mimic the structure of a native blood vessel, a process combining conventional needle based electrospinning and cell electrospaying was investigated. Thereby,

an electrospun fibrous network, mimicking the extracellular matrix of the human body, was infiltrated with cells to rebuild the architecture of human tissue. A murine myoblast model cell line (C2C12) was used to study the influence of the spinning process on cell viability and differentiation. A microfluidic-based cell encapsulation protocol was established and adjusted to protect the cells from toxic solvents used during the spinning process, followed by controlled release of the cells. By this, the incorporation of cells into a three-dimensional fibrous network was successfully shown and the viability of the cells was maintained due to the protective effect of the capsules.

Further, the scaffold materials were assessed in terms of cyclic mechanical performance under similar loading conditions as found in VAD's and their response to blood under semi-static incubation was tested. Two different fiber materials, namely polyurethane (PU) and poly(vinylidene fluoride-co-hexafluoropropylene) (PVDFhfp) were combined based on their unique mechanical performance and / or suitable hemocompatibility, respectively to obtain a blend fiber. By partially embedding the blend electrospun network into an elastic silicone material, a novel surface, potentially applicable for pulsatile membranes in VAD's was obtained based on the enhanced performance in terms of blood response. Since the aim of the final application is to maintain a confluent autologous endothelial cell layer, which acts as a barrier between the artificial surface and blood, the surface was cultivated with a confluent layer of cells and tested in a bioreactor system that allows for application of cyclic mechanical loading under flow.

The surface response to flow of endothelial cells cultured on the blend fiber network was investigated. A comparison between fibrous scaffolds without smooth muscle cells and scaffolds incorporating smooth muscle cells, mimicking the blood vessel architecture, is envisioned. By this, the influence of smooth muscle cells on the behavior of the endothelial cells can potentially be studied. A protocol was established for the smooth muscle cells, during which they were stimulated with ascorbic acid and fibronectin to produce a collagenous extracellular matrix to improve the adhesion of the endothelial cell layer.

In conclusion, this thesis presents the development, characterization and performance of a newly designed biomimetic scaffold, to be applied as a novel interface to improve the quality of ventricular assist devices. The biomimetic material was designed to resemble the hierarchically structured architecture of native blood vessels. The potential of this approach was successfully tested *in vitro*. In the future, the potential for long-term endothelialisation as well as investigation in an *in vivo* animal model to better understand the response under physiological conditions can be targeted, to further assess the applicability in a VAD.

Zusammenfassung

2 500 000 000 – die durchschnittliche Anzahl an Herzschlägen während des Lebens eines 70-jährigen Menschen. Das Herz ist ein unglaubliches, von der Natur entwickeltes Organ, welches bis heute unmöglich nachzubauen ist. Trotz, oder gerade wegen dieser unglaublichen Leistung, ist das Herz anfällig für Krankheiten oder Versagen. In den meisten Fällen sind die Konsequenzen fatal.

Seit Jahrzehnten versuchen Ärzte, Biologen und Ingenieure Lösungen zu entwickeln um das menschliche Herz zu heilen oder zu ersetzen. Bis heute müssen sich die meisten Patienten, die sich im Endstadium einer Herzerkrankung befinden, auf Spenderorgane verlassen, was zu grossen Problemen auf Grund von Mangel an Spenderorganen oder Nichteignung der Patienten, führen kann. Als alternative Behandlungsmöglichkeit wurden sogenannte "ventricular assist devices" (VAD) entwickelt – künstliche Pumpen, die das Herz dabei unterstützen den Blutfluss aufrechtzuerhalten – um die Zeit bis zur Transplantation oder Heilung zu überbrücken, oder um permanent im Patient zu bleiben. Ein grosser Nachteil dieser Geräte ist das vergleichsweise hohe Risiko von Thrombosen im Inneren der Pumpe, da sich die künstliche Oberfläche der Pumpe in permanentem Kontakt mit Blut unter hohen Scherkräften befindet, was wiederum die Bildung von Blutgerinnseln auslösen kann.

Das Ziel dieser Arbeit war es, einen neuartigen biomimetischen Ansatz zu designen und zu entwickeln, um diesen auf der Oberfläche von VADs anzuwenden um deren Lebensdauer zu erhöhen, sowie das Risiko von Thrombosen zu reduzieren. Blutgefässe im menschlichen Körper sind aus mehreren Lagen von glatten Muskelzellen (SMC) die in eine extrazelluläre Matrix eingebettet sind aufgebaut. Auf diesen Schichten sitzt eine eng vernetzte Monolage von Endothelzellen (EC) die die anti-thrombotischen Eigenschaften regulieren. Für den biomimetischen Ansatz wurde eine elektrogessponnene Matrix, die ähnlich eines Blutgefässes, sowohl SMCs als auch ECs beinhaltet, als Grenzfläche angestrebt. Dafür mussten drei Hauptthematiken innerhalb der Studie behandelt werden, nämlich die Entwicklung von lebenden zell-infiltrierten Gerüsten aus Nanofasern, die Anpassung von den mechanischen Eigenschaften sowie der Blutverträglichkeit

des Gerüstmaterials und schlussendlich die Analyse der Endothelzellantwort auf dem neu entwickelten Gerüst.

Um die Struktur eines Blutgefäßes nachzuempfinden, wurde ein Prozess, der konventionelles Elektrosponnen mit dem elektrischen Sprühen von Zellen verbindet, untersucht. Dafür wurde ein elektrosponnenes Netzwerk, welches stark der extrazellulären Matrix im menschlichen Körper ähnelt, mit Zellen infiltriert um die Architektur von menschlichem Gewebe nachzubauen. Eine Myoblasten Zelllinie aus der Maus (C2C12) wurde verwendet, um den Einfluss des Spinnprozesses auf die Überlebensrate der Zellen und deren Potential zur Differenzierung zu studieren. Ein auf Mikrofluidik basierendes Einkapselungsprotokoll wurde entwickelt und angepasst, um die Zellen vor den toxischen Lösungsmitteln zu schützen, die während des Prozesses verwendet wurden und die darauffolgende gezielte Freisetzung der Zellen analysiert. Dadurch konnte die Einbettung von Zellen in ein dreidimensionales Fasernetzwerk erfolgreich nachgewiesen werden und das Überleben der Zellen durch die Einkapselung erfolgreich erreicht werden.

Darüber hinaus wurden die Gerüstmaterialien in Bezug auf deren zyklisches mechanisches Verhalten, unter ähnlichen Lastbedingungen wie in einem VAD, sowie deren Verhalten im Kontakt mit Blut, unter semi-statischen Bedingungen, getestet. Zwei unterschiedliche Fasermaterialien, Polyurethan (PU) sowie Poly(vinyliden fluoride-co-hexafluoropropylen) (PVDFhfp) wurden auf Grund ihrer einzigartigen mechanischen Eigenschaften, bzw. passenden Blutverträglichkeit kombiniert um eine Mischfaser zu erzeugen. Durch partielles Einbetten dieses Mischfasernetzwerkes in ein elastisches Silikonmaterial konnte eine neue Oberfläche erzeugt werden, die aufgrund ihrer verbesserten Blutantwort potentiell in einem pulsatilen VAD Anwendung finden könnte. Da das finale Ziel der Anwendung der Erhalt einer autologen konfluenten Lage aus Endothelzellen als Barriere zwischen dem Blut und der künstlichen Oberfläche ist, wurde die Oberfläche mit einer konfluenten Lage aus Zellen in einem Bioreaktorsystem getestet, welches gleichzeitig eine zyklische mechanische Belastung der Membran als auch die Anwendung von Fluss erlaubt.

Die Endothelzellantwort gegen Fluss auf den Mischfasernetzwerken wurde getestet und ein Vergleich mit biomimetischen Netzwerken welche glatte Muskelzellen beinhalten wurde angestrebt nach dem Modell von Blutgefäßen. Darüber könnte der Einfluss der glatten Muskelzellen auf das Verhalten der Endothelzellen potentiell analysiert werden. Es wurde ein Protokoll für die glatten Muskelzellen etabliert, während dessen sie mit Ascorbinsäure und Fibronectin dazu stimuliert wurden ihre eigene extrazelluläre Matrix aus Kollagen zu synthetisieren, um die Adhäsion einer Endothelzellschicht zu verbessern.

Zusammenfassend präsentiert diese Arbeit die Entwicklung, Charakterisierung und Leistung eines neuen biomimetischen Gerüsts, um es als neue Grenzfläche für ventrikuläre Assistenzsysteme anzuwenden und deren Qualität zu verbessern. Das biomimetische Material wurde designt um die hierarchisch strukturierte Architektur von Blutgefäßen nachzuempfinden. Das Potential dieses Ansatzes wurde erfolgreich *in vitro* getestet. In der Zukunft können das Langzeitverhalten der Endothelzellen sowie Untersuchungen in einem *in vivo* Tierexperiment angestrebt werden, um die Antwort unter physiologischen Bedingungen besser zu verstehen und die Anwendbarkeit in einem VAD weiter zu beurteilen.

Contents

1	Background.....	1
1.1	Function of blood vessels and the endothelium.....	2
1.1.1	Angiogenesis.....	3
1.1.2	Vascular permeability.....	4
1.1.3	Metabolism.....	5
1.1.4	Leukocyte trafficking.....	7
1.1.5	Hemostasis.....	8
1.1.6	Vascular pathology.....	10
1.2	Vascular graft engineering.....	11
1.2.1	Scaffold materials.....	13
1.2.2	Scaffold types and manufacturing methods.....	15
1.2.3	Tissue engineering of vascular grafts.....	18
1.3	The combined process of electrospinning and cell electrospraying ..	20
1.4	Ventricular assist devices.....	22
2	Scope of the thesis	23
2.1	Thesis motivation.....	24
2.2	Thesis aims.....	25
2.3	Thesis outline.....	27
3	Cell electrospraying	29
3.1	Abstract.....	30
3.2	Introduction.....	31
3.3	Materials and methods.....	34
3.3.1	Materials and reagents.....	34
3.3.2	Cell culture.....	34
3.3.3	Microfluidic device fabrication.....	35

3.3.4	Microcapsules formation and cell encapsulation.....	35
3.3.5	Capsule separation.....	36
3.3.6	Capsule characterization.....	36
3.3.7	Spraying of capsules and cell release.....	37
3.3.8	Cell viability.....	38
3.3.9	Cell characterization.....	38
3.3.10	Analysis of residual solvent in electrospun membranes.....	39
3.3.11	Electrospinning/capsule spraying.....	39
3.3.12	Statistical analysis.....	40
3.4	Results.....	40
3.4.1	Cell encapsulation.....	40
3.4.2	Capsule purification and processing.....	42
3.4.3	Cell characterization.....	43
3.4.4	Cell release from microcapsules.....	46
3.4.5	Hybrid biograft fabrication.....	47
3.5	Discussion.....	49
3.6	Conclusion.....	53
3.7	Acknowledgements.....	53
3.8	Appendix.....	54
4	Blend fiber production.....	55
4.1	Abstract.....	56
4.2	Introduction.....	56
4.3	Materials and methods.....	58
4.3.1	Spinning solutions and fibre production.....	58
4.3.2	Fibre characterisation.....	59
4.3.3	Protein adsorption.....	60
4.4	Results and discussion.....	61

4.4.1	Solution characteristics and fibre morphology	61
4.4.2	Surface properties of electrospun membranes	63
4.4.3	Protein adsorption on PUR or PUR/PVDFhfp membranes....	70
4.5	Conclusion	74
4.6	Acknowledgements	74
4.7	Appendix	75
5	Fiber surface functionalization	77
5.1	Abstract.....	78
5.2	Introduction	79
5.3	Materials and methods	82
5.3.1	Materials and reagents	82
5.3.2	Membrane preparation and embedding into silicone.....	82
5.3.3	Scanning electron microscopy	83
5.3.4	Material characterization	83
5.3.5	Mechanical testing of membranes.....	84
5.3.6	Zeta potential measurement	85
5.3.7	Fibrinogen adsorption.....	85
5.3.8	Fibrin clot formation.....	86
5.3.9	Immunohistochemistry after blood incubation.....	87
5.3.10	Bioreactor tests	87
5.3.11	Statistics	88
5.4	Results and discussion.....	88
5.4.1	Surface properties of electrospun membranes	88
5.4.2	Mechanical characterization of electrospun membranes	92
5.4.3	Effect of fiber surface composition on hemocompatibility.....	94
5.4.4	Fabrication and characterization of PUPV-RTV	98
5.4.5	Surface endothelialization under flow	101

5.5	Conclusion	103
5.6	Acknowledgements	103
5.7	Appendix	104
6	Biomimetic co-culture approach	107
6.1	Abstract.....	108
6.2	Introduction.....	108
6.3	Materials and methods	111
	6.3.1 Materials and reagents	111
	6.3.2 Cell culture substrates	111
	6.3.3 Cell culture.....	111
	6.3.4 Immunofluorescence	112
	6.3.5 Collagen synthesis.....	112
6.4	Results and discussion	113
	6.4.1 Seeding of ECs on blend fiber membranes	114
	6.4.2 Boosting collagen formation.....	115
	6.4.3 Control of SMC phenotype.....	117
6.5	Conclusion	118
7	Appendix: Pore size fine-tuning	119
7.1	Introduction.....	120
7.2	Materials and methods	121
	7.2.1 Materials and reagents	121
	7.2.2 Electrospinning and electrospraying.....	121
	7.2.3 Capillary flow porometry.....	122
	7.2.4 Cell culture.....	122
	7.2.5 Scanning electron microscopy	122
	7.2.6 Fluorescence microscopy	123
7.3	Results and discussion	123

7.3.1	Electrospinning/particle spraying.....	123
7.3.2	Porosity measurements	124
7.3.3	Cell culture.....	126
7.4	Conclusion	129
8	Synthesis.....	131
8.1	Summary and conclusion	132
8.2	Limitations of this work	135
8.3	Outlook	137
9	Bibliography	139

List of figures

Figure 1.1: Blood vessel architecture	3
Figure 1.2: Mechanisms of vascular permeability.....	5
Figure 1.3: Leukocyte trafficking via the endothelium	8
Figure 1.4 Mechanism of thrombus formation	10
Figure 3.1: Graphical abstract	31
Figure 3.2: Microfluidic encapsulation process.....	41
Figure 3.3: Capsule purification.....	42
Figure 3.4: Capsule characterization.....	43
Figure 3.5: Assessment of cell viability.....	45
Figure 3.6: Cell differentiation.....	46
Figure 3.7: Cell release from capsule.....	47
Figure 3.8: Measurement of residual solvents	48
Figure 3.9: Cell incorporation into the scaffold.....	49
Figure 3.10: Cell viability after electrospraying.....	54
Figure 4.1: Graphical abstract	56
Figure 4.2: Fiber characterization	65
Figure 4.3: XPS analysis	67
Figure 4.4: Surface fluorine concentrations.....	68
Figure 4.5: Protein adsorption.....	73
Figure 4.6: Viscosity measurements.....	75

Figure 4.7: XPS spectra.....	76
Figure 4.8: Water contact angle.....	76
Figure 5.1: Graphical abstract	79
Figure 5.2: STEM EDX measurements	91
Figure 5.3: Mechanical characterization.....	92
Figure 5.4: Membrane interactions with fibrinogen and blood.....	95
Figure 5.5: Fabrication and characterization of embedded fibers.....	99
Figure 5.6: Bioreactor test.....	101
Figure 5.7: Surface characterization.....	104
Figure 5.8: Zeta potential measurement.....	105
Figure 5.9: Mechanical characterization in PBS at 37°C.....	105
Figure 6.1: Cell seeding approaches	114
Figure 6.2: EC seeding	115
Figure 6.3: Collagen stimulation	116
Figure 6.4: Collagen quantification.....	117
Figure 6.5: SMC phenotype control	118
Figure 7.1: SEM image of electrospun membrane.....	120
Figure 7.2: Electrospinning and particle spraying	124
Figure 7.3: Porosity before and after PEO removal.....	126
Figure 7.4: Fluorescence images of cells cultured on PET.....	127
Figure 7.5: SEM images of cells cultured on PET	128

Abbreviations

4'6-Diamin-2-phenylindol (DAPI)

Adenosine tri-phosphate (ATP)

Analysis of variance (ANOVA)

Ascorbic acid (AscAc)

Confocal Laser Scanning Microscope (CLSM)

Coronary artery disease (CAD)

Dimethylformamide (DMF)

Dimethyl sulfoxide (DMSO)

Dulbecco's modified Eagle Medium (DMEM)

Endothelial cell (EC)

Extracellular matrix (ECM)

Endothelial nitric oxide synthase (eNOS)

Energy dispersive X-ray spectroscopy (EDX)

Enzyme-linked immunosorbent assay (ELISA)

Ethylenediaminetetraacetic acid (EDTA)

Expanded polytetrafluoroethylene (ePTFE)

Fetal calf serum (FCS)

Fibrinogen (FG)

Fluorescence-activated cell sorting (FACS)

Fluorinated diamond-like carbon (F-DLC)

Gas chromatography – mass spectrometry (GC-MS)

Gaseous secondary electron detector (GSED)

Hexafluoroisopropanol (HFIP)

High angle annular dark field (HAADF)

Human umbilical vein endothelial cells (HUVEC)

Human serum albumin (HSA)
Lactate dehydrogenase (LDH)
Mouse myoblast cell line (C2C12)
Nitric oxide (NO)
Paraformaldehyde (PFA)
Phosphate buffered saline (PBS)
Plasminogen activation inhibitor (PAI-1)
Platelet activation factor (PAF)
Platelet factor 4 (PF4)
Platelet-rich plasma (PRP)
Poly(4,4'(hexfluoroisopropylidene)diphenol octane) (6FBA)
Poly(bisphenol A octane) (BA-C8)
Polycaprolactone (PCL)
Polydimethylsiloxane (PDMS)
Poly(ethylene glycol) (PEG)
Poly(ethylene oxide) (PEO)
Polyethylene terephthalate (PET)
Poly(N-vinyl-2-pyrrolidone) (PVP)
Poly(styrene-co-p-hexafluorohydroxyisopropanol- α -methyl styrene) / poly(4-vinyl pyridine) (PS(OH)PVPy)
Polyurethane (PU)
Polyurethane – PVDFhfp blend (PUPV)
Poly(vinylalcohol) (PVAL)
Poly(vinyl chloride) (PVC)
Poly(vinyl caprolactam) (PVCL)
Poly(vinylidene fluoride) (PVDF)
Poly(vinylidene fluoride-co-hexafluoropropylene) (PVDFhfp)

Potassium chloride (KCl)

Propidium iodide (PI)

Prothrombin fragment 1+2 (F1F2)

Pulsatile ventricular assist device (PVAD)

Room temperature (RT)

Room temperature vulcanizing silicone (RTV)

Root means square roughness (S_q)

Scanning Electron Microscope (SEM)

Scanning Transmission Electron Microscope (STEM)

Smooth muscle cell (SMC)

Solid phase microextraction (SPME)

Standard deviation (SD)

Surface modifying macromolecules (SMM)

Tetraethylammonium bromide (TEAB)

Tetrahydrofuran (THF)

Tissue culture polystyrene (TCPS)

Tissue engineering (TE)

Transforming growth factor β (TGF- β)

Vascular cell-adhesion molecule 1 (VCAM1)

Vascular endothelial growth factor (VEGF)

Ventricular assist device (VAD)

Very late antigen 4 (VLA4)

Vesiculo-vacuolar organelle (VVO)

Von Willebrand factor (vWF)

Wall shear stress (WSS)

Water contact angle (WCA)

X-ray photospectroscopy (XPS)

1.1 Function of blood vessels and the endothelium

The major role of the blood vessel system is to transport oxygen, nutrients like glucose, amino acids, fatty acids or vitamins and metabolic waste products such as carbon dioxide, urea and creatinine throughout the human body to maintain the function of tissues and organs (Levick 1991, Sandoo *et al* 2010). Depending on the site in the body and their dimensions, they have to withstand high pressure caused by the systolic output during the cardiac cycle via the pulmonary artery. To withstand such high levels of pressure, the blood vessel wall contains a hierarchical organization that consists of three layers, the tunica externa, the tunica media and the tunica intima, being the outer, middle and inner layer, respectively (Rutten 1995). The tunica externa mostly consists of a layer of connective tissue and interconnected thick bundles of collagenous fibrils that is wrapped around the tunica media. By this, it supports the mechanical strength of the vessel and restricts the deformation of the vessel. In the inner part, the media, multiple layers of resting elongated spindle-like SMCs that are embedded in an extracellular matrix of elastin and collagen fibrils are present. Depending on the type of vessel, different amounts of such SMC layers are situated in the media based on the mechanical load and function. The innermost part of the vessel is comprised of an interconnected monolayer of ECs, the endothelium, which is aligned in direction of the blood flow to minimize the effect of shear stress and separated from the media via a thin basal lamina. The basal lamina is mostly composed of collagen IV, laminin, nidogen and perlecan and provides not only a barrier to the media but can also act as a semipermeable membrane for filtration of macromolecules and permeability barrier for cell infiltration (Pollard *et al* 2008). The architecture of a blood vessel can be seen in Figure 1.1.

In the human body, the endothelium consists of up to 60×10^{12} ECs covering an area of up to 1000 m^2 (Félétou 2011) on the luminal surface which is the interface to blood. The term endothelium itself was first introduced by Wilhelm His, a swiss anatomist in 1865. Back then, it was only considered a simple diffusion barrier to prevent blood cell infiltration into the vascular matrix (Félétou 2011). Nowadays it is recognized as a dynamic organ that plays an important role in the maintenance of the vascular homeostasis as a key player in vasomotion, thrombosis, platelet aggregation and inflammation (Galley and Webster 2004).

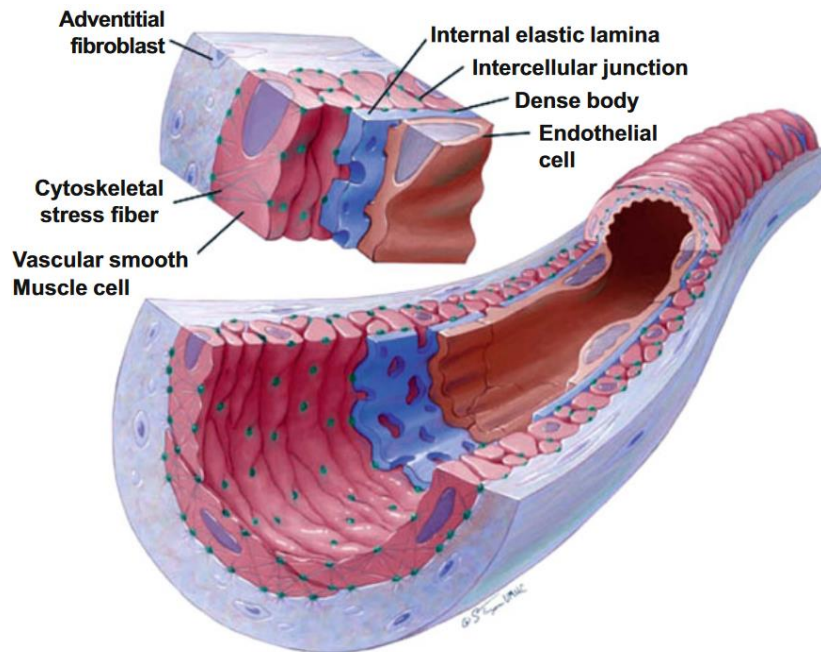


Figure 1.1: Blood vessel architecture

The different layers of the blood vessel can be seen with the corresponding cell types that are present in each layer. Image reprinted with permission by John Wiley and Sons (Martinez-Lemus 2012).

1.1.1 Angiogenesis

The term vasculogenesis refers to the process of *de novo* formation of new vessels. Angiogenesis on the other hand describes the sprouting of preexisting vessels by ECs (Muñoz-Chápuli *et al* 2004). This process plays a major role during the embryonic and postnatal development. However, it also occurs during tissue damage, wound healing, nutrient or oxygen deprivation and pathological conditions like cancer, inflammation or arthritis (Vandekeere *et al* 2015). In healthy blood vessels, ECs can stay quiescent for years, however upon activation by one of the before mentioned conditions, they switch their phenotype to migrate, to proliferate and to remodel the environment forming new vessels in the so-called sprouting angiogenesis process (Russell and Peters 2008, Vandekeere *et al* 2015). To regulate the process of angiogenesis, a well-defined balance between pro- and antiangiogenic agents is involved triggering the cellular migration of ECs

(Rousseau *et al* 1997). Three main mechanisms are involved in the cell migration process. Chemotaxis describes the directional movement of the cells towards a gradient of chemoattractants like vascular endothelial growth factor (VEGF) or basic fibroblast growth factor. Haptotaxis on the other hand refers to the migration towards immobilized ligand gradients due to integrin binding to the ECM. Mechanotaxis is triggered by mechanical forces (wall shear stress – WSS) applied to the cells by the blood flow on the surface of the vessel wall (Lamallice *et al* 2007). Upon activation, two major EC phenotypes are involved in capillary sprouting, so called tip cells and stalk cells. The sprouting process is led by the tip cells, which navigate the formation of new vessels. Stalk cells on the other hand are highly proliferative and follow the tip cells to elongate the branch and gradually form the vascular lumen (Motherwell *et al* 2018).

1.1.2 *Vascular permeability*

The endothelial lining represents a semi-permeable barrier between the tissue and blood. Via this barrier the exchange and transfer of solute factors and molecules is controlled (usually molecules smaller than 40 kDa), while at the same time exchange of larger molecules and cells is hindered as it would require a disruption of the endothelial barrier to enable transportation (Claesson-Welsh 2015). Additionally, small plasma proteins like albumin are known transport vehicles for fatty acids and vitamins via the barrier (Nagy *et al* 2008).

The transport of larger molecules occurs via controlled formation of leaks that can be described by two major models, either by formation of transendothelial channels, so-called vesiculo-vacuolar organelles (VVO), or the transient dissolution of endothelial junctions. All these described mechanisms highly depend on the type of tissue, vessel type and tissue-specific transport kinetics (Aird 2007). An illustration of the transportation mechanisms can be seen in Figure 1.2.

Junctions between adjacent endothelial cells are impermeable under normal conditions due to the presence of intercellular tight junctions and adherens junctions. Stimulation with e.g. VEGF, reactive oxygen species or inflammatory

species like bradykinin or histamine can however cause a temporal disruption of intracellular junctions. These paracellular junctions then allow for transportation of macromolecules (Claesson-Welsh 2015).

VVOs have been identified to mainly contribute to the transport of macromolecules towards the underlying tissues (Kohn *et al* 1992). Even though the origin of VVOs was believed to originate from caveolae – small cavities – the detailed process is currently not understood (Claesson-Welsh 2015).

In certain intestinal tissues like e.g. endocrine glands or kidney peritubular capillaries, where fast exchange of molecules is mandatory, a fenestrated endothelium is present in the vessels. These fenestrations act as permiselective barrier to transport water, small ions, sugars, amino acids and small peptide hormones (Stan *et al* 2013).

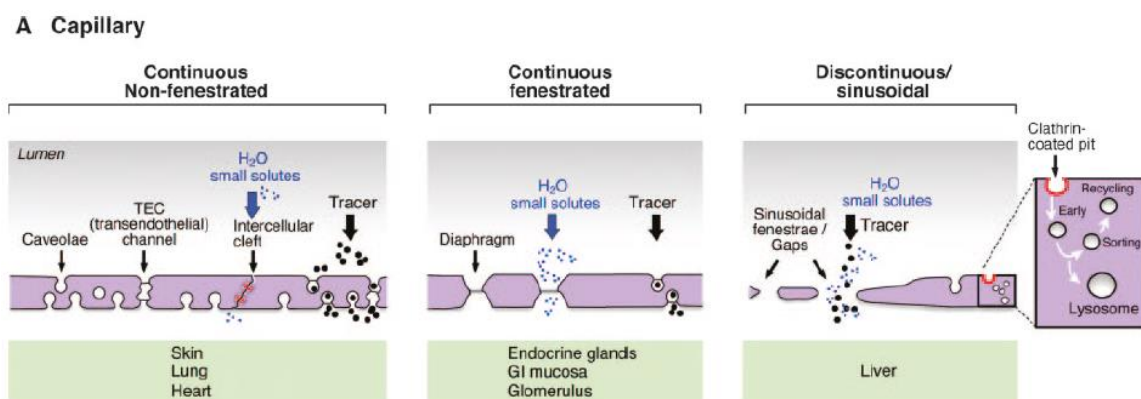


Figure 1.2: Mechanisms of vascular permeability

*The different mechanisms of vascular permeability for the transport of soluble factors and molecules. Depending on the tissue type, the vascular wall provides a barrier for molecules and cells exceeding a certain size. The image was reprinted from Aird *et al.* with permission from Wolters Kluwer Health, Inc. (Aird 2007).*

1.1.3 Metabolism

Even though a healthy endothelium is considered as quiescent, it is by far not inert since ECs carry out important functions, metabolizing glucose, fatty acids

and amino acids to generate energy and biomass. These energy production processes are especially important during angiogenesis when phenotypic changes of the ECs occur to allow proliferation and migration (Eelen *et al* 2015, De Bock *et al* 2013).

Glucose is taken up via diffusion by glucose transporters in ECs controlled by VEGF. Glucose accumulates in the proximity of the intracellular junctions and the locations of glucose transporters. By this, a concentration gradient is formed between the cytosol and the interstitial space, which is likely to be responsible for the glucose transport via the cell (Gaudreault *et al* 2008). Inside the cell, glucose is processed via glycolysis, an important process for ECs since they generate about 80% of adenosine tri-phosphate (ATP) via this pathway (De Bock *et al* 2013). Upon VEGF stimulation, ECs can greatly increase their glycolytic flux when higher amounts of energy are required, e.g. during cell migration due to cytoskeleton remodeling (Eelen *et al* 2015).

During proliferation, fatty acid uptake in ECs is upregulated as an additional source of energy. Apart from that, it is assumed that energy synthesis via fatty acid oxidation compensates the energy loss under glucose-deprived conditions (Dagher *et al* 2001). However, ECs are also responsible for transportation of fatty acids to consuming organs like the heart via the endothelial barrier (Eelen *et al* 2015).

Amino acids like glutamine, proline, and serine are essential sources of energy for rapidly growing cells. Especially glutamine is important during cell proliferation. Under oxidant injury by increased levels of reactive oxygen species, which inhibits glyceraldehyde 3-phosphate dehydrogenase, an important player in the glycolytic cycle, ATP synthesis is hampered (Harjes *et al* 2012). Uptake of glutamine, the most abundant amino acid in the plasma, compensates for the resulting energy loss to maintain cellular viability. Furthermore, it has been shown that glutamine minimizes the amount of nitric oxide (NO) secreted by ECs by reducing the availability of glyceraldehyde-3-phosphate dehydrogenase, an important cofactor of endothelial nitric oxide synthase (eNOS) (De Bock *et al* 2013).

1.1.4 Leukocyte trafficking

If inflammatory reactions occur in the human body, leukocytes, which are continuously circulating in the bloodstream, are sent by the host immune system to the site of inflammation. To enter the affected location and to start defending the host, leukocytes need to pass the vessel wall, a process called leukocyte trafficking or extravasation. Since the luminal wall is lined with a continuous layer of ECs, the immune cells first need to pass this barrier. This procedure of transendothelial migration can be separated into different main stages, initial leukocyte attachment, rolling, arrest and transmigration (Aird 2007, Luscinskas *et al* 2002). The detailed mechanisms of each individual step during transendothelial migration, a process which has been first discovered more than 200 years ago, are gradually better understood (Ley *et al* 2007, Salmi and Jalkanen 2005).

During the first stages of the cascade, the initial attachment and rolling of leukocytes is initiated by specific selectins and their corresponding ligand (i.e. P-selectin glycoprotein ligand 1), which is able to interact with all selectins and is mainly involved in the process. Among others, these selectins include L-selectin, P-selectin as well as E-selectin. Both, P-selectin and E-selectin are expressed by inflamed ECs, whereas only P-selectin is expressed by the leukocyte cells (Ley *et al* 2007). Since this binding procedure is reversible, the rolling process along the inflamed endothelium is mediated until the cells enter the arrest phase (Hogg and Berlin 1995). The catch bond like character of the selectins allows for fast attachment and release between the cell-types and enables a strong link despite the high levels of shear stress of up to 3 Pa present on the luminal surface (Butcher and Picker 1996, Marshall *et al* 2003). Rolling and attachment is further initiated by the interaction of the leukocyte-specific ligands with surface integrins like e.g. very late antigen 4 (VLA4) with vascular cell-adhesion molecule 1 (VCAM1). Leukocyte arrest is finally mediated by EC secreted chemoattractants that cause formation of stable attachment via leukocyte specific integrins with adhesion molecules expressed by the ECs (Ley *et al* 2007).

To finally migrate through the EC layer, two possible pathways are known. Either the migration takes place through the intracellular space – the paracellular route,

or directly via the ECs in the transcellular route (Feng *et al* 2002). The whole process occurs with only minimal disruption of the endothelial structure. To enable migration in-between ECs a redistribution of junctional molecules takes place to facilitate a paracellular route. Adherens junctions such as VE-cadherin can actually be disrupted upon arrival of leukocytes to enable extravasation via the generated intracellular gap (Shaw *et al* 2001). Until lately, the paracellular pathway was believed to be the only route. However, it has been found that migration can occur via before mentioned VVOs that are responsible for transportation of macromolecules. This can however be only observed by a minority of leukocytes (Ley *et al* 2007). An overview of the whole process can be seen in Figure 1.3.

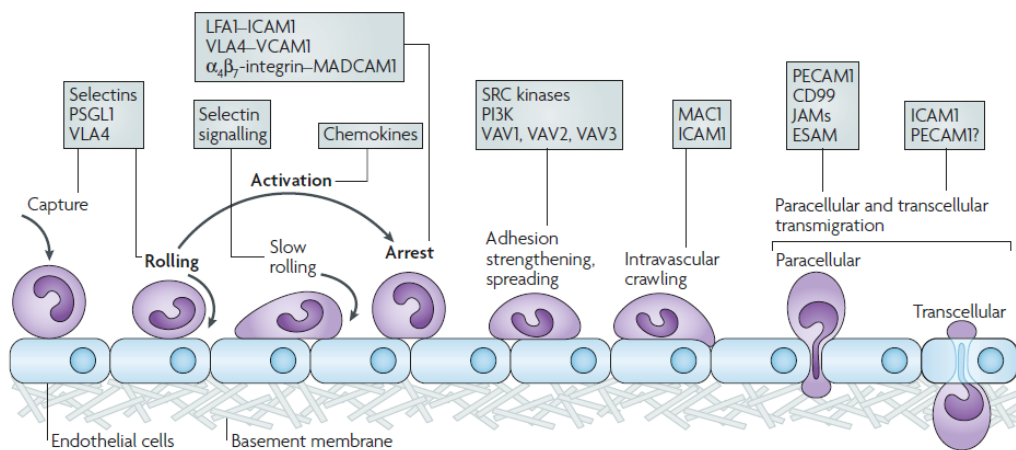


Figure 1.3: Leukocyte trafficking via the endothelium

The different stages of leukocyte trafficking into the underlying tissue can be seen. After the capture and rolling stage, leukocytes enter the arrest phase before finally passing the endothelium either via the para- or transcellular path. The image was reprinted with permission from Springer Nature (Ley *et al* 2007).

1.1.5 Hemostasis

One of the most important tasks of endothelial cells is not only to provide an antithrombotic, hemocompatible surface but also the control of hemostasis in case of blood vessel injury. Regulation of hemostasis includes a variety of processes

such as control of coagulation, platelet adhesion and activation, fibrinolysis, platelet disintegration and, to a certain extent, vasoregulation (Van Hinsbergh 2012). After blood vessel damage, and thus a disruption in endothelial integrity, the underlying layer of ECM and SMCs is exposed to the blood flow. This loss of integrity is rapidly counteracted by the formation of a hemostatic plug. Von Willebrand factor (vWF), which is produced by ECs, plays a major role in the formation of such plugs by triggering initial platelet recruitment and the subsequent multistep formation of a thrombus (Wu and Thiagarajan 1996). An overview of the coagulation cascade can be seen in Figure 1.4.

Circulating platelets bind to the vascular wall to subendothelial collagen via the GPIIb/IX/V glycoprotein receptor assisted by vWF, which serves as a ligand (Moncada and Higgs 2006). Upon secretion of ADP, serotonin, fibrinogen and thromboxane A₂, further platelet recruitment, activation and aggregation of platelets is triggered. Apart from that, the released molecules initiate contraction of smooth muscle cells, which finally facilitates the plug formation (Wu and Thiagarajan 1996, Félétou 2011). On site, fibrinogen is cleaved by thrombin to form fibrin, which polymerizes into a network together with platelets to form the final blood clot. The whole initiation of the cascade requires tissue factor, which is located in the subendothelial layer and is activated when being exposed to blood flow (Moncada and Higgs 2006).

ECs are also able to steer the fibrinolytic mechanism to counteract the excessive formation of a blood clot when the closure of the wound is fully established. Plasminogen, an inactive enzyme is constantly present in the vascular system under healthy conditions. To activate the enzyme, ECs start secreting two different types of plasminogen activators – tissue-type plasminogen activator and urokinase-type plasminogen activator (Félétou 2011). The activated protease plasmin subsequently starts degrading fibrin and the remaining clot.

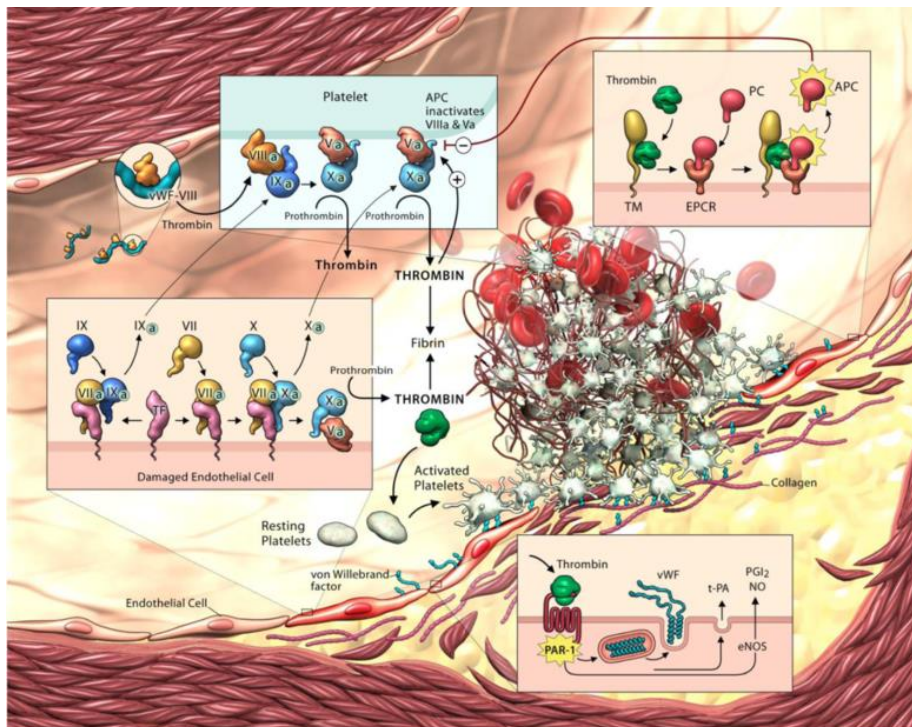


Figure 1.4 Mechanism of thrombus formation

The different steps of the coagulation cascade, which finally lead to the formation of a blood clot can be seen in this schematic illustration. The image was reprinted with permission from Yau et al (Yau et al 2015). (<https://creativecommons.org/licenses/by/4.0/>)

1.1.6 Vascular pathology

The complex set of tasks that the endothelium has to fulfill, makes it vulnerable to a variety of disorders related to dysfunction of ECs, which can all result in major complications for the host. It is important to mention that EC dysfunction is not related to EC activation, since the cells are generally highly responsive to environmental stimuli as e.g. during tissue repair, angiogenesis and immune response (Aird 2008).

A dysfunctional endothelium can be characterized by different features such as reduced vasodilation, proinflammatory state or prothrombotic phenotype. Consequently, cardiovascular diseases like hypertension, coronary artery disease, chronic heart failure, peripheral vascular disease, chronic kidney failure or viral

infections are all related to a dysfunctional endothelium (Wu and Thiagarajan 1996, Rajendran *et al* 2013).

Under normal conditions, the endothelium provides a functional barrier. Conditions of disturbed flow at e.g. branching points of the vasculature, or the presence of elevated levels of reactive oxygen species can impair the function of ECs. Under disturbed flow, ECs are known to reduce their alignment in the direction of the flow, and become activated to start secreting higher amounts of procoagulative and/or vasoconstrictive agents (e.g. endothelin, vWF or superoxide) (Jennette and Stone 2014). Upon activation, ECs also start secreting growth factors as well as reactive oxygen species to regulate inflammatory responses by expression of surface cell adhesion molecules (as described before). As a result, of all these harmful conditions, the barrier function of the endothelium is lost and toxins as well as inflammatory cells are entering the tissue (Claesson-Welsh 2015, Rajendran *et al* 2013).

While leukocyte trafficking is pivotal for the immune response of the body, excessive infiltration can cause acute and chronic inflammatory diseases such as atherosclerosis, diabetes mellitus, rheumatoid arthritis and others. In brief, during atherosclerosis leukocytes, T-cells as well as monocytes are being attracted and migrate into the arterial wall. On site, monocytes can differentiate into foam cells that trigger proliferation of SMCs. The uncontrolled proliferation of SMCs causes structural alterations, which end up narrowing the lumen (Moncada and Higgs 2006). If the vessel is narrowed, the blood supply can no longer be maintained, causing malnutrition of organs, or in the worst case stroke. Under such conditions, the vessel needs either to be widened with a stent, or completely replaced.

1.2 Vascular graft engineering

Diseased blood vessels need to be either replaced or a bypass around the obstruction in the vessel needs to be applied. Most of these coronary and peripheral vascular graft procedures utilize autologous vessels, such as the saphenous vein or the internal mammary artery (Ravi and Chaikof 2010). However, the use of autologous vessels is complicated by the additional extraction surgery,

which can cause donor site morbidity. Additionally, the availability of autologous tissue is always limited and long-term patency of the graft cannot be guaranteed. Failure rates of saphenous vein bypass grafts after 10 years account for 50% of all patients (Pashneh-Tala *et al* 2015).

As an alternative solution to autologous vessels, synthetic graft materials can be implanted. For large diameter substitutes such as the aorta, iliac artery or the proximal femoral artery, Dacron – a polyethylene terephthalate (PET) based material is commonly used. For replacements of small-diameter vessels (<6-8 mm), either autologous vessels or expanded polytetrafluoroethylene (ePTFE) are preferentially selected (Buja and Schoen 2015). Even though synthetic materials are implanted since many years, they usually perform less well compared to autologous vessels. Artificial graft materials are often causing complications like thrombus formation and thus embolism, fibrous hyperplasia, infection, pseudoaneurysm and structural degeneration. Material related issues include fabric fragmentation as well as graft dilation and inability to grow with adolescent patients (Buja and Schoen 2015). Most of the before mentioned problems like thrombosis, intimal hyperplasia or atherosclerosis arise due to absence of an autologous layer of ECs on top of the luminal graft surface (Pashneh-Tala *et al* 2015).

To overcome these issues related to vascular grafts, several approaches of tissue engineered vessels have been investigated. First introduced in 1988, the term tissue engineering (TE) was meant for "the application of principles and methods of engineering and life sciences toward the fundamental understanding of structure-function relationships in normal and pathological mammalian tissues and the development of biological substitutes to restore, maintain or improve tissue function" (O'Brien 2011). By this definition, it merges the research fields of cell biologists, biomaterial engineers and physicians and many others.

The aim of TE approaches is to rebuild native tissue with autologous patient-derived cells, to avoid immune rejection of the graft. However, to guide the formation of new tissue, in most cases a porous three-dimensional scaffold is necessary. This scaffold is intended to serve as a platform for the cells to attach, proliferate, migrate and start with the formation of novel tissue *in vitro* before the

implantation *in vivo*. Stimulation of tissue formation is often induced with additional supply of growth factors or cytokines. Based on their stimuli, formation of specific tissue types can be triggered. These three major contributors (cells, scaffold, growth factors) – often called the tissue engineering triad – decide on the outcome of the engineered tissue (Jafari *et al* 2017).

1.2.1 Scaffold materials

Materials used for scaffolding in tissue engineering can be either stable or degradable and their origin can be synthetic, naturally occurring or a mixture of both. Based on the chemical composition and their architecture, their influence on cell fate can be crucial. It has often be stated that the structure itself should facilitate cellular attachment and growth and provide a porous architecture for the transport of nutrients and waste products. To be considered suitable for TE, five main scaffold criteria need to be considered (O'Brien 2011).

(i) Cytocompatibility

As already mentioned before, one of the main prerequisites to be applied as a scaffold is the material's compatibility with cells. Cells need to grow and spread on/inside the scaffold before they start with the synthesis of ECM. To be considered as biocompatible, the response to the host tissue also needs to be addressed. For successful implantation, inflammatory responses or foreign body reactions and fibrous capsule formation should be avoided (Babensee *et al* 1998).

(ii) Biodegradability

One of the principles in TE is the assumption that new tissue is formed inversely correlated to the degradation of the scaffold. After complete dissolution of the scaffold, the newly synthesized tissue is able to carry out all the structural functions of the previous architectural support. The extracellular space that becomes available is subsequently filled with ECM. Byproducts of the degradation

process need to be transported away from the site without causing cytotoxic or inflammatory reactions (O'Brien 2011).

(iii) Mechanical support

Apart from cellular response, the scaffold needs to closely mimic the mechanical properties of the host tissue. Depending on the tissue type, this requirement is difficult to achieve. Especially for bone tissue or tendon. Post implantation, it needs to be considered that the mechanical properties of the scaffold will be drastically affected if degradable scaffolds are selected. Depending on the cellular performance, a huge loss in mechanical stability might be the result (Ravi and Chaikof 2010).

(iv) Architecture

A major factor for cellular infiltration and nutrition supply within a scaffold is the architecture of the construct. Mostly influenced by the pore size as well as the type of interconnected porosity, cells infiltration can be observed (Jafari *et al* 2017). However, the actual pore size required for infiltration is strongly debated (Murphy *et al* 2010). To maintain viability, the porous network is mandatory to transport nutrients to the cells as well as waste products away from the scaffold. Several tissues require vascularization, so the scaffold dimensions need to be sufficient for angiogenesis.

(v) Manufacturing process

As a last point, the fabrication method for the scaffold needs to be addressed. To be available for the medical market, the production of the material needs to be up scalable. In that regard, also the achievement of a good manufacturing practice standard is critical (O'Brien 2011). This prerequisite is a limiting factor for many research-lab based approaches that already could proof successful use of their materials *in vitro* or *in vivo*.

1.2.2 Scaffold types and manufacturing methods

To engineer scaffolds according to the previously discussed requirements, several techniques have been utilized. They all differ in the final architecture of the construct in terms of pore-size, pore-size distribution, interconnectivity and processability of different materials respectively.

Solid free form fabrication or rapid prototyping describes a method, which is capable of precisely reproducing the architecture of a defect or missing tissues. The structure is fabricated directly from a computer-aided design model that is often obtained by MRI or CT scans of the patient. The structure is built by repetitive build-up of 2D layers from the material in a layer-by-layer approach usually from a powder bed or extrusion. Such processes include selective laser sintering, fused deposition modeling or 3D printing. Selected material classes of polymers, metals or ceramics can be processed by these techniques. Drawbacks of this technology are the size-limitation of small features, or the limitation in materials choice. Nano-sized interconnected porous networks with a highly regular microstructure cannot be fabricated via these techniques. Advantages include the reproducibility of manufactured parts, precise geometry as well as potential for up-scaling and the possibility to use non-toxic components for the process (Weigel *et al* 2006, Hutmacher 2000).

More recently, the technique of 3D bioprinting has gained a lot of attention. The principle of the process remains the same; however, instead of using conventional materials for the additive process, bioinks made of poly(ethylene glycol) (PEG) based hydrogels, alginate or agarose are used to fabricate 3D scaffolds. These bioinks include cell-suspensions, cell-laden hydrogels, microcarriers, cell/tissue spheroids and decellularized matrix components (Duan 2017). The cells are directly deposited at the site of interest in a three-dimensional fashion, without the need for post-seeding procedures. Scaffold structures with mixtures of several cell-types and functional materials can be fabricated. One drawback however remains, the limitation in available materials and overall considered weak mechanical performance of such bioprintable materials. Since the cells are directly implemented during the printing process, toxic solvents or cross-linkers and elevated temperatures need to be avoided (Ji and Guvendiren 2017).

Solvent casting/particulate leaching techniques make use of a porogen, mostly salt or other soluble particles that are embedded in a polymer solution. After evaporation of the solvent, a solid layer with the porogen inside the matrix is fabricated. Subsequently the porogen is selectively solubilized and leached out of the scaffold. Depending on the particle size and density, scaffolds with different pore sizes and overall porosity can be obtained. The method is simple to apply and can be performed with most soluble polymers, however the particle distribution is generally difficult to control and an interconnected porosity cannot be guaranteed (Janik and Marzec 2015, Ma 2004).

Thermally induced phase separation describes the process when a thermodynamically unstable polymer solution is separated into a polymer-depleted and a polymer-rich phase induced by removal of heat energy (liquid-liquid phase separation). Other mechanisms like solid-liquid or theoretically liquid-solid phase separation rely on either polymer crystallization in solution (solid-liquid) or solvent crystallization before the polymer (liquid-solid), respectively. Nature and strength of polymer-solvent interactions determine the progression of the process. The polymer solution can be cast into the desired shape before the solidification process of the polymer-rich phase is triggered. The polymer-depleted phase will turn into pores during the process of solvent sublimation or extraction. Based on the process components and conditions, different pore sizes and geometries can be obtained (Lu *et al* 2013, Weigel *et al* 2006).

Gas foaming is another straight forward method for scaffold fabrication. The procedure can be carried out by injection molding or by use of a high-pressure chamber in an autoclave. Formation of pores is either induced by expansion of gaseous phases such as CO₂ and ammonia gas that are formed during the procedure (e.g. polyurethane reacts with ammonium bicarbonate), or by decomposition of substances that are added during the process. The process is generally difficult to control, resulting in relatively large pore sizes (Weigel *et al* 2006).

A different approach is the addition of different foaming agents such as nitrogen, water, fluoroform or CO₂ that can be added to the polymer melt. This allows for better control of pore size within the range of 500 - 2000 μm and does not require

the usage of toxic solvents. However, the general issue of missing interconnectivity and pore size distribution remains (Janik and Marzec 2015).

Hydrogel fabrication to engineer water-containing polymeric gel scaffolds. They are physically or chemically cross-linked hydrophilic polymeric networks incorporating a huge amount of retained water. They consist of one or more monomer types resulting in cross-linked homopolymer or copolymer networks of either neutral, anionic or cationic charge depending on their building blocks. In addition, they can be categorized according to their physical structure, that can either be amorphous, semi-crystalline, hydrogen-bonded, supramolecular or hydrocolloidal (Vlierberghe *et al* 2011). The potential of using synthetic polymers, natural polymers or blend systems of both opens up a large variety of applications in TE. Synthetic hydrogels can be modified with naturally occurring cell-binding motifs, such as fibronectin, laminin or collagen, providing a suitable environment for host cells. To further mimic the ECM environment, hydrogel modifications with growth factors or peptides have been widely investigated (Zhu and Marchant 2011). Another interesting feature of hydrogels is the possibility to directly load the gels with cells. Cells can be added directly in the precursor solutions when non-toxic cross-linking protocols are applied (Hillel *et al* 2007). Mechanical properties of the gels can be tuned to a certain extent by controlling the cross-linking process; however, a mechanically stable substrate, maintaining the originally desired properties is difficult to obtain. Higher cross-linking densities enhance the stiffness of the gels, but can cause brittleness. To tune the mechanical properties of hydrogels, reinforcement with a stronger fibrous component has been suggested (Yodmuang *et al* 2015).

Electrospinning has been first introduced in the 1930s and is one of the most investigated scaffold fabrication methods in TE. In electrospinning, fibrous scaffolds with tunable fiber diameter can be obtained that can closely mimic the dimensions of e.g. collagen fibrils (50-500 nm) in the human body. Based on the similar architecture to the native ECM, it has been proposed as an ideal substrate for cell culture (Ma 2004). A major advantage of the electrospinning technique is the plethora of polymers that can be processed. To process polymers via electrospinning, they need to be dissolved with a suitable solvent in an optimal concentration with adjusted viscosity. The process itself requires application of

high voltage that is applied e.g. to a needle, which is gradually extruding the polymer solution. As soon as the polymer is ejected, the polymer solution is accelerated towards a target with either opposing or neutral charge. During the travel time of the jet, the solvent evaporates and fibers are drawn during the time of flight. Based on the solution parameters such as viscosity, conductivity and solvent evaporation as well as the process parameters (applied voltage, distance to collector, temperature, humidity) the fiber size can be steered. The technique also allows for introduction of growth factors, peptides, drugs or other functional molecules that are either released from the fibers or present on their surface (Lu *et al* 2013).

1.2.3 Tissue engineering of vascular grafts

A first attempt to apply a tissue engineered vascular graft was performed by Weinberg and Bell in 1986 (Weinberg and Bell 1986) with a collagen gel in combination with vascular cells. Unfortunately, the durability of the construct was however impaired by the poor mechanical properties of the collagen gels, which are not sufficient to withstand the hemodynamic forces inside the vessel. Since then, several attempts have been investigated to reconstruct vascular grafts via TE. Some of the approaches utilize one of the previously described methods of scaffold fabrication, some others are considered as scaffold-free techniques.

In one of these attempts, a biodegradable polyglycolic acid scaffold was implanted as an autologous vascular graft *in vivo* and remained patent for up to 1 month. One drawback of such degradable scaffolds is the rapid dissolution, which is often accompanied with acidic byproducts that can cause inflammation or premature loss in mechanical integrity (Zhang *et al* 2007).

Cell-sheet engineering is a method where *in vitro* 2D cell culture of e.g. stromal cells such as SMCs or fibroblasts is used to fabricate sheets of cell-derived ECM (with or without decellularisation). These sheets can subsequently be wrapped around a tubular structure to shape the tunica media without initial use of a support scaffold. This tubular structure can then be wrapped with another layer of fibroblast-derived tissue to mimic the adventitia. The inner lining of the tubular

structure is then further seeded with ECs. The resulting graft showed promising mechanical performance and was successfully implanted for up to 20 months, yet the long-culture times and thus related costs and effort still limit this approach for clinical applications (Kumar *et al* 2011, McAllister *et al* 2009).

Another scaffold-free manufacturing technique to reconstruct native blood vessels is based on a self-assembling strategy with the guidance of a bio printer without any additional scaffold material. To fabricate such constructs in a desired shape, with high throughput and in a reproducible fashion, a rapid prototyping process in which cell-laden capsules made of ECM proteins like collagen are "printed" into the desired shape. One in the right shape the tissue needs to mature. It remains to be seen how those structures will perform under physiological conditions in a long-term application (Norotte *et al* 2009).

Decellularized tissue entirely composed of ECM components is another substrate that can be used for culturing autologous cells. By removing all cellular components from the tissue with chemical agents, any immunogenic reactions with the host system can be avoided. Since the extracellular components remain intact, mechanical properties of the scaffold are minimally impaired. The decellularized matrix is afterwards populated with patient derived cells that spread within the provided scaffold. Even though this approach seemed promising, it has been found that such decellularized grafts were more susceptible to aneurysm compared to synthetic graft materials. Possible explanations might be the lack of cellular repopulation of the graft (Pashneh-Tala *et al* 2015).

Another versatile technique to fabricate blood vessel structures is the electrospinning method. A huge advantage of the electrospinning approach is the possibility to blend several materials to steer the mechanical properties of the scaffold and to control the cellular response. Generally, depending on the diameter of the collector, different vessel diameters can be produced according to the desired shape (Ercolani *et al* 2015). In one approach, the idea was to provide a scaffold made of different ECM components such as collagen and elastin that might help in the development of a fully functional tissue. Both ECM components were electrospun on a cylindrical collector in a layer-by-layer approach. Post-seeding with SMCs, the results revealed cellular infiltration into the electrospun network.

Cells were proliferative and started to align in a circumferential direction. The intimal layer was fully covered with ECs being an indication of a functional endothelium (Boland *et al* 2004). Despite these promising results, cellular mechanisms like migration within such an environment and nutrient supply still need to be addressed.

1.3 The combined process of electrospinning and cell electrospraying

One of the most prominent drawbacks of the electrospinning process is the low pore size of the scaffolds, which directly correlates with the fiber diameter in randomly oriented networks. Nonetheless, in most configurations, a nanofibrous structure is preferred to closely mimic the size of the ECM components and to facilitate cellular attachment (Ma 2004). Even though some authors report on cellular infiltration (Boland *et al* 2004), it is generally assumed that infiltration can hardly be achieved for nanofibrous membranes (Nam *et al* 2007), a major drawback for the engineering of living tissues. Considering the size of a cell, the pore size needs to be adjusted accordingly to facilitate infiltration. Techniques to increase the porosity of electrospun membranes have been investigated. One way to enhance porosity is by introducing a sacrificial fiber, where two polymers are simultaneously spun on a collector in a co-electrospinning process. After the process, one of the polymers can selectively be dissolved without interfering with the other polymer (Baker *et al* 2012). Another approach is the so-called cryo-electrospinning process, during which ice crystals are deposited within the network during the process by cooling the collector to 200 – 220 K. When the ice dissolves after the process, scaffolds with increased pore sizes can be achieved (Simonet *et al* 2007).

A fairly new method for fabrication of cell-incorporated 3D scaffolds was introduced by combining conventional electrospinning and electrospraying of cells. This method was first described by Stankus *et al.* in 2006 (Stankus *et al* 2006). In their study, a simultaneous process of fiber spinning and electrospraying of cells onto a rotating mandrel was investigated. Interestingly, no loss in cellular viability

after up to 7 days in culture was observed after the spraying process, even though the toxic solvent hexafluoroisopropanol (HFIP) was utilized. Applying the same technique, a tubular graft was fabricated in a follow-up study. There, SMCs were integrated into the fibrous network and tested for mechanical properties, showing similar compliance values compared to native blood vessels, indicating the high potential of this approach in the fabrication of viable grafts (Stankus *et al* 2007). In other studies Ekaputra *et al.* and Paletta *et al.* confirmed the feasibility of this approach to fabricate *in-situ* cell-integrated scaffolds (Ekaputra *et al* 2008, Paletta *et al* 2011). Electrospraying of a murine fibroblast cell line into a poly(DL-lactide-co-glycolide) scaffold did also not affect the viability of the cells (Seil and Webster 2011). To demonstrate cellular integrity and to exclude damage on a molecular level, the gene expression profiles of human brain astrocytoma cells post electrospraying were analyzed in a study carried out by Eddaoudi *et al.* No significant alterations in terms of protein expression profile or post-translational modifications were found in the cells transported in the electric field (Eddaoudi *et al* 2010). In fact, Carter *et al* confirmed the functionality of electrosprayed spleen cells both *in vitro* as well as in an *in vivo* mouse model. They incorporated the cells in a layer-by-layer approach and subsequently assessed the viability of the cells within the construct (Carter *et al* 2011).

Instead of spraying the cells in a parallel process, a similar approach of incorporating living organisms into fibers was investigated (Yeo *et al* 2016, Letnik *et al* 2015). In fact, viable fiber constructs carrying yeast cells with a core-shell geometry were fabricated and kept in culture for 21 days (Letnik *et al* 2015). Also, Yeo *et al.* were able to introduce human osteosarcoma cells into an alginate-based fiber with sustained viability in a combined process of bioprinting and electrospinning (Yeo *et al* 2016).

All these alterations of the conventional electrospinning process indicate that there is still a lot of potential to improve the electrospinning technique towards the realization of 3D tissues in a single step process. Generally, it can be mentioned that due to the benign effects of the cell-spraying process the technique can be used as a versatile tool for the controlled delivery of cells. Based on the flexibility in cell sources and potential of utilizing several cell types as well as polymers,

especially the combined process with electrospinning provides an encouraging method for the fabrication of numerous engineered tissues in the future.

1.4 Ventricular assist devices

Since the first design of a VAD, pump thrombosis is considered a major problem due to interactions of a foreign material with blood. Apart from thrombosis, such devices are generally prone to adverse events such as stroke bleeding and infection (Kirklin *et al* 2013). In older generations of pulsatile VADs (PVAD) incorporating relatively large dimensions, the performance of the device is not directly impaired when small clots were formed on the surface; however, dislodgment of blood clots was likely to cause an embolic stroke to the patient (Tchantchaleishvili *et al* 2014). In continuous flow VADs – operated with a small impeller – blood clots can cause malfunction of the whole device. Additionally in such continuously operating VADs the blood experiences high speed and turbulent flow patterns that further can induce coagulation of the blood (Chiu *et al* 2014).

Since most of these adverse reactions are triggered by the pump surface itself, numerous approaches to improve hemocompatibility have been investigated. Some of these modifications include textured, sintered titanium surfaces, coatings with titanium nitride, diamond-like carbon and heparin, texturing with microfibers or application of polyurethane vascular patches (Schmid Daners *et al* 2017). Still, anti-coagulation therapy is applied post-surgery in all patients. Nonetheless, due to the difficulty of patient-specific anticoagulation-therapy the risk of either over- or under-anticoagulation remains. Gastrointestinal bleeding, intracranial bleeding or hemolysis and thrombosis are likely to occur consequently (Tchantchaleishvili *et al* 2014).

Based on these issues, a stable layer of autologous endothelial cells on the surface of the pump is therefore considered a promising solution to avoid any adverse reactions with blood similar as being present in human blood vessels. By applying such a cell lining on the surface of a VAD, the antithrombotic properties would be provided by the protective barrier function of the ECs, without requirement of a drug therapy.

2 Scope of the thesis

2.1 Thesis motivation

Despite the recent technological advances within the field of surface engineering for medical applications, a truly hemocompatible surface is not existing (Wnek and Bowlin 2008). Most materials utilized for blood contacting applications or devices, exhibit a certain degree of thrombogenicity. Depending on the application, consequences of blood coagulation can be severe. Numerous approaches aim for reduced interactions of synthetic materials with blood, to obtain bio-inert surfaces (Seib *et al* 2014, Zhu *et al* 2015). Alongside the chemical and morphological functionalization of surfaces, drug therapy by either release from the materials surface or external application is still common.

Antithrombotic properties of an autologous endothelium as present in the human body are considered the optimal blood interface, but to date, cannot be recreated via engineering approaches. Therefore, strategies utilizing autologous patient-derived cells to generate surfaces with luminal coverage of ECs represent a promising approach in the design of highly hemocompatible surfaces or blood vessel substitutes. Most approaches are based on surface functionalization to improve the attachment of the cells via grafting of specific peptides or other adhesive biomolecules (Jun and West 2004, Lin *et al* 2010). Other approaches aim for improved cell surface attachment by specific patterns that can induce both, a protective effect against shear stress from the blood flow and offer anchoring points for the cells (Stefopoulos *et al* 2017). All these attempts showed an improved cellular response; however, in most cases the interactions with underlying SMCs that can be decisive for endothelial cell fate are neglected.

Therefore, the ultimate goal is to engineer an artificial surface based on the architecture of a native blood vessel comprising both SMCs, ECs and extracellular matrix. There are numerous tissue engineering (TE) strategies using a combination of biodegradable scaffolds in combination with host cells, where a remodeling of the tissue via extracellular matrix formation by the host cells takes place (Dhandayuthapani *et al* 2011). To engineer a surface that is under constant mechanical load and shear flow, as for example present in PVADs, with living tissue, a stable scaffold containing the host cells is mandatory to avoid delamination at the interface or internal material damage.

Electrospun membranes are known since about 20 years within the field of biomedical engineering. It has been proposed that the substrate architecture is advantageous for cellular attachment (Agarwal *et al* 2008). Besides the suitability for cell culture, the electrospinning technique offers a broad variability in materials choice, fiber morphology and fiber organization. Numerous medically relevant polymers have been processed into fibrous scaffolds. Some of these polymers are proposed to be highly hemocompatible based on their considered inertness. Despite the amount of research done within this field, the possibilities to fabricate electrospun scaffolds that incorporate living cells are still limited. This is also due to the fact, that most micron- to submicron-sized scaffolds possess pore sizes that are too small to allow for cellular infiltration. Therefore, adaptations to the conventional electrospinning process are required to enable the *in situ* fabrication of cell-infiltrated scaffolds.

The motivation of this thesis was to enhance the electrospinning technique by combining the procedure with a cell spraying approach. To enable utilization of such a biomimetic scaffold, a fiber with enhanced properties in terms of mechanical response as well as hemocompatibility needs to be developed. A stable bonding procedure to functionalize surfaces with such membranes also needs to be explored.

2.2 Thesis aims

The overall aim of this thesis was to engineer a biomimetic scaffold that resembles the design of a native blood vessel in the human body that can be utilized as an interface to shield artificial surfaces from adverse interactions with blood. To achieve this, several tasks had to be addressed ranging from process engineering, to material evaluation and assessment of cellular as well as blood responses. The basis of the approach was the development of an electrospinning process to fabricate a scaffold made of non-degradable polymers that can be used as an interface with blood. Apart from the engineering aspect of producing viable cell infiltrated 3D scaffolds, these membranes were investigated in terms of hemocompatibility, with focus on platelet adhesion and the formation of a fibrin

clot. Additionally, interactions with endothelial cells, which in the end will be responsible for the protective properties of the biomimetic structure, were assessed.

Development of a method that combines conventional fiber electrospinning with cell-electrospraying

Fabrication of electrospun scaffolds has been developed since two decades due to their architecture and interconnected porosity closely matching the structure of extracellular matrix inside the human body. However, based on the small size of the pores present in such scaffolds, cellular infiltration is difficult to achieve. Therefore, a combined process of cell-electrospraying and electrospinning was envisioned that offers the opportunity of fabricating cell-infiltrated 3D electrospun scaffolds *in situ*. In order to obtain viable 3D constructs the effect of cytotoxicity deriving from utilized solvents during the process needed to be evaluated.

Tailoring of scaffold material for enhanced hemocompatibility

The presence of foreign artificial materials in blood-contacting devices, or vascular grafts can cause thrombus initiation and propagation if surface hemocompatibility is not given. Apart from the biological response of such materials, mechanical forces present within this environment need to be considered. Within this objective, the cyclic response of electrospun membranes to mechanical load was addressed. The fiber composition had to be adjusted to enable the fabrication of a membrane that can sustain numerous cycles of deformation. Apart from that, the aim was to characterize the interactions of the membrane material with biomolecules and blood, to better understand mechanisms that cause the initiation of blood clot formation on artificial polymeric scaffolds.

Assessment of cellular response

The endothelium is a complex structure that interacts as an interface with the environment of neighboring cells as well as the blood flow. Based on the environment the functionality of endothelial cells in terms of anti-inflammatory response and resistance against wall shear stress can differ. One aspect, the potential of the scaffold for endothelialization needed to be evaluated. To do so, the usage of a bioreactor setting that applies both, cyclic deformation as well as fluid flow to the endothelial cells was planned to mimic realistic conditions as present in a VAD. Furthermore, the potential of smooth muscle cells to produce ECM was addressed to better control EC response to electrospun membranes. To do so the goal was to steer the phenotype of the SMCs to enable synthesis of a collagenous matrix. At first, the SMC phenotype had to be controlled to enable formation of a collagenous ECM. Subsequently a quiescent phenotype, as present in blood vessels, needed be achieved to ensure ideal conditions for EC seeding. The overall aim of this concept of having a co-culture construct was to investigate a beneficial effect of SMCs on the EC performance.

2.3 Thesis outline

Chapter 1 summarizes relevant background information about the physiology of the vascular system, current approaches within the field of vascular graft engineering as well as the combined process of electrospinning and cell-electrospraying. This knowledge is fundamental for the realization of this study.

Chapter 2 shortly summarizes the motivation of the study, the aims that were specifically targeted during the process and the outline of the thesis.

Chapter 3 presents the experimental procedure of the fabrication of a cell-infiltrated scaffold engineered by the combination of an electrospinning process with the electrospraying of encapsulated cells by microfluidics. The establishment of this process is of key importance for the envisioned biomimetic approach to rebuild the architecture of a native blood vessel.

Chapter 4 describes the initial study of an electrospun blend fiber possessing a core-shell like architecture. The fabrication process, characterization of these fibers and response to the adsorption of blood relevant proteins is investigated.

Chapter 5 includes the characterization of the fibrous electrospun membrane. For the final application in a pulsatile ventricular assist device (PVAD) specific requirements in terms of mechanical performance and hemocompatibility have to be met. To address these requirements, the membranes were mechanically tested in a cyclic strip biaxial test, incubated with human blood and analyzed with respect to relevant marker molecules, to better understand the scaffold material and its interaction with the environment and finally to predict the performance in an *in vivo* setting.

Chapter 6 deals with the important topic of endothelial cell performance on top of tailored electrospun membranes. A comparison of cells seeded on blank electrospun surfaces with a membrane incorporating smooth muscle cells is the final objective of the approach. Preliminary results are presented how the synthesis of a collagenous ECM environment can be created with the assistance of SMCs. The synthesized ECM is expected to facilitate a strong attachment of ECs.

Chapter 7 highlights the possibility of tuning the pore size of electrospun membranes. A preliminary study investigating the effect of electrospayed sacrificial polymer particles that are incorporated during the spinning process are investigated.

Chapter 8 summarizes all the investigated topics and results within this thesis. It forms a synthesis of all the studies and their major outcomes and puts them into the context of the final application. This chapter also includes a final conclusion as well as an outlook for future research.

3 Cell electrospaying

L. Weidenbacher, A. Abrishamkar, M. Rottmar, A.G. Guex, K. Maniura-Weber, A.J. deMello, S.J. Ferguson, R.M. Rossi, G. Fortunato

Note: This chapter has been published as: Electrospaying of microfluidic encapsulated cells for the fabrication of cell-laden electrospun hybrid tissue constructs, *Acta Biomaterialia* 64, 137-147 (2017). Permission from the publisher was not required.

L. Weidenbacher performed all experiments including electrospinning, fiber characterization, cell studies, capsule characterization and cell spraying. A. Abrishamkar performed the microfluidic encapsulation process. L. Weidenbacher analyzed the data and wrote the manuscript with contribution of all authors.

3.1 Abstract

The fabrication of functional 3D tissues is a major goal in tissue engineering. While electrospinning is a promising technique to manufacture a structure mimicking the extracellular matrix, cell infiltration into electrospun scaffolds remains challenging. The robust and *in situ* delivery of cells into such biomimetic scaffolds would potentially enable the design of tissue engineered constructs with spatial control over cellular distribution but often solvents employed in the spinning process are problematic due to their high cytotoxicity. Herein, microfluidic cell encapsulation is used to establish a temporary protection vehicle for the *in situ* delivery of cells for the development of a fibrous, cell-laden hybrid biograft. Therefore, a layer-by-layer process is used by alternating fiber electrospinning and cell spraying procedures.

Both encapsulation and subsequent electro spraying of capsules has no negative effect on the viability and myogenic differentiation of murine myoblast cells. Propidium iodide positive stained cells were analyzed to quantify the amount of dead cells and the presence of myosin heavy chain positive cells after the processes was shown. Furthermore, encapsulation successfully protects cells from cytotoxic solvents (such as dimethylformamide) during *in situ* delivery of the cells into electrospun poly(vinylidene fluoride-co-hexafluoropropylene) scaffolds. The resulting cell-populated biografts demonstrate the clear potential of this approach in the creation of viable tissue engineering constructs.

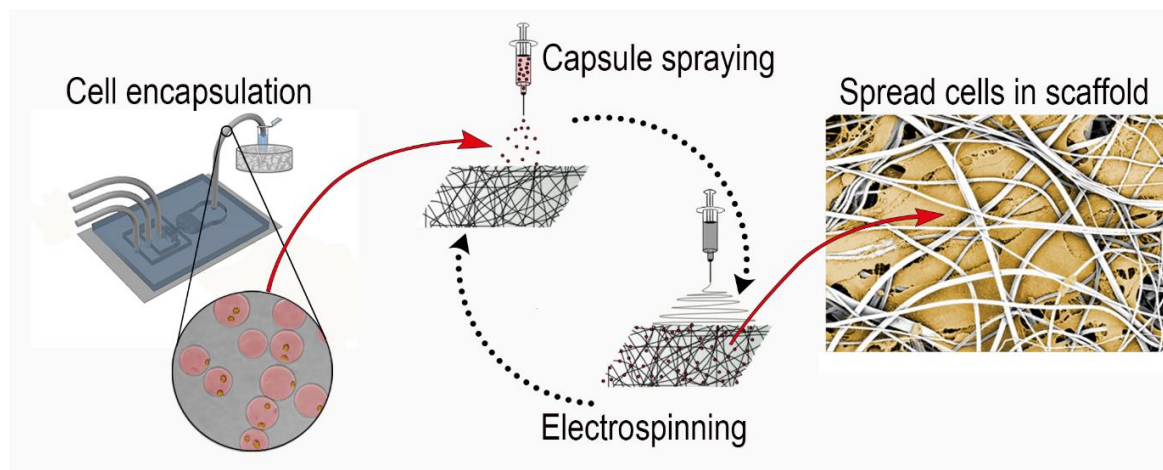


Figure 3.1: Graphical abstract

3.2 Introduction

In the field of tissue engineering, the development of artificial functional tissues is largely controlled by cell culture substrates that provide the tissue with specific biological, chemical, architectural and mechanical properties and cues. Despite a continual development of new manufacturing techniques that allow the engineering of 3D scaffolds, the ability to mimic native tissues in an efficient and reproducible manner remains a complex challenge.

In the human body, tissues are composed of spatially distributed cells within a tissue-specific extracellular surrounding made of various components (O'Connor and Adams 2010, O'Brien 2011). To mimic such a sophisticated environment using engineering approaches, not only the material choice and scaffold morphology need to be considered, but also the incorporation and subsequent interaction of host cells (which determine cell fate) within the construct (Griffith and Swartz 2006). While parameters such as average pore size and overall scaffold porosity are known to be of key importance for maintaining cellular function (Bergmeister *et al* 2015, Di Luca *et al* 2016, Telemeco *et al* 2005, Liu *et al* 2015a), cellular infiltration of a 3D scaffold and the formation of a multilayer, truly 3-dimensional tissue still remain a significant challenge.

Another prerequisite aside the scaffold architecture is the mechanical support, which should resemble the native tissue environment and can also be considered as a general requirement (Hollister 2005). This feature is limiting the usage of natural polymers for tissue engineered scaffolds since their mechanical support is too low. To adjust mechanical properties in a controllable manner, polymer blending (Sionkowska 2011) or crosslinking with potentially cytotoxic crosslinking agents or photoinitiators (Nguyen and West 2002, Liu *et al* 2008) is necessary. As a consequence, mostly synthetic polymers with superior intrinsic mechanical features (such as flexibility or modulus) are used for tissues for which adapted mechanical support is a prerequisite (Park *et al* 2015, Baker *et al* 2009). Stable polymers are applied *in vivo* for vascular and cardio-vascular intervention as vascular graft materials (Swathi and Elliot L 2010) or engineering of tri-leaflet heart valves (Bezuidenhout *et al* 2015). They are also being investigated for treatments of the spine (St. John 2014) or ligament (Legnani *et al* 2010). Besides these, they are commonly applied in designing advanced anti-adhesive or functional *ex vivo* wound dressings (Maitz 2015).

Furthermore, synthetic polymers are particularly attractive in terms of manufacturing standardization as well as off-the shelf availability when it comes to clinical requirements (O'Brien 2011).

Amongst these, poly(vinylidene fluoride-co-hexafluoropropylene) (PVDFhfp) is a highly fluorinated synthetic polymer with the potential for long term *in vivo* applications. Due to its chemical structure, it is highly resistant to hydrolytic, oxidative and enzymatic cleavage.(Ding *et al* 2009) In addition, since fluorinated surfaces have shown to enhance thromboresistance (Hasebe *et al* 2007, Xie *et al* 2010), PVDFhfp is a promising material for blood contact applications. It can also be exploited in the design of scaffolds in neuronal, cardiac or skeletal muscle tissue where electrical stimulation is beneficial (Balint *et al* 2013). Indeed, it has been found that electric stimuli can promote the differentiation of murine myoblast cells into functional contractile myofibrils, needed for engineering functional skeletal muscle tissue (Park *et al* 2008, Martins *et al* 2013).

A combination of electrospinning and cell electrospraying showed much promise for the incorporation of cells into three-dimensional fibrous scaffolds (Stankus *et*

et al 2006, 2007). Importantly, such an approach could be exploited to avoid post-seeding strategies, where seeding densities and cellular distribution are difficult to control (Chen *et al* 2011).

However, in most electrospinning processes, synthetic polymers must be first dissolved in cytotoxic organic solvents (Nam *et al* 2008), thus limiting their utility in cell-based applications. Whilst electrospinning from benign solvents has been investigated (Das *et al* 2015, Dalton *et al* 2006), its use has been limited to water soluble polymers, which in turn promotes rapid scaffold dissolution in the aqueous cell culture environment.

To overcome the issue of solvent toxicity, it has been suggested that cells should be “protected” during the manufacturing process (Stankus *et al* 2006), since simple post-processing methods allow the removal of residual solvents (Nam *et al* 2008).

Indeed, encapsulating cells in alginates, collagen or agarose (Hernández *et al* 2010), affords not only some degree of environmental protection but also a controlled release of cells (Steinhilber *et al* 2013). Such “microcarriers” have been widely investigated as potential delivery vehicles in therapeutic applications such as the treatment of myocardial diseases (Zhao *et al* 2016). Moreover, since the transport of cytokines and other molecules from such capsules to the surrounding tissue can occur with ease, there is much potential for application in cell-based therapies (Visted *et al* 2003, Uludag *et al* 2000). Conversely, it must also be remembered that capsules can inhibit or delay a host immune response by blocking immune cell recognition sites (Krishnan *et al* 2014).

In recent years, microfluidic technologies have been used to excellent effect in a range of biological applications such as synthesis of functional materials, drug discovery and single cell studies (Theberge *et al* 2010, Dittrich and Manz 2006, Rodríguez-San-Miguel *et al* 2016). In relation to the current studies, microfluidic tools have been shown to be especially useful in generating monodisperse capsules for single cell entrapment (Brouzes *et al* 2009, Tan and Takeuchi 2007) as well as in the controlled release of cells (Steinhilber *et al* 2013). Additionally, the combination of microfluidics with electrospinning and electrospraying has been shown to be a promising platform for a range of operations in cell biology and tissue engineering (Jun *et al* 2014, Hong *et al* 2010).

Herein, we describe how the use of electrohydrodynamic and microfluidic technologies can be applied to create a droplet-based microfluidic platform integrated with electrospraying/electrospinning for the fabrication of hybrid membranes composed of a synthetic polymer and living cells. Specifically, we leverage controlled droplet formation at a flow-focusing geometry to encapsulate cells in gelatin microcapsules for the generation of protective transport vehicles. Subsequent electrospraying of these carriers coupled with electrospinning of polymeric fibers is then demonstrated. Finally, we assess the effect of these processing steps on the viability and differentiation of C2C12 myoblast cells and the resulting hybrid constructs via flow cytometry of propidium iodide stained cells and immunohistochemistry staining for myosin heavy chain positive myoblasts.

3.3 Materials and methods

3.3.1 Materials and reagents

All materials were purchased from Sigma Aldrich (Buchs, Switzerland), unless otherwise noted. All materials were used as received and without any further purification. Cell culture supplements and reagents were from Thermo Fisher Scientific (Waltham, USA) and used as received.

3.3.2 Cell culture

All *in vitro* experiments were performed using a murine skeletal myoblast cell line (C2C12, ATCC, Manassas, USA) at passage 13 to 16. Cells were expanded/cultivated in Dulbecco's modified Eagle Medium (DMEM) supplemented with 10% fetal calf serum (FCS) and 1% penicillin (5 mg ml⁻¹)/streptomycin (5 mg ml⁻¹)/neomycin (10 mg ml⁻¹) incubated in a humidified environment at 37°C and 5% CO₂. When 90% confluency was reached, cells were harvested and suspended in 5% w/v gelatin (dissolved at 37°C in DMEM) derived from porcine skin in a 50 ml falcon tube (Corning, New York, USA). The solution was vortexed (Vortex Genie 2, Scientific Industries, New York, USA) and kept in a water bath at 37°C before

further use. All experiments were performed at a total concentration of 3×10^6 cells ml^{-1} .

3.3.3 *Microfluidic device fabrication*

Microfluidic devices were fabricated by replica molding of PDMS (SYLGARD 184 Silicone Elastomer Kit, Dow Corning®, USA) against a structured silicon master mold, previously fabricated using standard photolithographic methods, and described in detail elsewhere (Abrishamkar *et al* 2016). Briefly, a mixture of PDMS elastomer and curing agent at a 10:0.9 w/w ratio was poured over the master (previously treated with chlorotrimethylsilane) and cured in an oven at 70°C for two hours. The cured PDMS molds were then cut into rectangles (45 mm \times 25 mm) using a razor blade, with 1 mm diameter inlet and outlet holes formed using biopsy punches. Finally, PDMS molds were bonded to glass coverslips (76 mm \times 26 mm, Thermo Scientific, Switzerland) after plasma activation of both the glass and PDMS surfaces under corona discharge (Electro-Technic Products, USA; power input of 30 W at 4.5 MHz). The microfluidic device contains three inlets (two for continuous phase and one for dispersed phase) and one outlet. Integrated microchannels had widths ranging between 40 and 200 μm and a height of 45 μm . A schematic of the microfluidic design is presented in Figure 3.2 a.

3.3.4 *Microcapsules formation and cell encapsulation*

A cell-laden gelatin solution (3×10^6 cells ml^{-1}) and a carrier fluid consisting of light mineral oil (density: 0.838 g ml^{-1} at 25 °C) with 0.25% Span-80 were used to form microcapsules. A secondary oil flow (containing light mineral oil with 3% Span-80) was used downstream of the droplet generation region to control the segmented flow and enhance the formation of monodisperse microcapsules. Fluids were delivered to the inlets of the microfluidic device using a syringe pump system (neMESYS module, Cetoni GmbH, Germany), with the flow rates set to 5 $\mu\text{l min}^{-1}$ and 30 $\mu\text{l min}^{-1}$ for the gelatin and oil flows, respectively (Griffin *et al* 2015). The gelatin and oil flows are segmented at the flow focusing droplet geometry to form

microcapsules. The microcapsules are then driven through an expansion zone where the channel width expands from 60 to 200 μm over the length of 50 μm , enhancing the formation of stable microcapsules. Downstream, a secondary flow of oil (with higher surfactant concentration) is introduced at a flow rate of 35 $\mu\text{l min}^{-1}$. The generated microcapsules then pass through a bifurcation region comprised of 16 parallel (200 μm wide) microchannels, which further stabilize the microcapsules, before exiting the microfluidic device. The microcapsules were collected directly from the outlet into a 1 ml Eppendorf tube (Eppendorf, Switzerland), submerged in an ice bath, and allowed to settle. The microfluidic encapsulation process via microfluidics was run for 1.5 h before the subsequent oil extraction step.

3.3.5 Capsule separation

Excess oil was removed with a pipette before the extraction. The remaining liquid was then put on an electrospun PVDFhfp membrane (Mw: 400 000 Da, prepared as described in section 2.10). This allowed removal of any excess oil, leaving the microcapsules on the surface. These were then flushed into a petri dish with 200 μl of cold (4°C) cell culture medium. The process was repeated until the oil phase was fully adsorbed into the PVDFhfp membrane, with extracted capsules being stored in DMEM in an Eppendorf tube on ice.

3.3.6 Capsule characterization

Images of the capsules after the different production steps were taken using an optical microscope (Primovert equipped with an AxioCam 105 color, Zeiss, Oberkochen, Germany). The diameters of the capsules were measured using Image J (Schneider *et al* 2012). The average diameter of a total of 200 capsules was taken from three individual experiments. To determine the number of cells per capsule, 10 images (1141 capsules in total) from three individual experiments were analyzed and cell numbers manually counted. Additionally, we adopted a protocol

described by Mazutis *et al.* to estimate the number of cells encapsulated per capsule assuming Poissonian distribution (Mazutis *et al* 2013), Eq. 1:

Eq. 1:
$$P_x = \frac{e^{-\lambda} \lambda^x}{x!}$$

where P represents the probability of x cells per capsule and λ represents the mean number of cells per capsule calculated with the experimental parameters (by use of the initial cell concentration and the average capsule volume, x = number of cells).

3.3.7 *Spraying of capsules and cell release*

Capsules were sprayed in cell culture medium. A conventional electro spraying setup described elsewhere (Guex *et al* 2012a), modified for a vertical setup was used for all experiments. Briefly, 200 μ l of capsules in DMEM, purified from the light mineral oil as described in section 2.4, were placed in a 1 ml syringe tipped with a blunt 21G stainless steel needle (B. Braun, Melsungen, Germany). A positive voltage of + 9 kV was applied to this needle. A petri dish containing 500 μ l of cell culture medium was placed at 5 cm distance to the needle to collect the capsules. The petri dish was placed on a metal plate where a negative bias of - 3 kV was applied to direct the capsules into the dish.

Cell release from gelatin capsules was monitored using a confocal laser scanning microscope (CLSM, LSM 780, Zeiss, Germany). For live imaging, cells were stained with the lipophilic tracer DiD (20 μ g ml⁻¹). Gelatin from porcine skin, labelled with Oregon Green® was added to the gelatin used for the encapsulation at a ratio 1:1000 v/v. To induce gelatin dissolution and the release of the cells the temperature was increased to 37°C.

3.3.8 Cell viability

A LIVE/DEAD® staining kit for mammalian cells (Thermo Fisher, Waltham, USA) was used to stain living cells green (calcein AM, 4 mM in anhydrous DMSO, 1:2000) and dead cells red (ethidium homodimer, 2 mM in DMSO/H₂O 1:4 v/v, 1:2000). The staining was performed in DMEM cell culture medium instead of PBS. Other than that the protocol of the manufacturer was followed. Images were taken after 24 hours under cell culture conditions (37°C, 5% CO₂). Cells were stained for 10 minutes in DMEM prior to imaging. During this period cells were released from the gelatin microgel due to gelatin dissolution. Cells cultivated on tissue culture polystyrene TCPS (Corning, New York, USA) were used as positive controls and cells treated with 0.2 % digitonin (Sigma Aldrich, Switzerland) in DMEM for 5 minutes at 37°C as negative controls. For quantitative analysis of viable cells, a propidium iodide stain was used and measured by flow cytometry (Gallios, Beckman Coulter, Germany) (n=3 individual experiments). Capsules were kept in an incubator in an Eppendorf tube until the gelatin was fully dissolved. Subsequently, cells were centrifuged and stained for 15 minutes on ice. Staining solutions were prepared using a binding buffer (1x Annexin V Binding Buffer, BD Biosciences, Switzerland) and propidium iodide at the ratio 9:1 v/v. Living cells and dead cells were used as positive and negative control respectively. For the negative control, cells were heated to 57°C for 20 minutes to induce necrosis. The final percentage of dead cells was recorded by gating for higher signals of propidium iodide.

3.3.9 Cell characterization

After oil removal and spraying of the capsules, cells were cultivated until confluency was reached (approximately 4-5 days). Myotube formation of C2C12 cells was induced by change to serum deprived medium (DMEM supplemented with 1% horse serum (Gibco, Invitrogen, USA) and 1% PSN). Medium was changed every other day for a differentiation period of 7 days. Cells were stained for immunohistochemistry with fluorescent dyes for the nuclei (1:1000, DAPI) and actin (1:40, Alexa Fluor® 488 or 647 Phalloidin, Thermo Fisher Scientific). Differentiated cells were stained for myosin heavy chain (1:400, Sigma Aldrich,

Switzerland) conjugated to a fluorescently labelled secondary antibody (1:400, Goat anti mouse IgG, Alexa Fluor® 488, Thermo Fisher Scientific). Prior to staining, samples were blocked (5 % goat serum, 1 % FCS in PBS). Staining was performed in PBS supplemented with 1.5 % w/v skimmed milk (Rapilait, Migros, Switzerland). All experiments were repeated at least 3 times.

To observe incorporation of cells into the electrospun membrane, scanning electron microscopy was performed with an acceleration voltage of 2 kV and 10 mA current flow (Hitachi S-4800 (Hitachi High-Technologies, US, Illinois, USA). Prior to imaging, samples were fixed in modified Karnovsky solution (4 % paraformaldehyde, 2.5 % glutaraldehyde) for 1 hour and dehydrated in an ascending ethanol series from 50 % to 100 % (30 – 60 minutes incubation for each concentration) and finally dried in hexamethyldisiloxane for 5 minutes.

3.3.10 Analysis of residual solvent in electrospun membranes

The presence of residual N,N-dimethylformamide (DMF) (boiling point 153°C) in the membranes was measured via gas chromatography-mass spectroscopy (Head space GC-MS). An Agilent G1530A gas chromatograph coupled with an HP 5973 mass spectrometer was used for all experiments. Thereby, the sample was heated starting from a temperature of 50°C (held for 1 minute), which was ramped up to 250°C at a rate of 15°C min⁻¹, where the temperature was held for 1 min. Eluents were collected on a solid phase microextraction fiber (SPME Fiber 65 µm PDMS/DVB fused silica 24 Ga for use with manual holder, Sigma Aldrich, Switzerland) and separations performed on a HP-5MS GC column (Agilent technologies, USA) (30 minutes at room temperature).

3.3.11 Electrospinning/capsule spraying

The experiments were not performed under sterile conditions. However the device as well as the instruments were thoroughly cleaned with 70 % ethanol beforehand. Parameters for cell spraying were as described previously. For electrospinning, PVDFhfp was dissolved in DMF at a concentration of 35 % w/v. A planar stainless

steel plate collector was placed at a distance of 20 cm from a syringe filled with the polymer solution. The polymer solution was ejected at a flow rate of 20 $\mu\text{l min}^{-1}$ using a syringe pump (World Precision Instruments, Sarasota, USA, model: Aladin 1000). To characterize the intrinsic pore size of the polymeric membrane, capillary flow porometry was used (The POROLUX™ 1000, POROMETER nv, Belgium). The cell-laden membrane was fabricated in a layer-by-layer approach. After 60 minutes of electrospinning, capsules were sprayed on top of the membrane at a flow rate of 50 $\mu\text{l min}^{-1}$. In order to spray the required amount of cells in a volume of 200 μl , the spraying duration was 4 minutes. Subsequently a layer of PVDFhfp was spun for 5 minutes on top of the capsules. To remove residual solvent, the biograft was then washed with cold PBS (4°C) for 60 minutes in a cell culture dish, with the PBS being changed every 10 minutes. After washing the membrane was cultivated under culture conditions in cell culture medium. To validate the reproducibility of this approach, the experiment was repeated three times.

3.3.12 Statistical analysis

Pearson correlation coefficient (r^2) was calculated between the frequency distributions of predicted values from Eq. 1 and experimental data ($n=3$) of encapsulated cells per capsule. An unpaired two-tailed Student's t-test was used to determine significance. Differences with p -value < 0.05 were considered statistically significant. Statistical analyses were performed in Graphpad Prism 7.

3.4 Results

3.4.1 Cell encapsulation

The microfluidic device used herein is designed to generate stable gelatin-in-oil microcapsules, with diameters between 40 and 140 μm , at a rate of 150-200 per second (Griffin *et al* 2015). Cell-laden gelatin and oil flows were injected at 5 $\mu\text{l min}^{-1}$ and 30 $\mu\text{l min}^{-1}$, respectively, leading to formation of microcapsules with an average diameter of 112 $\mu\text{m} \pm 30 \mu\text{m}$ (Figure 3.2). To overcome potential backpressure issues, which occur in long microchannels and can cause failure of

the chip, flow rates were optimized as previously described (Mazutis *et al* 2009). Microcapsules passed through a short expansion zone where they were stabilized due to shear. Downstream a second flow of continuous phase was introduced from both sides at the flow rate of $35 \mu\text{l min}^{-1}$. This auxiliary flow of continuous phase guides the flow of generated microcapsules to the centerline of the channel, improving the monodispersity of the microcapsules and suppresses the jetting along the channel.

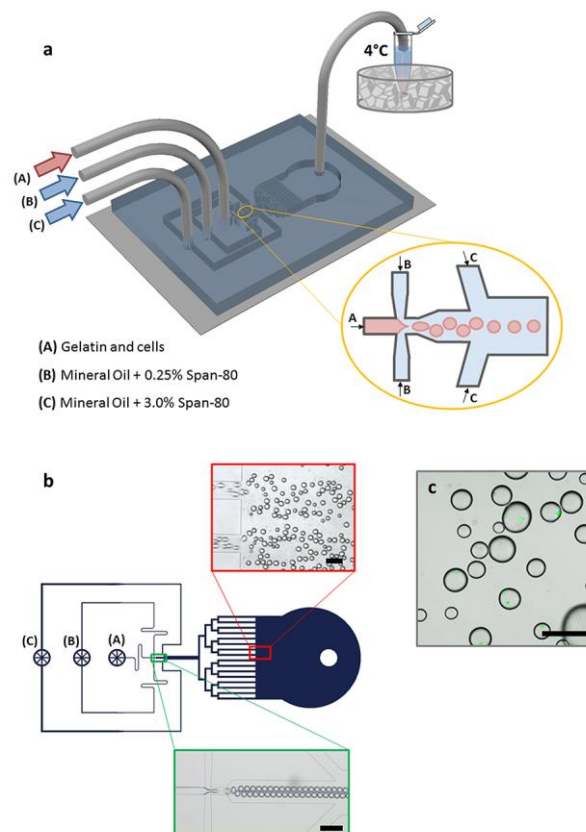


Figure 3.2: Microfluidic encapsulation process

(a) Schematic illustration of the microfluidic device and the encapsulation process including the collection of the generated microcapsules in an ice bath. The inlay schematically illustrates the droplet generation region. (b) The design of the microfluidic device, with the optical micrographs of its different sections during the process. (c) Microcapsules collected in oil with cells stained with a live dye showing the result of the encapsulation process. Scale bars: $200 \mu\text{m}$.

3.4.2 Capsule purification and processing

The different process steps for capsule purification are shown in Figure 3.3. After the purification the capsules were sprayed into a cell culture dish filled with cell culture medium. Significantly, and as shown in Figure 3.4 a and b, electrospraying had no influence on the morphology of the formed capsules. All capsules remained intact without any major deformation or swelling, with an average diameter of $112 \mu\text{m} \pm 30 \mu\text{m}$ ($114 \mu\text{m} \pm 31$ before spraying, $110 \mu\text{m} \pm 29 \mu\text{m}$ after spraying). Within the measured capsules ($n=1141$), a total number of 1729 cells were successfully encapsulated with 66 % of the capsules being laden with cells (Figure 3.4 c). A good agreement ($r^2=0.984$, $p=3.3 \cdot 10^{-11}$) was found between estimated values (from Eq. 1) and experimental data (Figure 3.4 c).

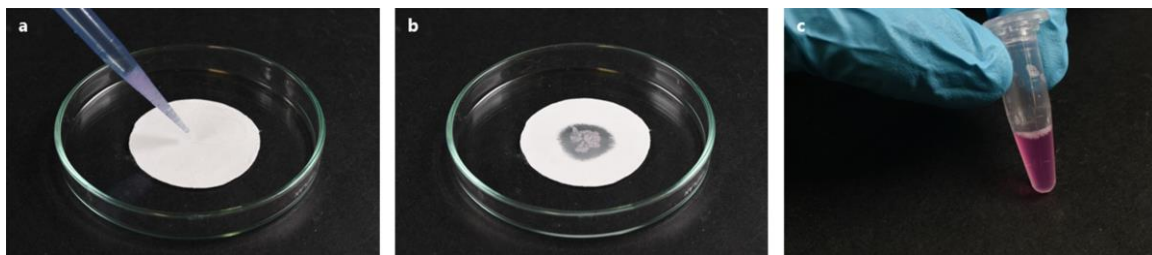


Figure 3.3: Capsule purification

Purification of the microgel capsules from the oil phase. (a) The oil containing the capsules is added onto the hydrophobic membrane. (b) After 1-2 minutes the oil was completely absorbed by the membrane. (c) The capsules were flushed with $200 \mu\text{l}$ of DMEM and stored in an Eppendorf vial on ice.

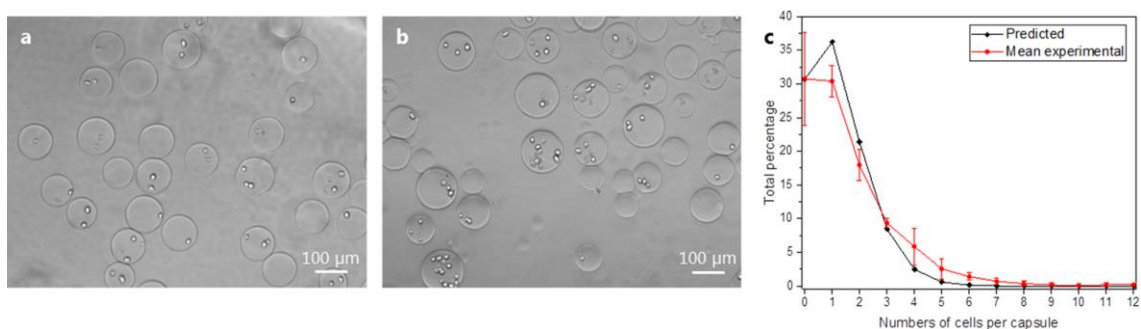


Figure 3.4: Capsule characterization

(a) Collected capsules after the oil extraction on a PVDFhfp membrane and resuspension in cell culture medium. (b) The shape and size of capsules are maintained after spraying capsules from a 21G needle into a petri dish filled with cold cell culture medium, with an average capsule size of $112 \mu\text{m} \pm 30 \mu\text{m}$. (c) Comparison between experimental data and prediction model (based on Poissonian distribution) for the encapsulation process. Data represents mean \pm SD of $n=3$ independent repetitions in the experimental group and predicted values from Eq. 1.

3.4.3 Cell characterization

LIVE/DEAD staining results, both after capsule extraction and after spraying, are presented in Figure 3.5 (a, d and g). Fluorescence images confirm that cell viability was not significantly impaired after each processing step when compared to the positive control. This is further supported by flow cytometry data (Figure 3.5 c, f and i) with 84 %, 82 % and 81 % ($n=3$) of the cells being viable in the control group, after the oil removal and after the capsules have been sprayed by the electrostatic field, respectively (measured by counting PI positive cells). The scatterplots shown in Figure 3.5 b, e and h, allow identification of viable and dead populations, as dead cells reveal lower forward scatter signals and higher side scatter signals. Interestingly, discrimination was less obvious for the control group.

After cultivating the cells in differentiation medium for 7 days, the impact of the process steps on differentiation potential (into multinucleated myotubes) was assessed.

Figure 3.6 a depicts differentiated cells after oil removal. By staining for actin and cell nuclei it can be seen that single cells merged and formed elongated myotubes, as expected for C2C12 myoblasts. No differences were observed compared to both experimental groups (Figure 3.6 b and c). Additionally, all groups investigated were positive for the specific myosin heavy chain marker (Figure 3.6 d-f).

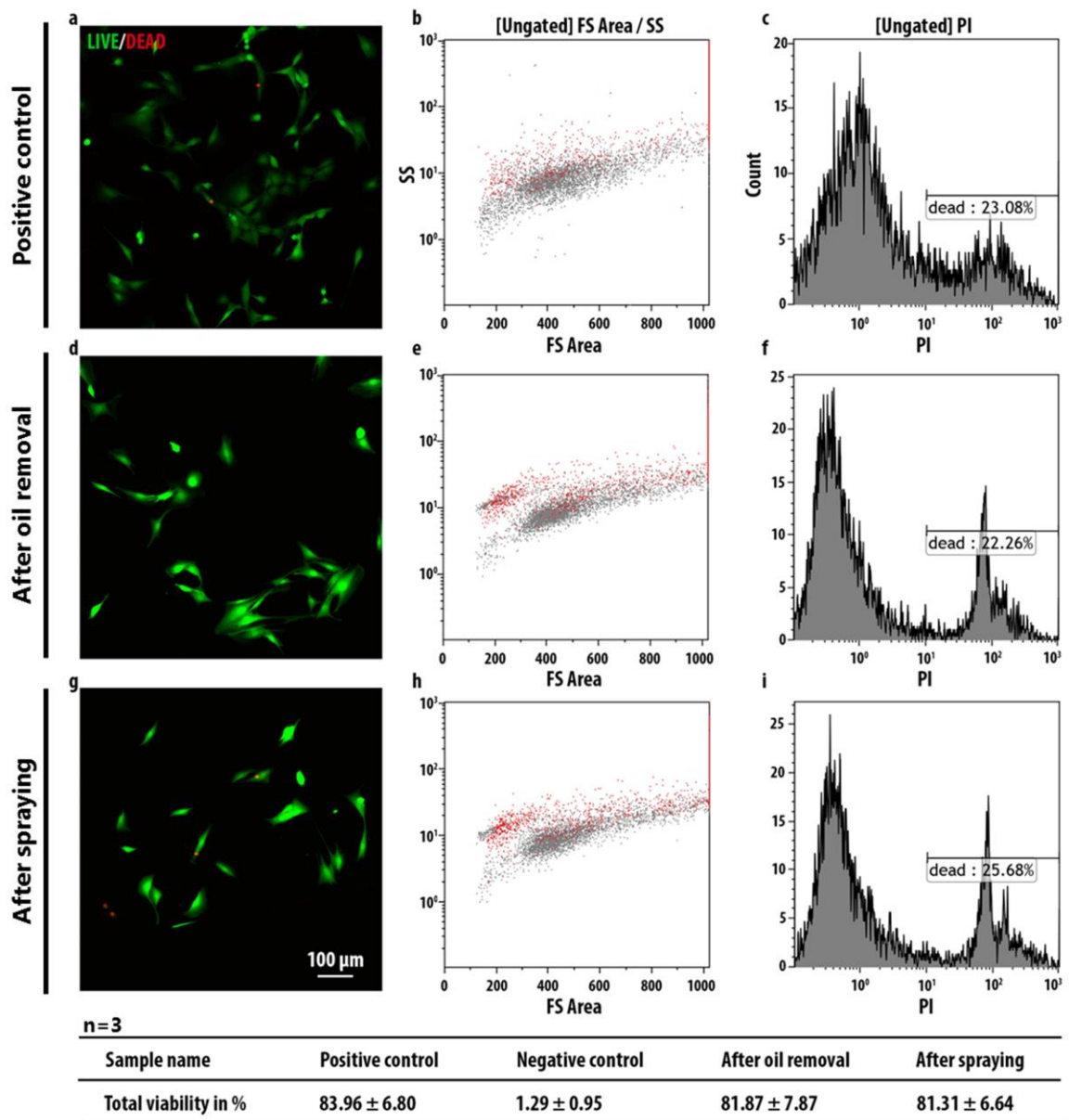


Figure 3.5: Assessment of cell viability

Viability of cells after different process steps. Cells were released from the gelatin capsules and attached to TCPS after a 24-hours incubation period at 37°C. Viability was measured via LIVE/DEAD staining as well as flow cytometry. Associated results for the different process steps can be seen: (d-f) after oil removal and resuspension in DMEM and (g-i) after spraying the capsules in DMEM with 9 kV into cell culture medium into a petri dish. (a-c) Untreated cells served as control.

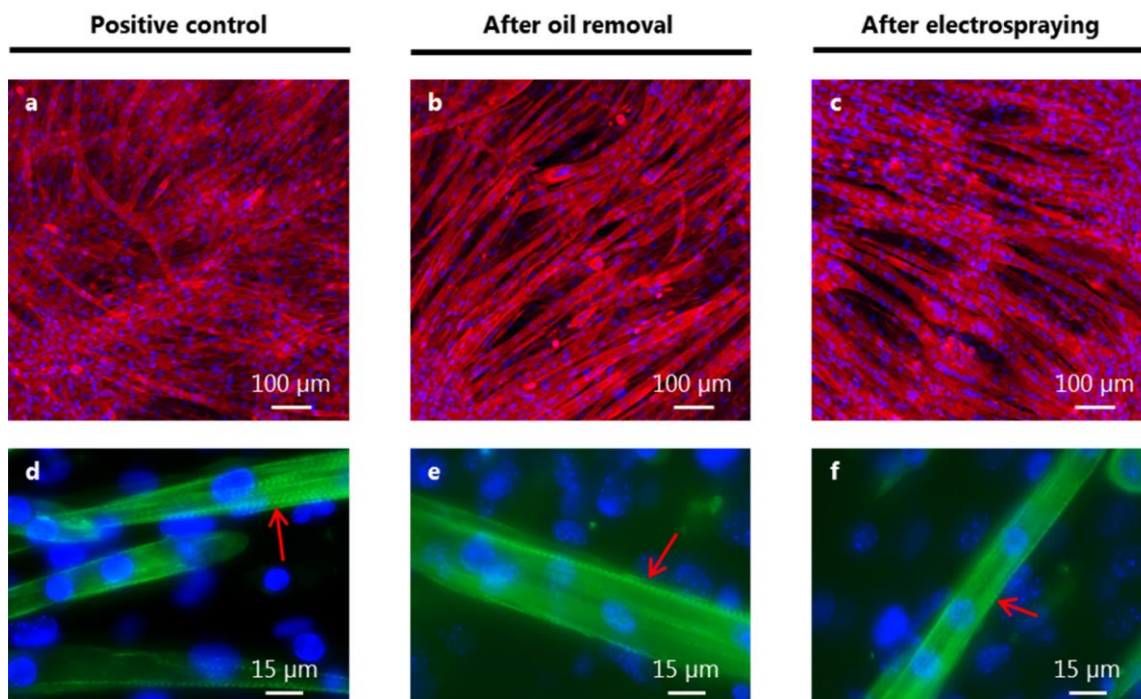


Figure 3.6: Cell differentiation

Confocal laser scanning image of differentiated C2C12 cells (b) after encapsulation and removal of oil (c) as well as after the spraying process. (a) Untreated cells were used as control. Single cells merge to form typical bundle-like structured tubes. (d-f) All myotubes expressed myosin heavy chain as indicated by the red arrows.

3.4.4 Cell release from microcapsules

Cell release from capsules is shown in Figure 3.7. Fluorescence images, taken after 1, 15 and 30 minutes, illustrate the dissolution of gelatin capsules over time at 37°C with signal from the Oregon green labelled gelatin diminishing after 15 minutes due to water uptake. Complete dissolution of the gelatin occurs after approximately 30 minutes (Figure 3.7 c). The first signs of cell attachment to the dish can be observed by the formation of cellular protrusions that appear after capsules are fully dissolved, with the low intensity background signal resulting from dissolved fluorophore in the solution. Subsequent adhesion was also observed during LIVE/DEAD imaging experiments, with Calcein AM positive cells

remaining attached and spread over the substrate 24 hours after release (Figure 3.5).

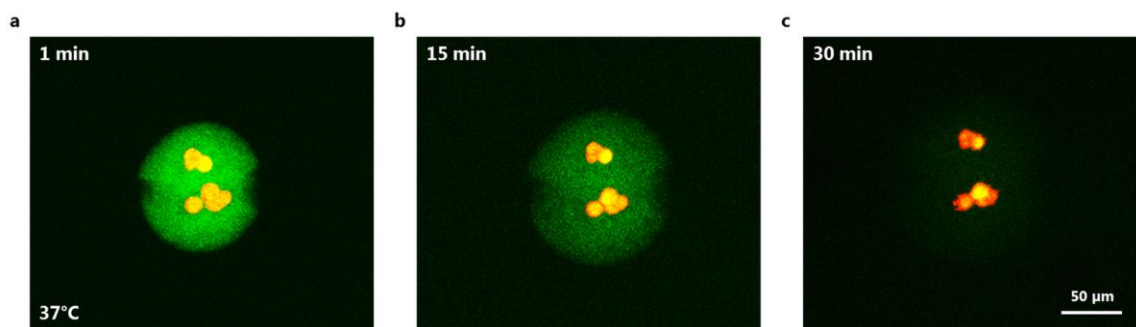


Figure 3.7: Cell release from capsule

Release of C2C12 cells from gelatin capsules monitored by time lapse imaging. After 30 minutes at 37°C cells are released and start attaching onto the substrate. After 30 minutes, the first signs of cellular protrusions are visible, indicating the start of attachment to the underlying TCP substrate.

3.4.5 Hybrid biograft fabrication

The protective effect of the encapsulation was shown by the LIVE/DEAD staining of C2C12 cells after the combined process without encapsulation (Figure 3.8 b) as well as with encapsulation (Figure 3.8 c). Combined electrospinning of PVDF/hfp and electrospraying of non-encapsulated cells was unsuccessful, since all cells were necrotic (Figure 3.8 b). Head-space GC-MS measurements indicated high amounts of “residual” DMF directly after electrospinning (Figure 3.8 a). While residues on the membranes were also measured after 2 hours of storage in air, samples stored in PBS showed only a very small peak deriving from DMF.

Cell survival after the encapsulation process was significantly increased as demonstrated by the higher number of calcein AM positively stained cells (Figure 3.8 c). Cell proliferation within the biograft was reported by higher cell numbers on day 7 as seen in Figure 3.8 d. Living as well as dead cells were counted based on these images (n=5 per group) revealing values of 0 % (a), 77.75 % ± 13.64 % (b)

and $87.08\% \pm 3.95\%$, respectively. We never experienced issues concerning contamination when the constructs were transferred into cell culture.

The presence of spread cells underneath the fiber layer was confirmed by SEM imaging of the construct produced by the described layer-by-layer process (Figure 3.9 a and b). This observation could be made in all the performed experiments ($n=3$). Only small areas without cells were observed. Additionally, immunohistochemistry staining for actin and cell nuclei confirmed the cellular attachment to the scaffold (Figure 3.9 c).

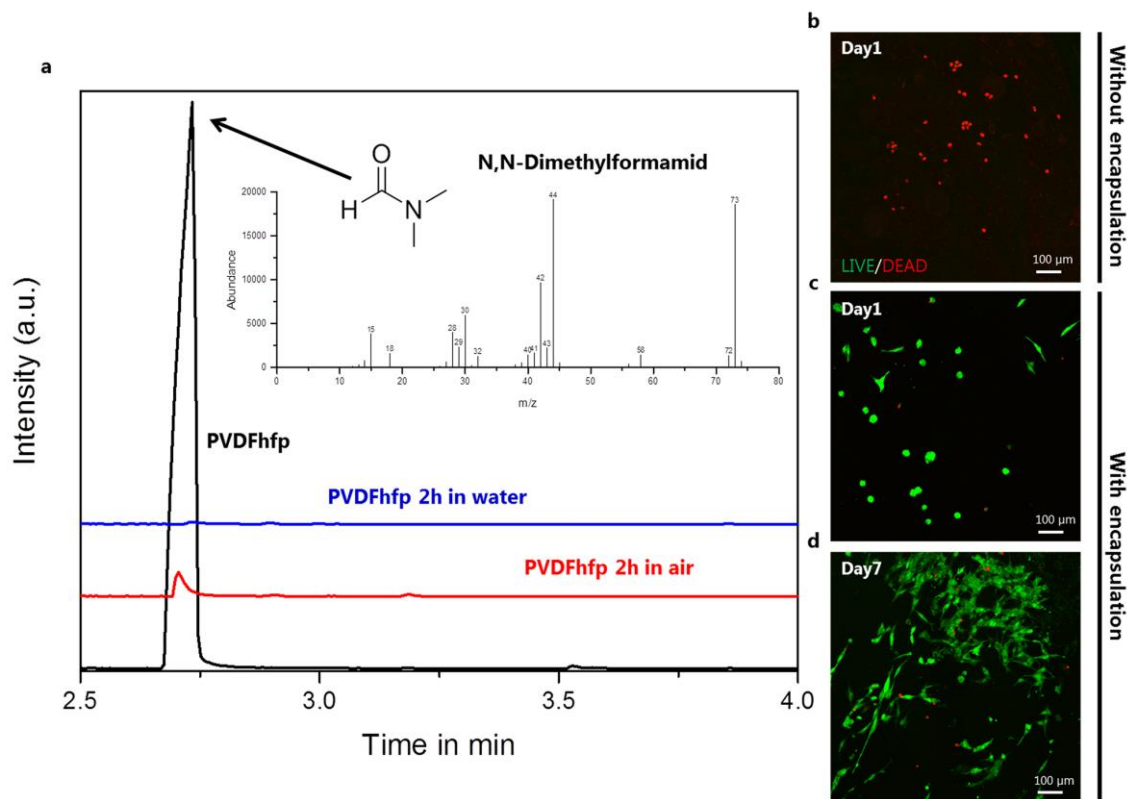


Figure 3.8: Measurement of residual solvents

(a) Mass spectra of electrospun membranes measured by GC-MS. The peak for residual DMF is depicted for the differently treated samples. LIVE/DEAD staining of C2C12 cells (b) sprayed into the membrane without encapsulation, (c) with encapsulation (d) as well as with encapsulation after 7 days in culture ($n=3$).

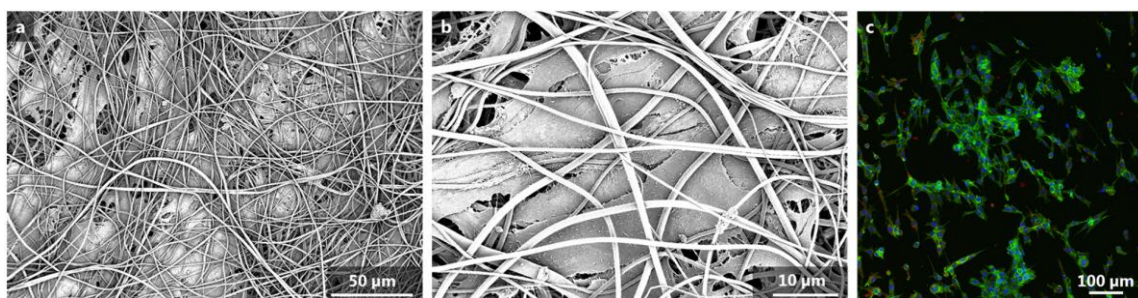


Figure 3.9: Cell incorporation into the scaffold

(a and b) SEM micrographs of cells spread underneath a layer of electrospun fibers indicating the successful incorporation of C2C12 cells into the PVDFhfp scaffold. Images were taken after 7 days in culture. (c) The corresponding confocal laser scanning images confirm the presence of spread cells. Cells were stained for actin (green) and nuclei (blue).

3.5 Discussion

Production of scaffolds for *in situ* integration of cells to create functional 3D tissues is hampered by the usually required application of cytotoxic solvents or cross-linking agents (Telemeco *et al* 2005, Liu *et al* 2008). Since fiber formation by electrospinning is highly dependent on the solvent system used (according to the used polymer), non-cytotoxicity cannot always be achieved as many synthetic polymers do not dissolve in e.g. aqueous solutions. For the reported polymer PVDFhfp, DMF is required to ensure spinning of homogenous fiber morphologies, and cytotoxicity of residual DMF within the fibers was observed after electrospinning (Figure 3.8 b). It is likely that the amount of remaining solvent in as-spun PVDFhfp is considerable due to a strong affinity of the solvent towards the polymer. DMF carrying a carbonyl group is able to form Lewis acid-base pairs with polymers like poly(vinylidene fluoride) (Ye *et al* 2012), leading to semi-stable bonds with slow evaporation of the solvent. Similar interactions of polymers with solvents, e.g. hexafluoroisopropanol (HFIP) with polycaprolactone, were described by Nam *et al.* revealing solvent desorption over extended periods of time (Nam *et al* 2008). This affinity depends on the polymer-solvent combination as e.g. Stankus *et al.* did not observe any adverse effects with respect to cell survival when

poly(ester urethane)urea was used with HFIP (Stankus *et al* 2006). Furthermore, DMF has a relatively low vapor pressure implying slow diffusion kinetics compared to solvents with a high volatility like chloroform, THF or HFIP. In general it can be stated that solvents with a low vapor pressure remain longer in the fibers (Kidoaki *et al* 2005). While washing the membranes for 2 hours with water removed most of the remaining solvent (Figure 3.8 a), such an incubation step is not compatible with the approach of *in situ* integration of cells in the scaffold. Therefore, microfluidic cell encapsulation was utilized for the temporary protection of cells to maintain cell viability during the fabrication of hybrid biografts.

From the various techniques that have been described for the fabrication of microencapsulated cells (Young *et al* 2012, Tan and Takeuchi 2007), a microfluidic platform was selected due to the ease with which highly monodisperse microcapsules can be produced and because of the potential to control capsule size, throughput and encapsulation efficiency in a direct manner. The described microfluidic system allowed the preparation of microcapsules with an average diameter of $112 \mu\text{m} \pm 30 \mu\text{m}$. With the capsule size being a limiting factor for a successful electro-spraying process, this was well within the intended size range of $< 500 \mu\text{m}$, being a limiting factor for a continuous electro-spraying process.

Establishing the optimal parameters for cell encapsulation, experimental parameters like flow rate, cell concentration as well as gelatin concentration were optimized, to achieve a stable process with low numbers of empty capsules. It was found that initial cell concentrations not only affected the efficiency of the process, but also the overall viscosity of the gelatin phase, which in turn influenced the performance of the microfluidic approach. Higher cell concentrations lead to faster gelation of the gelatin within the microfluidic channels and blockage of the tubing within a few minutes (data not shown). However, Clausell-Tormos *et al.* observed that as soon as the initial cell concentration drops below a certain number, the probability of encapsulating more than one cell decreases to values of $p \leq 7 \%$ (Clausell-Tormos *et al* 2008). Therefore, cell densities were chosen to achieve single cell encapsulation resulting in 66 % of the capsules carrying at least one cell. The efficiency of the cell encapsulation process was also modelled assuming Poissonian distribution and the predicted occupancies were in good agreement with experimental observations (Figure 3.4 c). Indeed, Mazutis *et al.* (Mazutis *et al* 2013)

previously utilized this model to obtain capsules with the majority of droplets containing one cell. The results in the present study highlight the versatility of the microfluidic cell encapsulation process and the potential to adapt the process to meet individual requirements.

After the microfluidic encapsulation a dispersion of cell-laden capsules in oil is obtained. Different methods such as centrifugation or dissolution of oil have been proposed to purify the microfluidic capsules (Mazutis *et al* 2013, Tan and Takeuchi 2007). However, either the dissolution of oil in hexadecane had a negative influence on the stability of the capsules, or the forces applied to the capsules during centrifugation initiated fusing of the gelatin micro-spheres (data not shown). A purification protocol using hydrophobic filtration paper has previously been used to remove the oil phase (Lee *et al* 2014). Adaption of this approach, by using electrospun nanofibrous PVDFhfp membranes (known for their high porosity, oleophilic properties and the potential to split oil from water for purification purposes (Patel *et al* 2013)) allowed uptake of the oil within 2 minutes, so that capsules could be easily flushed from the membrane surface to the cell culture medium. Importantly, capsules were observed to maintain their shape and monodispersity throughout all the experimental steps including the subsequent electro spraying process where shear forces are applied, indicating sufficient mechanical stability of the capsules. One major advantage of gelatin was the possibility of triggering the cell release from the capsules in cell culture without the use of any additional treatments.

It has been previously reported that electro spraying of murine hematopoietic stem cells has no negative effect on either viability or phenotype (Bartolovic *et al* 2010). No changes of cell viability were also observed for C2C12 cells within our study (Figure 3.10). In the current study, it was shown that both the cell encapsulation as well as the following electro spraying process do not negatively influence the behavior of myoblasts in terms of viability and myotube differentiation. Indeed a total of 81 ± 6.6 % of the cells were viable after the encapsulation, spraying and the release steps. In the control group 84 ± 6.8 % of the cells were alive (Figure 3.5). Additionally, cells were found to proliferate between day 1 and day 7 as observed by increasing cell numbers positively stained with calcein AM (Figure 3.8 c and d). As indicated by immunohistochemical analysis, characteristic

differentiation of C2C12 cells into myotubes had occurred after culture in serum deprived media, with expression of myosin heavy chain being evident after 7 days (Figure 3.6). Such phenotypical expression is in good agreement with results reported e.g. by Ricotti *et al.* with respect to the C2C12 behavior in terms of proliferation and differentiation cultured on nanofiber membranes surfaces (Ricotti *et al* 2012).

Furthermore, successful *in situ* integration of cells to create a hybrid biograft using a layer-by-layer approach based on electrospinning and electrospraying could be demonstrated (Figure 3.9). SEM analysis showed the incorporation of cells in-between the spun layers without migration to the membrane surface SEM analysis showed the incorporation of cells in-between the spun layers without migration to the membrane surface due to the small mean pore size of 2.22 μm . This is an important finding since it demonstrates the possibility to spatially control the distribution of a cell population within a membrane. The electrospun layer seems to provide a barrier, mimicking natural barriers (such as the basement membrane found in blood vessel walls), where spatial separation of different cell types is required. This is especially relevant for vascular applications, since smooth muscle cell proliferation and migration in the vascular system can cause pathological conditions such as intimal hyperplasia (Louis and Zahradka 2010).

To further benefit from this potent combination of electrospinning and cell electrospraying, the experimental setup can be further developed to allow a simultaneous collection of fibers and encapsulated cells on a rotating drum. Overall, the presented approach suggests that complex functional tissues with spatially separated cells can be designed and fabricated.

3.6 Conclusion

The described method, which exploits microfluidic cell encapsulation and electro-spraying/-spinning, provides a novel platform for controllable manipulation of cells and fabrication of hybrid biografts composed of viable cells and fibrous synthetic polymer scaffolds. Based on the protective effect of the microcapsules, cells are shielded from cytotoxic solvents utilized during electrospinning. Spraying cell-laden capsules does not affect viability or phenotype characteristics of the processed cells. Furthermore, the presented results provide a better understanding of solvent behavior during electrospinning. Finally, the presented approach has the potential to be adapted for different cell types and scaffold materials, and thus is likely to be an useful tool for targeted tissue reconstruction in applications such as vascular substitutes or other hierarchically structured 3D tissues.

3.7 Acknowledgements

The authors thank Dr. Mario Novkovic (Institute of Immunobiology, Kantonsspital St. Gallen) for the helpful assistance with the statistics. We are grateful to Elisabeth Michel (GC-MS measurements) and Dr. Nils Bohmer (FACS analysis) for their skillful help. This work is part of the Zurich Heart project of “Hochschulmedizin Zurich”

(<http://www.hochschulmedizin.uzh.ch/en/projekte/zurichheart.html>).

3.8 Appendix

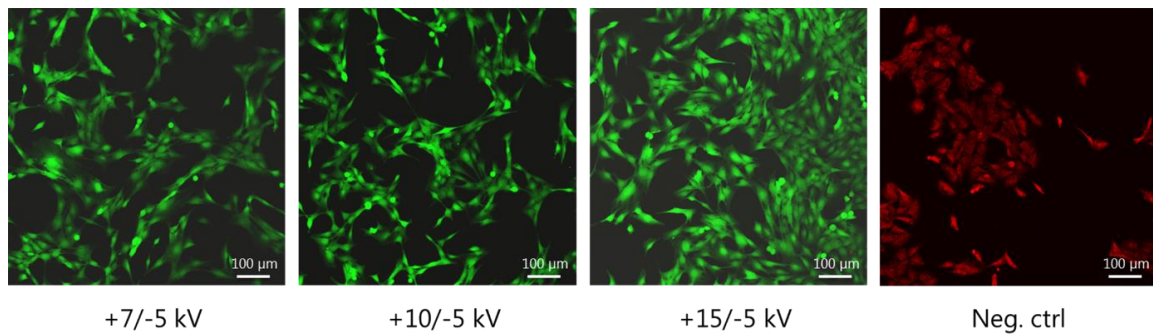


Figure 3.10: Cell viability after electrospaying

Control experiment to demonstrate the potential of utilizing cell electrospaying. C2C12 cells were electrospayed into petri dishes with different positive voltages. Subsequent LIVE/DEAD staining revealed no differences in cell viability between the tested groups. The negative control was treated with digitonin to induce cell death.

4 Blend fiber production

A.G. Guex, L. Weidenbacher, K. Maniura-Weber, R.M. Rossi, G. Fortunato

Note: This chapter has been published as: Hierarchical self-assembly of PUR/PVDFhfp blends into highly hydrophobic electrospun fibres with reduced protein adsorption profiles, *Macromolecular Materials and Engineering* 302, 1700081 (2017). Reprinted with permission from John Wiley and Sons.

L. Weidenbacher performed electrospinning experiments as well as the protein adsorption study and assisted A.G. Guex with the manuscript writing process. A.G. Guex and G. Fortunato designed the study, characterized the fibers and wrote the manuscript with contribution of all authors.

4.1 Abstract

Electrospinning of blend systems, combining two or more polymers, has gained increasing interest for the fabrication of fibres that combine properties of the individual polymers. Here, a versatile method to produce hydrophobic fibres composed of poly(vinylidene fluoride-co-hexafluoropropylene) (PVDFhfp) and polyurethane (PUR) is presented. PVDFhfp containing fibres are expected to reduce protein adsorption. In a one-step process, blend solutions are electrospun into homogeneous non-woven membranes with fibre diameters in the range of 0.6 ± 0.2 to 1.4 ± 0.7 μm . Surface fluorine concentrations measured by XPS show an asymptotic dependency in function of the PVDFhfp to PUR ratio, reaching values close to pure PVDFhfp at a weight per weight ratio of 10% PVDFhfp to 90% PUR. This fluorine enrichment on the surface suggests a gradient structure along the fibre cross-section. At increased surface fluorine concentration, the contact angle changes from $121 \pm 3^\circ$ (PUR) to $141 \pm 4^\circ$ (PUR/PVDFhfp). Furthermore, these highly hydrophobic fibres present significantly reduced fibrinogen or albumin adsorption compared to PUR membranes.

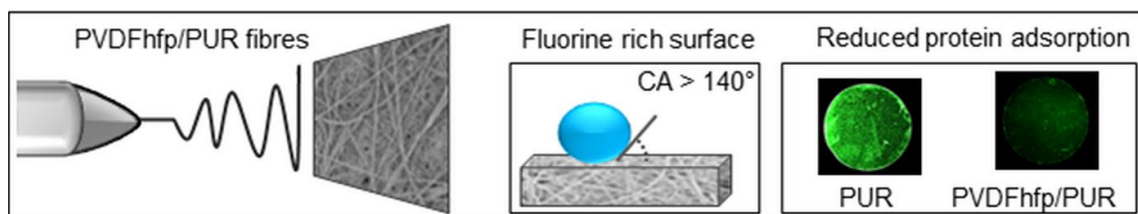


Figure 4.1: Graphical abstract

4.2 Introduction

Electrospun nano- to micron-scale fibres and functional membranes have been increasingly studied in a variety of research fields, such as filter technology (Ahn *et al* 2006), sensor development (Aussawasathien *et al* 2005), fuel cell industry (Mollá and Compañ 2011), tissue engineering, and regenerative medicine (Liu *et al* 2012). Surface functionalities of polymeric systems are thereby of particular interest since they control chemical and catalytic activity, wettability, cytocompatibility, and adhesive or antifouling properties. When used as implants

for medical purposes, cell material interactions are governed by chemical and physical surface properties that trigger initial protein adsorption, and regulate further downstream signals for cell adhesion, cell proliferation, and/or differentiation (Castner and Ratner 2002). Typically, improved biointerfaces and surface functionalisation are addressed by post-treatment such as plasma coating processes (Guex *et al* 2012b, 2014, Savoji *et al* 2014), layer by layer assembly (Mei *et al* 2014, Croisier *et al* 2014), photochemical surface modifications (Versace *et al* 2013), wet chemical treatment (Zhou *et al* 2013), or gas phase induced coating processes (Zimmermann *et al* 2008). Recently, fluorine-functionalised surfaces have gained increasing interest in the field of biomedical applications due to their outstanding properties of hydrophobicity and oleophilicity, chemical resistance, low friction coefficient and mechanical stability. Furthermore, coatings with fluorinated surface modifying macromolecules (SMMs) (Jahangir *et al* 2002, Massa *et al* 2005) or fluorinated diamond-like carbon films (F-DLC) (Saito *et al* 2005, Hasebe *et al* 2007) were reported to present promising materials for implants with anti-thrombogenic character, indicated by significantly reduced fibrinogen adsorption and platelet activation. However, SMMs and F-DLC post-functionalisation requires additional modification steps which hampers rapid material manufacturing. Fluorinated polymers, such as poly(vinylidene fluoride) (PVDF) or poly(vinylidene fluoride-co-hexafluoropropylene) (PVDFhfp) were therefore increasingly studied as bulk materials to introduce fluorinated groups, and used for biomedical applications, for instance in the form of electrospun membranes (Guo *et al* 2012, Liu *et al* 2010, Weber *et al* 2010). In vitro, PVDFhfp membranes presented low protein adsorption profiles with subsequently reduced platelet adhesion (Ahmed *et al* 2014), and have been utilised as polymer coatings in drug eluting stents in clinical trials for occlusive artery diseases (Ding *et al* 2009). In contrast to promising results in these studies, perfluorinated polymers place a considerable burden on environmental health and hence efforts are made to reduce their application (Beachley *et al* 2013).

In an effort to reduce the amount of incorporated fluorinated polymer, we have developed blend systems of PVDFhfp and polyurethane (PUR) with a low PVDFhfp to PUR ratio. In a one-step electrostatic spinning process, we aimed for the formation of fibres with PVDFhfp enriched surfaces (Wei *et al* 2006, Fortunato *et*

al 2014). Fibre morphology and surface chemistry was characterised, and concomitant adsorption of fibrinogen and albumin was assessed fluorometrically.

4.3 Materials and methods

4.3.1 Spinning solutions and fibre production

Poly(vinylidene fluoride-co-hexafluoropropylene) (PVDFhfp, Mw: 400,000 Da), N,N-dimethylformamide (DMF), and tetraethylammonium bromide (TEAB) were of analytical grade and obtained from Sigma-Aldrich, Switzerland, without any further purification. Polyurethane (PUR, Elastollan C95A55, Mw: 85,790 Da) was obtained from BASF (Germany).

All polymer solutions were produced at a total polymer concentration of 14.5 % w/v and dissolved in DMF. Blends of PUR and PVDFhfp at variable relative concentrations were produced by direct addition of both polymers to DMF. Relative PVDFhfp to PUR concentrations (wt%) were 0%, 1%, 2%, 10% or 20%. To increase the electrical conductivity, TEAB (0.1 M in DMF, 0.5 $\mu\text{L}\cdot\text{g}^{-1}$ polymer solution) was added. Solutions were placed on a vertical shaker overnight prior to spinning. Electrospinning of pure PVDFhfp at the same polymer concentration (14.5 % w/v in DMF) resulted in bead formation and membranes were hence excluded from further investigations. Instead, 2-dimensional films of, drop casted from a 14.5% w/v PVDFhfp solution were used for surface chemical analysis (X-ray photospectroscopy).

Electrical conductivity of polymer solutions was measured using a Metrohm 660 conductometer (Metrohm, Herisau, Switzerland). The conductometer was calibrated using 0.001, 0.01 or 0.02 M potassium chloride (KCl) solution. KCl (Sigma Aldrich, Switzerland, puriss. P.a.) was dried at 110°C for 12 h before preparing the standards.

A rheometer (Paar Physica MCR 300, Graz, Austria) equipped with a plate – cone system was applied in controlled shear rate mode to assess shear viscosities in function of shear rate. Flow curves with shear rates varying from 0.01 – 500 s^{-1} were recorded at 20°C.

Fibres were produced by electrospinning as previously developed in our group (Guex *et al* 2012b, Fortunato *et al* 2014). In brief, an in-house built electrospinning device of two high voltage generators (aip Wild AG, Oberglatt, Switzerland), an infusion pump (KD scientific, Massachusetts, USA) and a planar stainless steel collector were placed inside a Faraday cage in a chemical hood. Fibres were processed at a flow rate of $10 \mu\text{Lmin}^{-1}$ through a needle of 0.8 mm diameter (Unimed S.A., Lausanne, Switzerland). A positive voltage of 9 kV was applied to the needle, and the collector was at a negative bias of -2 kV. The needle to collector distance was fixed at 20 cm. The fibres were assembled on a tin foil coated stainless-steel plate.

4.3.2 Fibre characterisation

4.3.2.1 Scanning electron microscopy (SEM)

Fibre morphology was characterised based on SEM images. Fibres were gold sputter coated prior to acquisition (8 nm, EM ACE600, Leica Microsystems, Heerbrugg, Switzerland). Images were acquired at an accelerating voltage of 2 kV and a current flow of $10 \mu\text{A}$ on a Hitachi S-4800 (Hitachi High-Technologies, Etobicoke, Canada). Fibre diameters were calculated based on 100 individual measurements (Image J freeware, <http://rsbweb.nih.gov/ij/>).

4.3.2.2 Scanning transmission electron microscopy (STEM)

Scanning transmission electron microscopy (STEM) was performed at 30 kV accelerating voltage and 10 mA current flow. Fibres were spun directly onto 200 mesh carbon coated copper grids (Plano, Wetzlar, Germany). Fibre staining was then performed using 30 mg RuCl_3 powder dissolved in 20 mL sodium hypochlorite for 60 min in a closed vessel. The formed RuO_4 is known to selectively stain oxygen containing polymers (Trent 1984).

4.3.2.3 X-ray photospectroscopy (XPS)

XPS analysis (survey spectra) was accomplished on a PHI LS 5600 instrument (Minnesota, USA) with a standard MgK α X-ray source. Energy resolution of the spectrometer was set to 0.8 eV/step at a pass-energy of 187.85 eV. The X-ray beam was operated at a current of 25 mA and an acceleration voltage of 13 kV. Elemental compositions were determined using atomic sensitivity factors of 0.314 (C1s), 0.733 (O1s), 0.499 (N1s), and 1.000 (F). High resolution spectra of the C1s chemical environment were acquired on a PHI 5000 VersaProbe II instrument (Minnesota, USA) with a monochromatic AlK α X-ray source. Energy resolution of the spectrometer was set to 0.125 eV/step and 29.35 eV. Carbon 1s at 284.5 eV was used as a calibration reference to correct for charge effects. Data analysis was performed by use of CasaXP software (Casa Software Ltd, United Kingdom). C1s transition was fitted using C-C and C-H at 284.5 eV, C-O and C-N at 285.9 eV, C=O and C-F at 288.7 eV, C-F₂ at 290.3 eV, and C-F₃ at 293.2 eV.

4.3.2.4 Static contact angle

Water-in-air contact angles were assessed on a drop shape analyser DSA24 (Krüss GmbH, Hamburg, Germany). Membranes were fixed on a metal holder in order to measure contact angles on a freely suspended membrane, with n=5 individual measurements per membrane. Contact angles were automatically calculated by the equipment software after an equilibration time of 1 min.

4.3.3 Protein adsorption

Protein adsorption on selected electrospun membranes (100% PUR or 20% PVDFhfp/80% PUR) was quantified fluorometrically. Membranes were fixed in 24-well culture plates, according to previously published protocols (Guex *et al* 2013). In brief, membrane discs of 10 mm in diameter were cut with biopsy punches, placed on cured poly(dimethylsiloxane) (PDMS, Sylgard 184, Sutter Kunststoffe AG, Switzerland) and fixed with insect pins (Sphynx, Ento Meier, Munich, Germany). Membranes were incubated in phosphate buffered saline (PBS, Sigma

Aldrich) at 37°C overnight, prior to protein incubation. Solutions containing either 10 $\mu\text{g}\cdot\text{mL}^{-1}$ of fluorescently labelled human serum albumin (HSA, Alexa Fluor 647 – Thermo Fisher Scientific, Rheinach, Switzerland) or fibrinogen (Fg, Alexa Fluor 488 – Thermo Fisher Scientific, Rheinach, Switzerland) were prepared for the study of protein adsorption from single protein solutions. Competitive adsorption of both proteins to the membranes was studied by use of a mixture of 10 $\mu\text{g}\cdot\text{mL}^{-1}$ HSA and 10 $\mu\text{g}\cdot\text{mL}^{-1}$ of Fg. Protein solutions were incubated for 30 min, 6 h, or 16 h, respectively, at 37°C. After three subsequent washing steps in PBS, patches were mounted on glass slides with cover slips. Fluorescence intensity was measured using a microarray scanner (Tecan Group Limited, Männedorf, Switzerland) at $\lambda_{\text{ex}} = 650 \text{ nm}$ and $\lambda_{\text{em}} = 665 \text{ nm}$ or (490/525 nm) for HSA or Fg, respectively. Measurements were performed in three individual experiments, with three replicates each. PBS incubated membranes served as control.

Protein concentration was not quantified but compared among conditions and expressed as fluorescence intensity (a.u.). Results are presented as mean \pm SD. Groups were compared by a Kruskal-Wallis test, followed by pairwise post-hoc analysis with a Mann-Whitney-U test. Results were accepted as significantly different for $P < 0.05$.

4.4 Results and discussion

4.4.1 Solution characteristics and fibre morphology

All investigated PUR / PVDFhfp blend systems yielded transparent solutions, indicative of complete solubility of both polymers at the chosen concentrations. Electrical conductivities and viscosities of spinning solutions are known to have a considerable influence on resulting morphology of electrospun fibres (Thompson *et al* 2007) and depend both on the solution concentration and the nature of the used polymers and solvents. An increased electrical conductivity of 5.1 $\mu\text{S}\cdot\text{cm}^{-1}$ of the spinning solutions was observed at a PVDFhfp concentration of 20% compared to pure PUR solutions (3.0 $\mu\text{S}\cdot\text{cm}^{-1}$), while at lower PVDFhfp concentration of 1, 2 or 10 %, no change in electrical conductivity was measured (Table 4.1). Solution rheological measurement revealed non-Newtonian flow behaviour for all spinning

solutions with shear thinning at shear rates above 10 s⁻¹. An increased viscosity of 5.9 Pa·s was found at 20 % w/w PVDFhfp, compared to 4.1 Pa·s for pure PUR solutions (measured at a shear rate of 0.1 s⁻¹; Table 4.1). At shear rates of 500 s⁻¹ solution viscosities were decreased for all PVDFhfp to PUR ratios, reaching 2.7 Pa·s for a 20% PVDFhfp solution, and 2.4 Pa·s for a pure PUR solution. Increased viscosities at higher PVDFhfp concentrations can be explained by the increased molecular weight of PVDFhfp compared to PUR (400,000 Da vs. 85,790 Da, respectively), and stronger intermolecular interactions induced by hydrogen bridge formation of PVDFhfp (Costa *et al* 2010). Interestingly, the viscosity of a 2 wt% PVDFhfp solution drops at low shear rates, which hypothetically arises from different polymer chain entanglements or arrangement at this particular ratio. At high shear rates, which is more representative for the situation at the Taylor cone, viscosities are comparable for the here reported spinning solutions. A shear thinning at these higher rates is attributed to a rearrangement and alignment of the polymer chains upon stirring. Viscosity flow curves are displayed in supplementary data, Figure 4.6.

Polymer solutions were processed by electrospinning into free-standing fibrous non-woven membranes (Figure 4.2 A). SEM image analysis revealed fibre diameters in the micrometer to sub-micrometer range for all PVDFhfp/PUR ratios (Table 4.1). Higher PVDFhfp to PUR ratios induced a decrease in fibre diameters towards a more homogenous diameter distribution in the sub-micrometer range: Pure PUR fibres displayed diameters of $1.39 \pm 0.7 \mu\text{m}$, whereas fibres processed from solutions of 20 wt% PVDFhfp displayed significantly smaller fibre diameters of $0.61 \pm 0.2 \mu\text{m}$ (n=100 for all fibres). The formation of electrospun fibres at smaller diameters at 20 wt% PVDFhfp can be attributed to an increased electrical conductivity of PVDFhfp-rich polymer solutions and an increased drawing process during fibre formation. These membrane morphologies and fibre diameters are comparable to previous studies, where processing of fluorinated polymers such as PVDF or PVDFhfp and the generation of non-woven membranes in the sub-micrometer range was reported (Costa *et al* 2010, Lalia *et al* 2013). STEM image acquisition after selective ruthenium staining provided evidence for the formation of gradient fibres, with a discontinuous polymer separation along the fiber axis. A dark, oxygen rich core indicates an increased accumulation of PUR in the core,

with a PVDFhfp-enriched surface layer. Representative images are displayed in Figure 4.2 B.

Table 4.1: Characteristics of spinning solutions and electrospun fibres

PVDFhfp to PUR ratio (wt%)	conductivity ($\mu\text{S}\cdot\text{cm}^{-1}$)	Viscosity at low shear rate (0.1 s ⁻¹) (Pa.s)	Viscosity at high shear rate (500 s ⁻¹) (Pa.s)	Fibre diameter (μm)	Contact angle (°)
0	3.0	4.1	2.4	1.39 \pm 0.7	121.5 \pm 3
1	2.5	5.1	2.5	1.87 \pm 0.7	142 \pm 2
2	2.6	4.4	2.4	0.77 \pm 0.3	135 \pm 2
10	3.6	5.5	2.7	0.68 \pm 0.2	141 \pm 4
20	5.1	5.9	2.7	0.61 \pm 0.2	141 \pm 3

4.4.2 Surface properties of electrospun membranes

Surface wettability is highly influenced by a material's surface energy, which depends both on chemical as well as topographical properties. Fluorinated polymers are particularly interesting for the generation of hydrophobic or superhydrophobic surfaces. Furthermore, appropriate polymer surface texturing allows for the generation of superhydrophobic properties, for instance by use of nano-scaled fibres or particles (Zhou *et al* 2013, Ge *et al* 2013, Liao *et al* 2014). Wettability of as spun membranes was assessed based on static contact angle measurement. PVDFhfp containing membranes displayed reduced wettability, indicated by contact angles higher than 140° compared to a contact angle of 121 \pm 3 ° for pure PUR membranes (Table 4.1). PUR/PVDFhfp membranes are therefore highly hydrophobic, yet do not fall into the class of superhydrophobic substrates, which are characterised by static water contact angles of >150°. Chen *et al.* demonstrated that superhydrophobic membranes could only be generated by additional silane functionalisation of PVDF polymers (Chen and Kim 2009). Interestingly however, comparison of our results to a study by Laila *et al.* in which electrospun membranes of PVDFhfp presented contact angles of 135 to 140° (Laila *et al* 2013) indicates that similar hydrophobicity could be achieved at low addition

of 1 or 2% PVDFhfp. Water in air contact angles are, however, not only determined by surface chemical properties, but are also highly influenced by surface morphology, in particular at the sub-micron or nano scale (Whyman *et al* 2008). Surface elemental composition of electrospun fibres was analysed by XPS (Figure 4.3, Figure 4.4, Table 4.2). Survey spectra are presented in supplementary data, Figure 4.7. Theoretical fluorine concentration (Figure 4.4) was calculated based on two assumptions: i) a homogenous mixture of PVDFhfp and PUR, and ii) a fluorine concentration of 53.4 at% for pure PVDFhfp (measured on drop-casted pure PVDFhfp). A 1 wt% PVDFhfp concentration resulted in a surface fluorine content of 12 at%, increasing to 19 at% for 2 wt% PVDFhfp, and reaching a value close to pure PVDFhfp for a content of 20 wt% (50.6 at%). Deconvolution of high resolution C1s spectra underpinned these findings and demonstrated a high fluorine content, indicated by additional peaks at higher binding energy representative of the C-F₂ (290.3 eV) and C-F₃ (293.2 eV) chemical environment. To this end, the considerably higher contact angle at low fluorine concentrations of 1 or 2 wt%, in comparison to PUR membranes, could be attributed to changes in surface chemical composition by the formation of gradient fibres.

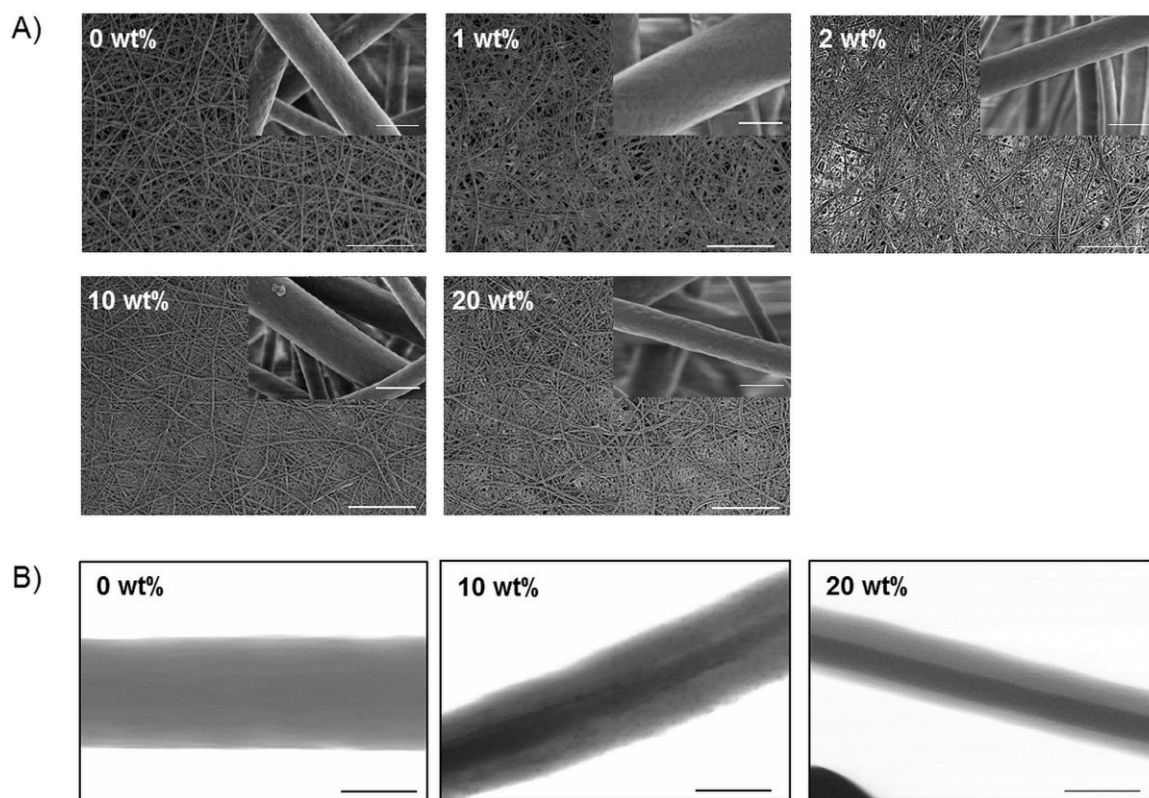


Figure 4.2: Fiber characterization

A) SEM images of electrospun fibres, produced from solutions of different PVDFhfp to PUR ratios (0-20 wt%). At higher PVDFhfp concentrations, fibres displayed smaller diameters with lower standard deviations, indicating more homogenous fibre distribution. Inserts present images of higher magnification, demonstrating the smooth surface of PUR/PVDFhfp fibres. Scale bars: low magnification 50 μm , higher magnification 1 μm . B) STEM images of PUR/PVDFhfp fibres, indicating fibre formation with an oxygen rich (PUR) core. Scale bar: 250 nm.

Table 4.2: Chemical surface composition

Electrospun PUR/PVDFhfp fibres, assessed by XPS on as spun membranes and membranes stored in air for six weeks. C-F₂ and C-F₃ were determined based on deconvolution of C1s chemical environment.

surface elemental composition in at%												
PVDFhfp to PUR ratio (wt%)	directly after spinning					six weeks post spinning					fitting C1s	
	C	O	N	F	F/C	C	O	N	F	F/C	C-F ₂	C-F ₃
0	76.4	20.9	2.7	0		76.4	21.3	2.4	0		0	0
1	67.7	18.4	2.0	12.0	0.18	69.4	19.4	2.9	8.4	0.12	2.9	0*
2	64	14.3	2.1	19.6	0.31	63.3	15.3	1.7	19.7	0.31	5.4	0*
10	48.1	2.6	0.5	48.8	1.01	47.9	2.7	0	49.4	1.03	11.0	3.8
20	47.0	2.3	0.1	50.6	1.08	49.5	3.5	0	47.0	0.95	27	5.8

* below detection limit

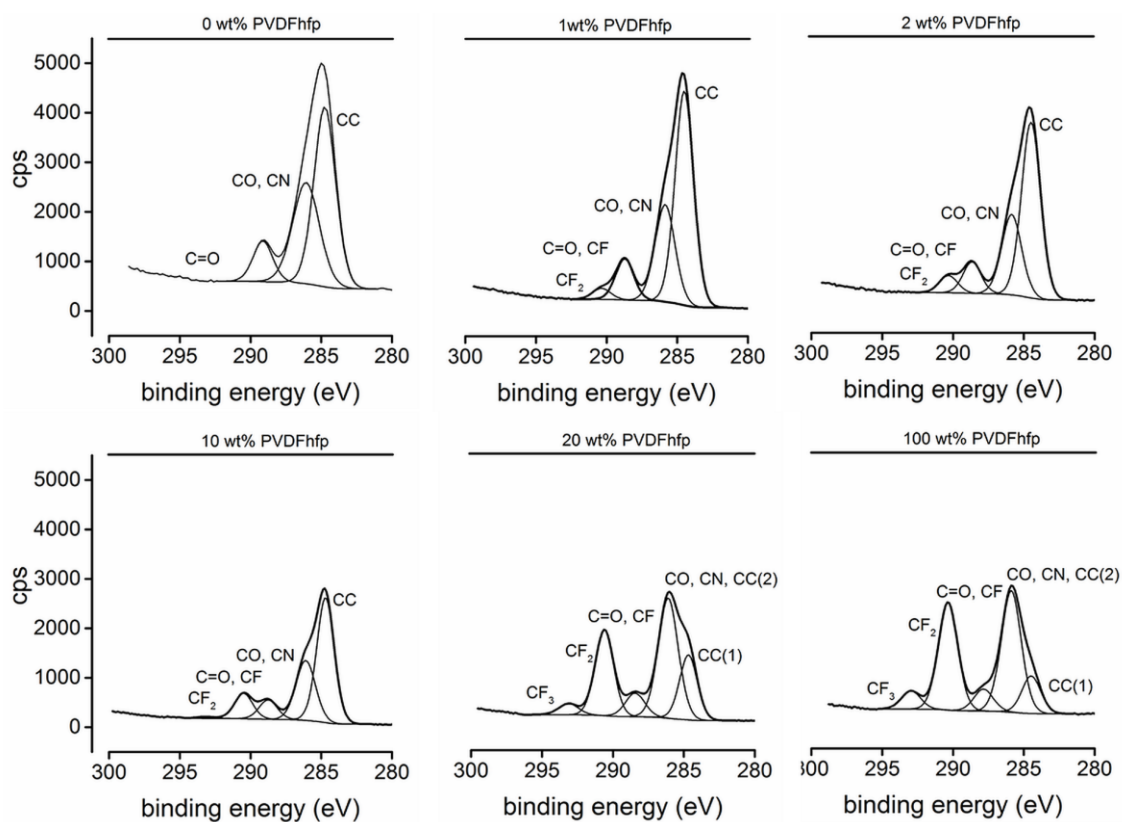


Figure 4.3: XPS analysis

XPS high resolution spectra of C 1s chemical environment. C1s transition was fitted using C-C and C-H at 284.5 eV, C-O and C-N at 285.9 eV, C=O and C-F at 288.7 eV, C-F₂ at 290.3 eV and C-F₃ at 293.2 eV.

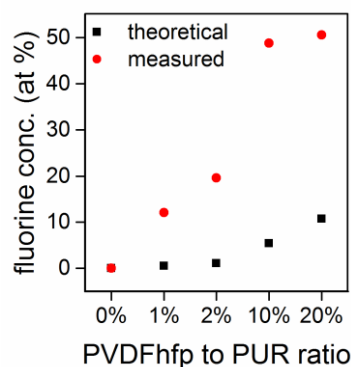


Figure 4.4: Surface fluorine concentrations

XPS measured surface fluorine concentration and theoretical values calculated for a fully homogenous polymer distribution within the fiber. Surface enrichment of PVDFhfp resulted in enhanced fluorine content compared to theoretical values of PUR/PVDFhfp blends. A concentration of 10 or 20 wt% PVDFhfp resulted in surface fluorine contents close to pure PVDFhfp.

Phase separation and resulting core-sheath fibre formation of polymer blends has been previously reported and explained by different theories: i) (Re)crystallisation has been identified as a possible factor influencing the surface fluorine content in fluorinated co-polymers (Cheung *et al* 2006, Wu *et al* 2009). Copolymers of poly(bisphenol A octane) (BA-C8) and Poly(4,4'-(hexfluoroisopropylidene)diphenol octane) (6FBA) were shown to form films of reduced fluorine content over time, as opposed to generally observed surface enriched fluorine contents in such systems. In these studies, the authors postulated an enthalpy driven process of crystallisation that moves and traps fluorinated segments into the bulk material. Experimental studies of PCL and poly(vinyl chloride) (PVC) blends presented a ratio dependent surface aggregation or crystallisation of PVC at a certain threshold (Clark *et al* 1989, 1991). At lower PCL to PVC ratios, bulk and surface chemical composition were identical, whereas at PCL concentrations higher than 40%, the surface was PCL enriched, switching to a PVC enriched surface at PCL concentrations higher than 90%.

ii) According to another hypothesis, polymer miscibility and interactions, and consequential surface chemistry were based on the formation of hydrogen bonds in a copolymer of poly(styrene-co-p-hexafluorohydroxyisopropanol- α -methyl styrene)/poly(4-vinyl pyridine) (PS(OH)PVPy) (Liu *et al* 2001). Surface enrichment of the low surface energy component can be reduced by stronger interactions of the polymers, and hydrogen bonding was increased by adjusting the hydroxyl content in the PS(OH) co-polymer. This resulted in comparable surface and bulk chemical composition.

With respect to the first theory, we could show by XPS measurements of our fibres directly after spinning and six weeks post spinning, that the same fluorine concentrations and shape of transitions were found over time, indicative for a stable fibre morphology and chemistry (Table 4.2). C-F₃ unites of PVDFhfp on the other hand are highly prone for hydrogen bond acceptance, whereas the urethane groups of PUR are potential hydrogen donors and also form hydrogen bonds upon crystallisation. Solutions of low PVDFhfp to PUR ratios were mixed into homogenous spinning solutions, whereas in other studies in our group, we observed that at ratios of 1:1, the two polymers were not miscible and a two phase solution was formed (results not presented). These observations, in line with XPS data on the very high surface fluorine content, indicate a low interaction between PVDFhfp and PUR and limit the hypothesis of hydrogen bridges between the two polymers. Our observations do not mirror previous results where surface and bulk chemistry were comparable upon polymer interaction via hydrogen bonds (Liu *et al* 2001).

Most likely, the formation of the presented fibres here, with a PVDFhfp enriched surface, is driven by surface exposure of the polymer with lower surface energy (Wei *et al* 2006). Fluorine containing segments of co-polymers are generally known to accumulate at the surface of polymer films, inducing fluorine enriched outer shells and bulk sections of low fluorine content in polymer films (Lei *et al* 2003, Ming *et al* 2002, Affrossman and Stamm 1998, Thomas *et al* 1998). This phenomenon could be translated to electrospun fibres of fluorinated co-polymers (Chen and Kim 2009, Hardman *et al* 2011, Valtola *et al* 2009, Deitzel *et al* 2002). Phase separation and surface aggregation of polymer segments has been demonstrated for blends of poly(vinyl alcohol) and poly(N-vinyl-2-pyrrolidone)

(PVAL/PVP) (Li *et al* 1998), poly(caprolactone) and poly(vinyl caprolactam) (PCL/PVCL) (Clark *et al* 1989, 1991), poly(styrene-co-p-hexafluorohydroxyisopropanol- α -methyl styrene)/poly (4-vinyl pyridine) (PS(OH)/PVPy) (Liu *et al* 2001), and poly(vinylidene fluoride-co-hexafluoro propylene)/ poly(ethylene oxide) (PVDFhfp/PEO) (Fortunato *et al* 2014). To our knowledge, it has not been demonstrated as a means of hydrophobisation of electrospun membranes.

4.4.3 Protein adsorption on PUR or PUR/PVDFhfp membranes

Upon biomaterial implantation, surfaces are covered by proteins from the blood plasma within seconds. Fibrinogen (Fg) adsorption in particular has been identified as a major trigger for further downstream platelet activation and thrombus formation (Zucker and Vroman 1969). Interestingly, Fg adsorption is influenced by the surface chemical and topographical characteristics of biointerfaces (such as hydrophilicity or roughness), and has further been reported to compete with the adsorption of other proteins in a time and concentration dependent manner (Vroman and Adams 1969, Nonckreman *et al* 2010, Roach *et al* 2005). Fluorinated substrates on the other hand were shown to reduce Fg adsorption and thereby suppress platelet activation (Massa *et al* 2005). We therefore investigated Fg adsorption with or without human serum albumin (HSA) at three different time points. Results of single or competitive protein adsorption are presented in Figure 4.5. Two main aspects were evaluated: i) surface protein accumulation over time on the respective membranes and ii) comparison of relative protein adsorption on PUR compared to PUR/PVDFhfp (at a 20 wt% ratio of PVDFhfp to PUR) membranes.

On both PUR and PUR/PVDFhfp membranes, the amount of Fg at the fibre surface increased over time. For HSA, however, protein adsorption levels remained in the same range, indicating a saturation of protein adsorption after 30 min. These discrepancies of protein adsorption kinetics between Fg and HSA can be explained by the conformational differences of these two proteins, the latter one being a highly globular, small (66.5 kDa) protein, whereas fibrinogen is a larger (340 kDa), rod shaped glycoprotein. Rod-shaped proteins may undergo a two stage adsorption

process, initially exposing their long axis parallel to the surface, yet self-assembling into a tightly packed arrangement with the longitudinal axis perpendicular to the surface (Roach *et al* 2005). Proteins thereby increase protein-protein interactions and reduce protein-substrate interaction. On hydrophilic substrates, dynamic protein adsorption-desorption has been observed, allowing for orientational rearrangements over time (Falde *et al* 2016). However, proteins tend to bind stronger and more permanently on hydrophobic substrates, impairing this rearrangement and tight packing, thereby reducing the total amount of bound proteins. We suggest that this rearrangement induced the altered protein adsorption pattern after long-term incubation (6 or 16 h) when comparing hydrophilic to hydrophobic substrates. On PUR/PVDFhfp membranes, the relative amount of Fg is significantly reduced after 6 h or 16 h incubation, compared to PUR membranes. PUR/PVDFhfp membranes therefore appear superior to PUR membranes with respect to protein adsorption prevention.

In contrast to rod-shaped proteins, HSA is a symmetric, globular protein, where no anisotropic rearrangement can be observed. We therefore hypothesise that the protein adsorption profile of HSA on either membrane can be attributed to a rapid coverage of the surface, followed by a steady-state situation without tight packing or increased protein adsorption over time. The relative amount of HSA, however, is significantly lower on PUR/PVDFhfp membranes compared to PUR membranes after 30 min or 6 h incubation. On PUR/PVDFhfp membranes, an overall reduced protein adsorption profile with a quicker saturation of protein concentration was shown. These observations are promising with respect to certain *in vivo* application, where reduced protein adsorption is desired. To better mirror such an *in vivo* situation, where implants come in contact with a cocktail of various proteins, competitive protein adsorption was studied by incubating membranes with a mixture of Fg and HSA. On both membranes, Fg adsorption, in competition with HSA, undergoes a similar adsorption profile as observed for single protein incubation with an increasing amount of Fg after 6 or 16 h compared to 30 min incubation time. In this situation of competitive protein adsorption, significant differences in Fg adsorption between PUR and PUR/PVDFhfp membranes were only observed after prolonged incubation for 16 h. Again, we hypothesise that the dynamic adsorption-desorption state, including orientational Fg re-arrangements on PUR membranes, is responsible for this observed increase over time. Fg binds

with stronger affinity to the membrane, replacing the smaller, more mobile HSA after an initial incubation period. Observations of a reduced amount of HSA on PUR membranes after 6 h further support this hypothesis.

In summary, an overall reduction in protein adsorption was observed on PUR/PVDFhfp membranes. This suggests an early saturation in total protein concentration, explained by reduced adsorption-desorption dynamics that restrict any further rearrangements of the rod-like Fg.

These results provide evidence that the PUR/PVDFhfp membranes presented here are interesting candidates for use in biomedical applications, where reduced protein adsorption is required. These observations mirror previously published results where fluorinated SMMs induced reduced protein adsorption (Jahangir *et al* 2002, Massa *et al* 2005). However, as discussed in a recent review by Falde *et al.* (Falde *et al* 2016) *in vivo* studies of protein adsorption on superhydrophobic membranes still reveal conflicting results with respect to protein adsorption and further research is needed to elucidate the underlying mechanism of surface fluorination or hydrophobisation, protein adsorption, and subsequent platelet activation or cell adhesion.

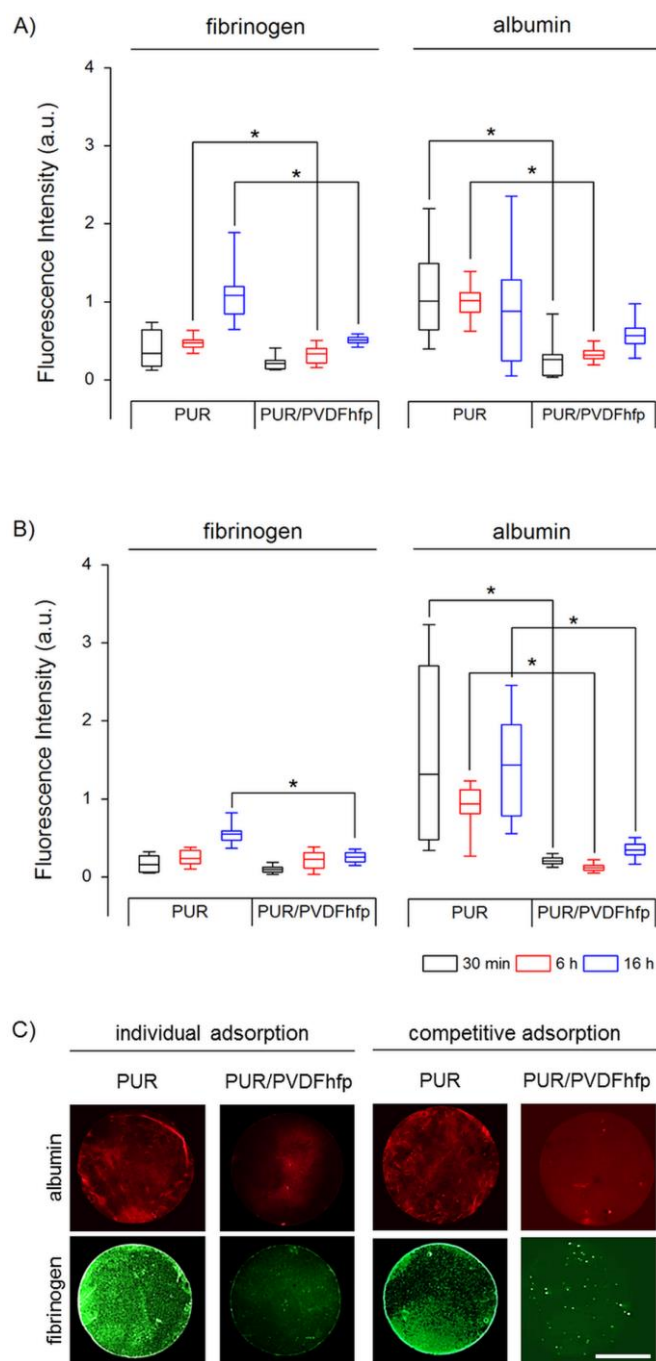


Figure 4.5: Protein adsorption

Single protein and B) competitive protein adsorption on PUR or PUR/PVDFhfp (20 wt% PVDFhfp) membranes over time. Adsorption of fluorescently labelled fibrinogen or human serum albumin was measured at different time points, after 30 min, 6 h or 16 h incubation. * $p < 0.05$, $n = 3$ with 3 replicates each. C) Representative images of protein incubated membranes; scale bar: 5 mm.

4.5 Conclusion

Electrospun non-woven membranes of PUR/PVDFhfp blends were developed and analysed for surface chemical composition. We demonstrated the formation of gradient fibres with fluorine enriched surfaces. This change in surface chemistry resulted in highly hydrophobic properties (contact angle of $141 \pm 3^\circ$) at low PVDFhfp to PUR ratios of 10 or 20 wt%. PVDFhfp. The current approach presents a versatile method for surface modification of electrospun fibres, addressing the increasing need for up-scalable yet simple processes. Further, our blend systems allows for a reduction in the use of fluorinated polymers without loss of surface functionalities. Membranes, spun from PUR/PVDFhfp blends were shown to reduce albumin and fibrinogen adsorption.

4.6 Acknowledgements

The authors are very grateful to Dr. Eike Müller and Dr. Markus Rottmar, Biointerfaces, Empa, St. Gallen, Switzerland for technical assistance with protein adsorption experiments and fruitful scientific discussion of the results. We would like to thank Dr. Philip Howes, ETH Zürich, Switzerland, for English proof reading of the manuscript.

4.7 Appendix

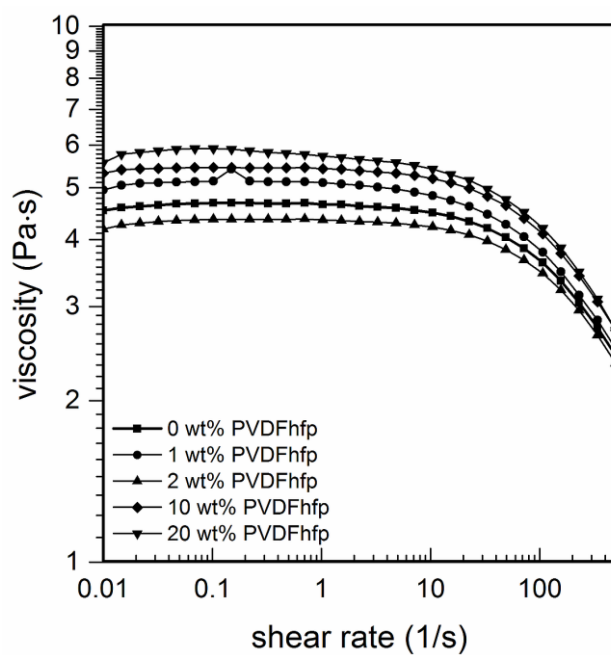


Figure 4.6: Viscosity measurements

Solution viscosities were assessed in function of shear rate. Flow curves with shear rates varying from 0.01 - 500 s⁻¹ were recorded at 20°C.

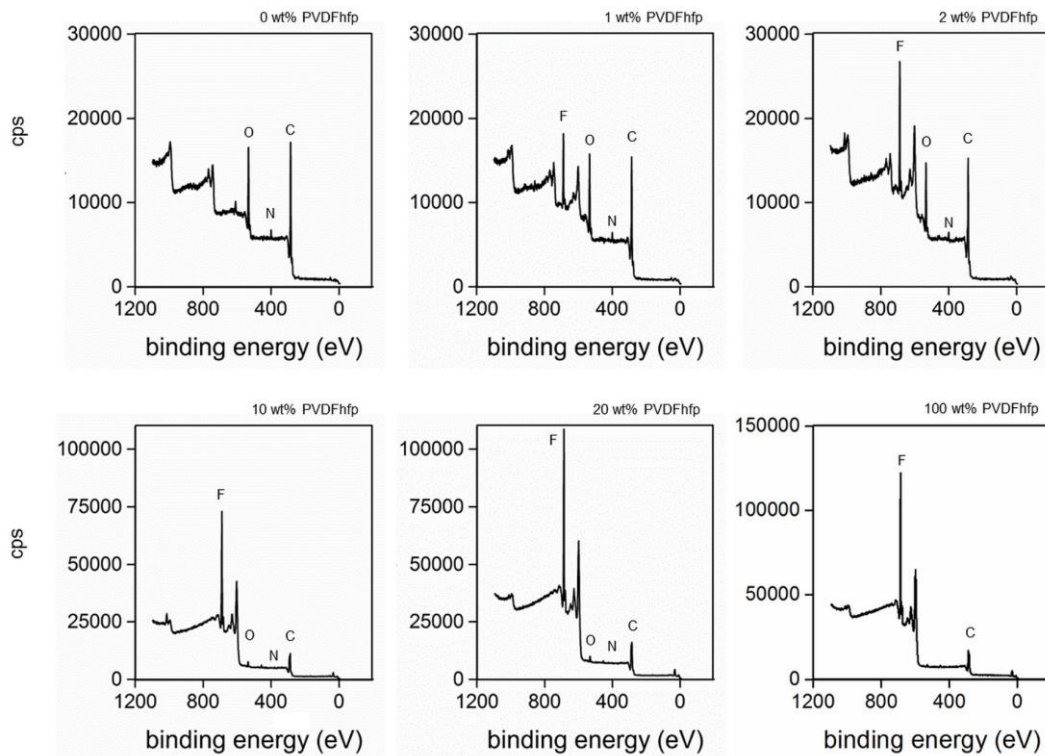


Figure 4.7: XPS spectra

XPS survey spectra of electrospun scaffolds of different PVDFhfp to PUR ratios. Blending with PVDFhfp resulted in high surface fluorine contents at a small percentage of 1 at%. A concentration of 20 wt% PVDFhfp resulted in a chemical surface composition comparable to pure PVDFhfp. The increase in fluorine concentration is clearly visible as the peak at 687 eV.

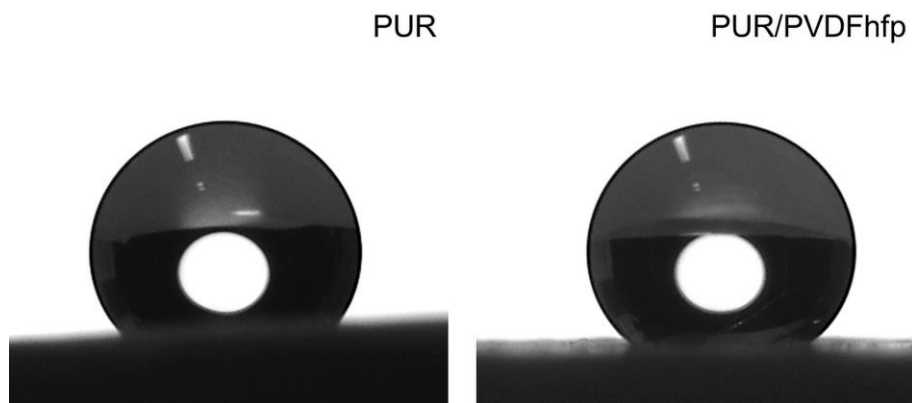


Figure 4.8: Water contact angle

Photographs of water in air sessile drop formation on PUR membrane and PUR/PVDFhfp membrane (20 wt% PVDFhfp).

5 Fiber surface functionalization

L. Weidenbacher, E. Müller, A.G. Guex, M. Zündel, P. Schweizer, V. Marina, C. Adlhart, L. Vejsadová, R. Pauer, E. Spiecker, K. Maniura-Weber, S.J. Ferguson, R.M. Rossi, M. Rottmar, G. Fortunato

Note: This chapter was submitted as: In Vitro Endothelialization of Surface Integrated Nanofiber Networks for Stretchable Blood Interfaces with Reduced Thrombogenicity.

L. Weidenbacher performed all the experiments including electrospinning, fiber characterization, membrane embedding, blood incubation and bioreactor tests. L. Weidenbacher analyzed the data and wrote the manuscript with contribution of all authors.

5.1 Abstract

Despite major technological advances within the field of cardiovascular engineering, the risk of thromboembolic events on artificial surfaces in contact with blood remains a major challenge and limits the functionality of ventricular assist devices (VAD) during mid- or long-term therapy.

Here, a nanofiber based approach that decreases the thrombogenicity while promoting the endothelialization capability of elastic silicone surfaces for next generation VADs is explored. A blend fiber membrane made of elastic polyurethane (PU) and low thrombogenic poly(vinylidene fluoride-co-hexafluoropropylene) (PVDFhfp) was partially embedded into the surface of silicone films. These blend membranes resist fundamental irreversible deformation of the internal structure and are stably attached to the surface, while also exhibiting enhanced anti-thrombotic properties when compared to bare silicone. The composite material supports the formation of a stable monolayer of endothelial cells within a pulsatile flow bioreactor resembling the physiological *in vivo* situation in a VAD. The nanofiber surface modification concept thus presents a promising approach for the future design of advanced elastic composite materials that are particularly interesting for applications in contact with blood.

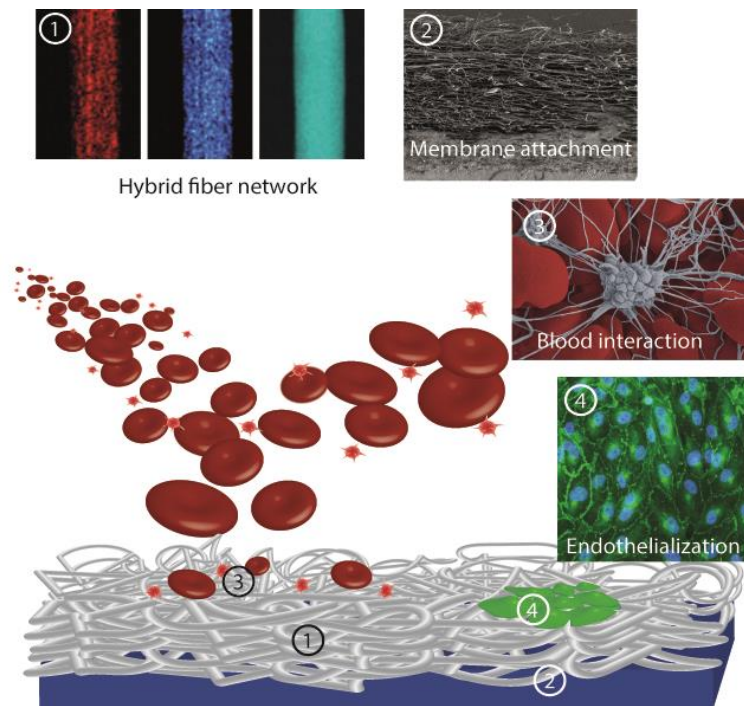


Figure 5.1: Graphical abstract

5.2 Introduction

To date, heart transplantation is the only curative treatment to save the life of patients suffering from end stage heart failure or congenital heart diseases. However, limited availability of donor organs, issues with patient eligibility and the rising number of new cases lead to the urgent need of alternative treatments. Temporarily supporting the function of the diseased heart, ventricular assist devices (VADs) are applied as bridge to transplant or recovery, and as destination therapy for patients ineligible for heart transplantation.^{1,2} Current state-of-the-art VAD therapies still bear the risk of blood clotting, bleeding, infections, or malfunction. Triggered by the interaction of blood with the exogenous surface of the pump,³ thrombosis was reported to account for 18.6% of the complications within the first 24 months post implantation,⁴ thus presenting a major challenge especially if VADs are applied as bridge to recovery or as destination therapy.^{2,5}

Over the past decades, turbodynamic and pulsation driven VADs have been developed. In pulsation operated VADs (PVAD), an elastic membrane is periodically deformed to pump the blood, mimicking the physiological action of the heart, which has been reported to increase the potential for myocardial recovery when compared to turbodynamic VADs.^{1,6} These elastic membranes should provide both long-term mechanical performance as well as hemocompatibility. In currently applied PVAD systems, a biostable polyether(urethane urea) material is used for this purpose.⁷ Due to their suitable elastic mechanical properties,⁸ hydrophobic nature, and chemical inertness, silicone based materials, such as polydimethylsiloxane (PDMS) or room temperature vulcanizing silicone (RTV), are commonly employed in medical applications⁹ and represent a promising alternative to currently applied materials for designing membranes in PVADs. However, despite the widespread use of silicones as implant material, uncontrolled protein adsorption as well as formation of thrombi and emboli have been reported.¹⁰⁻¹² Strategies to improve the hemocompatibility of silicone include tailored plasma derived coatings or poly(ethylene glycol) (PEG) based surface functionalization to decrease biomolecule adsorption.^{12,13} Furthermore, anticoagulation strategies based on heparin, or drug releasing surfaces for e.g. delivery of nitric oxide (NO)¹⁴ or other drugs have been reported.^{15,16} However, long-term stability of the functionalized silicone surfaces remains difficult to achieve.¹⁷ Besides, biofunctionalization of the surface with anticoagulant drugs, e.g. with heparin, could increase the risk of bleeding,¹⁸ and late stage thrombosis might occur in local drug delivery approaches after depletion of the drug reservoir.¹⁹ Therefore, new approaches to render silicone surfaces non-thrombotic are urgently required.

In the human body a single layer of endothelial cells (ECs) accounts for sustainable anticoagulant properties preventing thrombosis.²⁰ Mimicking the architecture of native blood vessels by covering the artificial material with a homogeneous functional EC layer presents the most promising, yet challenging strategy to avoid blood clot formation.²⁰ However, most approaches aiming for reduced interactions of materials with blood, avoid protein adsorption as well as cellular attachment and thus also impair surface endothelialization.²¹ Various strategies, including surface functionalization with adhesive peptides,²² surface patterning to protect the cells from shear stress caused by the bloodstream²³ or surface immobilization

of collagen IV or gelatin^{24,25} have been developed alongside with *in situ* re-endothelialization approaches²⁶ to improve the formation of a stable endothelium. To this end, biofunctionalization of artificial ePTFE surfaces via coating with fibrin and *in vitro* preseeding with autologous ECs allowed for a full surface coverage with a healthy endothelium *in vivo*.²⁷ On the other hand, electrospun scaffolds that mimic the fibrous structure of the native extracellular matrix^{28,29} were also found to foster stable endothelialization of diverse vascular grafts.³⁰ Due to the demonstrated biofunctionality, the flexibility in terms of materials choice and physicochemical properties of electrospun scaffolds, the application of electrospun membranes as an interface with blood seems worthwhile. To design larger medical devices such as a PVAD, integration of such fibrous scaffolds into soft base materials such as silicone presents a promising approach. However, stable bonding between an elastomeric silicone surface and an electrospun membrane that promotes endothelialization to enhance the performance of blood contacting devices has yet to be achieved.

To this end, electrospun poly(vinylidene fluoride-co-hexafluoropropylene) (PVDFhfp) membranes present an interesting scaffold, since they offer a low protein adsorption profile and reduced platelet adhesion.³¹ However, mechanical properties of PVDFhfp electrospun membranes do not allow for constant cyclic mechanical loading as present within a PVAD due to their low tensile strength.³² Blend electrospinning PVDFhfp with polyurethane (PU), which is known to exhibit remarkable cyclic elastic properties also at high strain levels,^{33,34} was shown to result in a fluorine-rich fiber surface.³⁵ While this blend membrane (PUPV) seems promising to fulfil both criteria, i.e. low thrombogenicity and enhanced elasticity, essential for the application in a VAD, blood response to such blend fiber membranes *in vitro* has not been investigated in detail, yet.

In the present study, we developed an electrospun PUPV membrane/silicone elastomer a composite and explored its potential for the long-term improvement of anti-thrombotic surfaces in a VAD. For this, the physicochemical properties, cyclic mechanical performance, and blood-interaction of PUPV membranes were assessed. Composite PUPV-RTV constructs were developed and thoroughly characterized for their mechanical properties, i.e. cyclic loading, and their thrombogenic potential. Finally, formation and stability of an endothelial cell lining

was investigated in a bioreactor setting,²³ combining fluid flow as well as pulsatile motion as present in an operating VAD. Our study successfully demonstrates the potential of a nanoscaled fibrous surface functionalization strategy to enhance the performance of blood-contacting implant surfaces to open up new possibilities in the design as well as manufacturing of a new generation of soft medical devices.

5.3 Materials and methods

5.3.1 Materials and reagents

All materials were purchased from Sigma Aldrich (Buchs, Switzerland), unless otherwise noted and used as received without any further purification. Cell culture supplements and reagents were obtained from Thermo Fisher Scientific (Waltham, USA) and used as received.

5.3.2 Membrane preparation and embedding into silicone

Electrospinning was performed by use of an in-house built setup as described elsewhere (Guex *et al* 2017). PVDFhfp (M_w : 400 000) was dissolved in dimethylformamide (DMF) in a concentration of 35% w/v. The polymer solution was filled in a 3 ml syringe (B. Braun, Melsungen, Germany) tipped with a 21 G blunt needle. Experiments were performed at a flow rate of 20 $\mu\text{L min}^{-1}$ and at voltages of + 14 kV at the needle tip and at - 5 kV at the collector electrode. Polyurethane (Elastollan C 95 A, BASF, Melsungen, Germany) was dissolved in DMF at a total concentration of 14.5% w/v. The same total concentration was used for the polymer blend of PU and PVDFhfp (ratio 4:1). Both PU as well as PUPV solutions were processed with a positive voltage of +14 kV and a negative voltage of - 4 kV at a flow rate of 10 $\mu\text{L min}^{-1}$. For all experiments a needle to collector distance of 25 cm was set.

For the embedding procedure, the two components of the RTV 4420 silicone (Bluestar Silicones, Lyon, France) were mixed in the ratio of 1:1 by stirring and degassed prior to casting. Custom built Teflon molds with a depth of 400 μm were

filled with the silicone and excess material was removed with a glass slide. The prefabricated electrospun membrane was placed on top of the uncured material and placed in a vacuum oven (SalvisLAB Vacucenter, Renggli AG, Rotkreuz, Switzerland) for 30 min at 60 °C to allow curing of the RTV.

5.3.3 *Scanning electron microscopy*

Scanning electron microscopy images were taken with an acceleration voltage of 2 kV and a current flow of 10 mA (Hitachi S-4800, Hitachi-High Technologies, Illinois, USA). Blood incubated surfaces were first fixed with a modified Karnovsky solution (4% paraformaldehyde, 2.5% glutaraldehyde) for 1 h and subsequently dehydrated in an ascending ethanol series from 50% to 100% (30-60 min incubation time per concentration) and hexamethyldisiloxane for 5 min. Samples were dried overnight prior to the gold-palladium sputtering process. Prior to imaging, samples were sputter coated with an 8 nm thick layer of gold-palladium.

All blood-incubated samples embedded in RTV were imaged with an environmental scanning electron microscope (Quanta 650, FEI Company, Hillsboro, USA) after fixation with the modified Karnovsky solution (and no further treatment) due to swelling of the material upon treatment with hexamethyldisiloxane. The samples were imaged at 100% humidity with a pressure of 8 mbar at 3 °C. An acceleration voltage of 7 kV was selected in combination with a gaseous secondary electron detector (GSED).

5.3.4 *Material characterization*

Membrane thickness was measured with a Fischerscope MMS® (Helmut Fischer GmbH, DIN ISO 2360).

Surface roughness was measured with a confocal 3D Optical Surface Metrology System (DCM8, Leica Microsystems AG, Switzerland) equipped with a Leica EPI 50x objective. For all samples the root-mean-square roughness (Sq) values were

measured on three different spots; the values were calculated according to ISO 25178 (2012).

To measure the water contact angle of the polymer membranes a drop shape analyzer was used (DSA25E, Krüss GmbH, Hamburg, Germany). Each surface was measured with $n=3$ individual measurements to determine the water contact angle value which was calculated by the supplied software.

X-Ray Photospectroscopy (XPS) analysis was performed on a PHI LS 5600 device (Physical electronics Inc., Chanhassen, USA) with an Mg K α X-ray source as described before (Guex *et al* 2017).

Scanning Transmission Electron Microscopy (STEM) and Energy Dispersive X-ray spectroscopy measurements were performed using an aberration corrected FEI Titan Themis³ 300 at an acceleration voltage of 300 kV. EDX maps were acquired using a Super-X detector in a single-pass mode to avoid densification and element migration. The fibers were dispersed on a TEM grid with a continuous carbon film (Plano GmbH, Wetzlar, Germany) and imaged in their pristine unaltered state (same electrospinning parameters as described above).

5.3.5 Mechanical testing of membranes

Uniaxial strain was imposed to rectangular samples with an aspect ratio of 1:5 (free length to width: 4 mm \times 20 mm) in a strip-biaxial setup using a MTS 793 test rig (MTS Systems, Eden Prairie, USA) as described elsewhere (Hopf *et al* 2016). After reaching the reference configuration, identified by a threshold tensile force ($F=0.01$ N), the samples were cyclically loaded at a frequency of 1 Hz to a maximum of 30% strain for a total of 2000 cycles. Tests were performed both, at room temperature in dry conditions and at 37 °C in PBS. Sample deformation in the loading direction was evaluated as gauge strain ε ,

$$\varepsilon = (L - L_0)/L_0 \tag{1}$$

where L and L_0 correspond to the sample length in deformed and reference configuration, respectively. The mechanical response of the materials was

characterized in terms of membrane tension (i.e. force divided by initial sample width). The inelastic part of the deformation was characterized with the residual strain ϵ^{res} , defined as the residual strain value in the sample after unloading each cycle (zero membrane tension). To measure the orientation of the fibers, their relative orientation on the surface was analyzed before and after the test via electron microscopy images with a potential bias of the analysis method in direction of the image axis.

5.3.6 Zeta potential measurement

The ζ -potential of PUR, PUPV, and PVDFhfp nanofibrous membranes was determined using an electro-kinetic flow-through ζ -potential analyzer (Mütek™SZZP-06, BTG Instruments GmbH, Wessling, Germany). During the measurement, a pulsating stream of fluid through the nanofibrous membrane was generated. Thereby, the diffuse double layer was sheared off and a local potential (streaming potential) was measured. The ζ -potential was then derived from the slope of the streaming potential ΔU [V] according to equation (2),

$$\zeta = \frac{\Delta U}{\Delta p} \times \kappa_B \times \frac{\eta}{\epsilon_r \cdot \epsilon_0} \quad (2)$$

with the pressure difference Δp [kg ms⁻²], the conductivity κ_B [A Vm⁻¹], the viscosity of the fluid η [kg ms⁻¹], the unit less dielectric constant ϵ_r , and the permittivity ϵ_0 [A s mV⁻¹].

Each experiment was performed in 3 repetitions with a differential pressure of $2.0 \times 10^4 - 2.5 \times 10^4$ kg ms⁻². The conductivity of 0.25 A Vm⁻¹ (2.5 mS cm⁻¹) and the pH between 5 and 9 were adjusted using a Titrator T90 (Mettler Toledo, Columbus, USA).

5.3.7 Fibrinogen adsorption

Fluorescence images were taken on a confocal laser scanning microscope (LSM 780, Zeiss, Germany) after incubation in fluorescently conjugated fibrinogen (FG-

Alexa633, 100 $\mu\text{g mL}^{-1}$ in PBS) for 1 h. To quantify the amount of adsorbed fibrinogen triplicates of PU, PUPV and PVDFhfp were incubated in fluorescently conjugated fibrinogen (FG-Alexa488, 100 $\mu\text{g mL}^{-1}$ in PBS) for 1 h, followed by three times washing with PBS. Subsequently, the membranes were incubated in 2% SDS in PBS and ultrasonicated for 30 min at 70 °C to remove the adsorbed protein. After a last washing step, fluorescence intensity of the residues was measured at 490 nm (Mithras2 Plate reader, Berthold Technologies). The experiment was repeated three times.

5.3.8 Fibrin clot formation

PVDFhfp, PUR as well as PUPV membranes (20 mm diameter) were placed in custom build Teflon molds and fixed to the bottom with Viton O-rings (Kubo Tech AG, Switzerland). The membranes were incubated in PBS overnight at RT prior to blood incubation with freshly taken partially heparinized human blood (0.43 IU mL^{-1}) supplemented with fluorescently conjugated fibrinogen (17 $\mu\text{g mL}^{-1}$, FG-Alexa488). After closing the molds with a lid, they were sealed with parafilm and placed on an orbital shaker at 10 rpm for 2 h (1 h for the comparison of RTV with PUPV embedded in RTV). Following the incubation, supernatants were collected and stabilized with EDTA before centrifugation at 2000 rpm. The plasma was stored at -20 °C for later analysis of coagulation markers. After carefully rinsing the membranes with PBS on the orbital shaker three times for 1 min, they were transferred into a 12 well plate and further processed for scanning electron microscopy and immunohistochemistry, respectively.

To determine platelet numbers attached to the surfaces, an LDH assay (CytoTox 96®, Promega AG, Fitchburg, USA) was performed according to the manufacturer's instructions. For this, electrospun surfaces were incubated with platelet rich plasma (PRP) for 30 min with the same setup as described above. Adsorbance was measured at 490 nm (Mithras2 Plate reader, Berthold Technologies).

5.3.9 Immunohistochemistry after blood incubation

Samples were fixed with a 4% paraformaldehyde (PFA) solution for 1 h in a 12 well plate. Subsequently the samples were blocked with 5% goat serum and 1% fetal calf serum (FCS) in PBS for 1 h. Activated platelets were stained with a CD62p-selectin antibody (1:100. Alexa Fluor® 645, Biolegend, San Diego, USA). Afterwards, cells were permeabilized in PBS containing 0.1% triton-X 100 for 10 min. In the last step, actin and cell nuclei were stained with Alexa Fluor® 546-conjugated phalloidin (1:200) and DAPI (1:1000), respectively. All antibodies were dissolved in PBS containing 1% FCS. Incubations were always followed by 3 times washing with PBS for 5 min.

5.3.10 Bioreactor tests

Embedded PUPV membranes (14mm diameter) were coated with gelatin by incubating them for 1 h in 1.5% gelatin dissolved in DI water. Subsequently, gelatin was crosslinked by incubation in 2% glutaraldehyde in DI water for 15 min. Samples were washed for 30 min in 70% ethanol and PBS containing 2 mM glycine overnight. Afterwards, the membranes were washed 5 times in PBS for 5 min in a 24 well plate.

1×10^5 human umbilical vein endothelial cells (Thermo Fisher Scientific, Waltham, USA) were seeded per sample and cultured for 5 days until confluency was reached. Cells were cultured in phenol red free Medium 200 supplemented with 2% (v/v) fetal bovine serum, hydrocortisone ($1 \mu\text{g mL}^{-1}$), human epidermal growth factor (10 ng mL^{-1}), basic fibroblast growth factor (3 ng mL^{-1}) and heparin ($10 \mu\text{g mL}^{-1}$). The embedded PUPV membrane was then placed in the bioreactor setting as described before (Bachmann *et al* 2016). Fluid flow was set to 0.5 L min^{-1} and the membrane was cyclically stretched to 8% at a frequency of 1 Hz for 18 h. The experiment was repeated three times. After the procedure cells were fixed with paraformaldehyde for 30 min, permeabilized with a 0.1% triton-X 100 solution and washed 3 times in PBS.

After blocking the samples for 2 h in 4% bovine serum albumin (BSA) in PBS, cells were fluorescently stained for the nuclei (1:1000 DAPI), actin skeleton (1:200, Alexa Fluor® 488, Thermo Fisher Scientific) and rabbit anti VE-cadherin primary antibody (Vascular Endothelial Cadherin, 1:400, Cell Signaling Technology, Danvers, USA) overnight at 4 °C. Afterwards, samples were washed 5 times in PBS and incubated with the secondary antibody anti-rabbit-Alexa Fluor® 633 (1:200, Thermo Fisher Scientific). Finally, samples were washed 5 times for 5 min in PBS prior to imaging on a confocal laser scanning microscope (LSM 780, Zeiss, Germany). All stainings were performed in PBS containing 4% BSA.

5.3.11 Statistics

Analysis of the statistical significance between two samples was performed either by one-way ANOVA or two-way ANOVA (results obtained from at least two donors) and Tukey-Kramer's post hoc test using GraphPad Prism 6 (GraphPad Software Inc., USA). Asterisk denote statistical significance as follows: * $p < 0.05$, ** $p < 0.01$, *** $p < 0.001$.

5.4 Results and discussion

5.4.1 Surface properties of electrospun membranes

By electrospinning of PU, PVDFhfp and the PUPV blend, nonwoven nanofiber membranes with homogenous morphologies and fiber diameters between 490 ± 190 nm (PU), 607 ± 188 nm (PVDFhfp) and 518 ± 164 nm (PUPV) were fabricated. Obtained membrane thickness values ranged from 112.4 ± 13.5 μm (PU), to 106.6 ± 12.3 μm (PVDFhfp) and 96.4 ± 19.1 μm (PUPV) (Table 5.1).

Table 5.1: Physico-chemical surface properties and membrane features

Parameter	PU	PUPV	PVDFhfp
Fiber diameter [nm]	490 ± 190	518 ± 164	607 ± 188
Membrane thickness [μm]	112.4 ± 13.5	96.4 ± 19.1	106.6 ± 12.3
Roughness [μm]	0.82 ± 0.27	1.73 ± 0.06	1.44 ± 0.22
Water contact angle [°]	133.5 ± 1.3	140.4 ± 0.7	144.8 ± 0.4
Zeta potential (pH = 7) [mV]	-55.2 ± 2.5	-97.1 ± 3.2	-103.5 ± 9.1
Surface concentration F [at.%]	0	41	54

Surface roughness was determined via non-destructive confocal 3D surface metrology (Table 5.1, Figure 5.7). Obtained roughness values were within the same range for all materials, being lowest for PU ($0.82 \pm 0.27 \mu\text{m}$) and highest for PUPV ($1.73 \pm 0.06 \mu\text{m}$).

Wettability of the membranes was assessed via static water contact angle measurements. As shown in Table 5.1, PU had the lowest contact angle ($133.5 \pm 1.3^\circ$) and PVDFhfp the highest ($144.8 \pm 0.4^\circ$). Notably the contact angle of the blend PUPV ($140 \pm 0.7^\circ$) was in between PU and PVDFhfp, indicating that the blend possesses a surface enriched with PVDFhfp as reported by our group (Guex *et al* 2017). Generally, contact angles were slightly higher based on the smaller size of the fibers that we aimed for in this study.

In addition to wettability, surface charge crucially determines the electrostatic interaction with biomolecules, which are comprised of various charged groups (Park *et al* 2016, Gitlin *et al* 2006). Therefore, the ζ -potential was measured in buffer solution for PU, PUPV as well as PVDFhfp in dependency of the pH value (Figure 5.8). Over the entire pH range, all surfaces possessed a negative ζ -potential. At a physiological pH value of 7, PVDFhfp had the lowest zeta potential ($-103.5 \pm 9.1 \text{ mV}$) and PU the highest ($-55.2 \pm 2.5 \text{ mV}$). The ζ -potential of PUPV ($-97.1 \pm 3.2 \text{ mV}$) was close to that of pure PVDFhfp, indicating a similar surface chemistry and underpinning the idea of the preferred localization of the PVDFhfp polymer at the

surface of the nanofibers. The strong negative ζ -potential of the PVDFhfp might be the result of the strong dipole moment of the C-F bond (O'Hagan 2008). Interestingly, the measured values for the ζ -potential of the PVDFhfp nanofibrous scaffolds at pH 7 are similar e.g. to previously reported values for PVDF based ultrafiltration membranes measured in tap water at pH 7.6 (Bendixen *et al* 2014). Values for PU are also supported by the literature (Lin *et al* 2015).

To gain information on the surface chemical composition, the fibers were analyzed by X-ray photoelectron spectroscopy (XPS). A fluorine concentration of the PUPV blend fibers (polymer weight ratio of 4:1 (PU:PVDFhfp)), close to the concentration known for PVDFhfp was measured (41 at.% and 54 at.% fluorine, respectively). This observation indicates that the blend fiber structure is composed of a core made of mostly PU and a surface that is highly enriched with the fluorinated polymer PVDFhfp, despite the relatively low amount of PVDFhfp in solution. Phase separation during the electrospinning process is expected to take place with the fluorinated polymers having the tendency to orient towards the surface due to their lower surface energy (Cheung *et al* 2006). Incomplete phase separation during the process and surface imperfections might explain the lower amount of detected fluorine. Such surface enrichment of one compound has been demonstrated for different blend systems being dependent on surface energy evolution, solubility of respective polymers and the polymer blend ratio (Bogntizki *et al* 2001, Li *et al* 2014b).

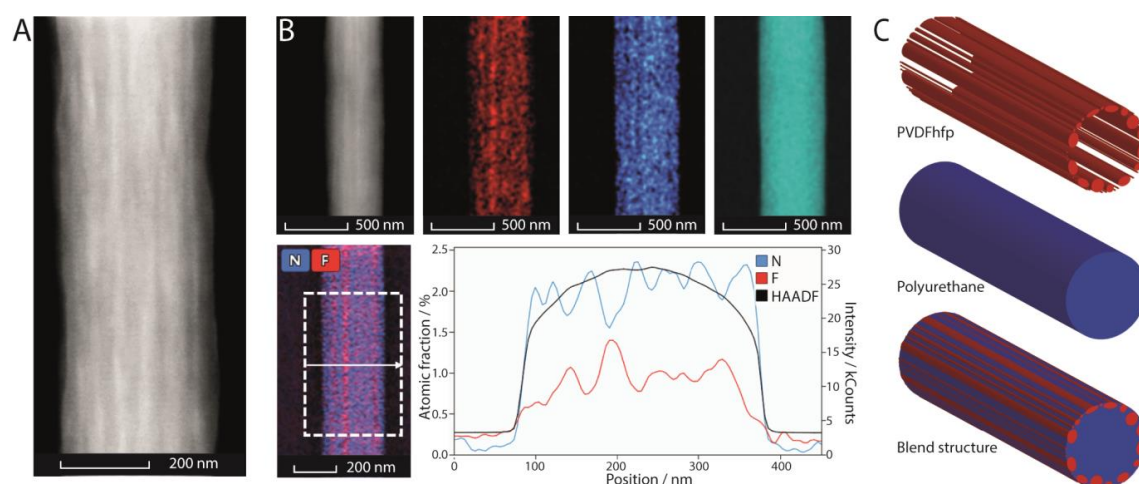


Figure 5.2: STEM EDX measurements

A) Representative high-angle annular dark field image of a single PUPV fiber. B) Single-pass EDX mapping of fluorine, nitrogen and carbon in red, blue and turquoise respectively (top) and a line scan perpendicular to the fiber axis (bottom). C) Schematic representation of the polymer distribution in blend fibers consisting of a PU core and a surface enriched by stripe-like domains of PVDFhfp (bottom image).

To investigate the nano-scale architecture of single blend fibers in detail and further confirm the hypothesis of a core-shell structure, scanning tunnel electron microscopy EDX (STEM EDX) analysis was performed in plan-view. A Z-contrast difference could be observed via high angle annular dark field imaging (HAADF) in stripe-like segments along the fiber axis, suggesting zones of material with higher Z-number and/or density (Figure 5.2 A). EDX mapping of those segments revealed an accumulation of fluorine with a concurrent depletion of nitrogen, deriving selectively from PU, as visible in the line scan shown in Figure 5.2 B. Carbon was homogeneously detected throughout the fiber. While fluorine was detected all over the fiber surface, the enriched segments might originate, based on the polymorphous structure of PVDFhfp, from crystalline domains with higher fluorine densities (Cui *et al* 2015).

Taken together physiochemical characterization of the surfaces revealed a similar surface topography, chemistry, wettability and ζ -potential for the PUPV blend and

PVDFhfp indicating a PVDFhfp enriched fiber surface structure in a more in-depth analysis as reported previously (Guex *et al* 2017). Via STEM EDX analysis, we could finally confirm the hypothesis of core-shell-like structured fibers consisting of a core of PU and a surface enriched with rod like segments of PVDFhfp along the fiber axis as sketched in Figure 5.2 C.

5.4.2 Mechanical characterization of electrospun membranes

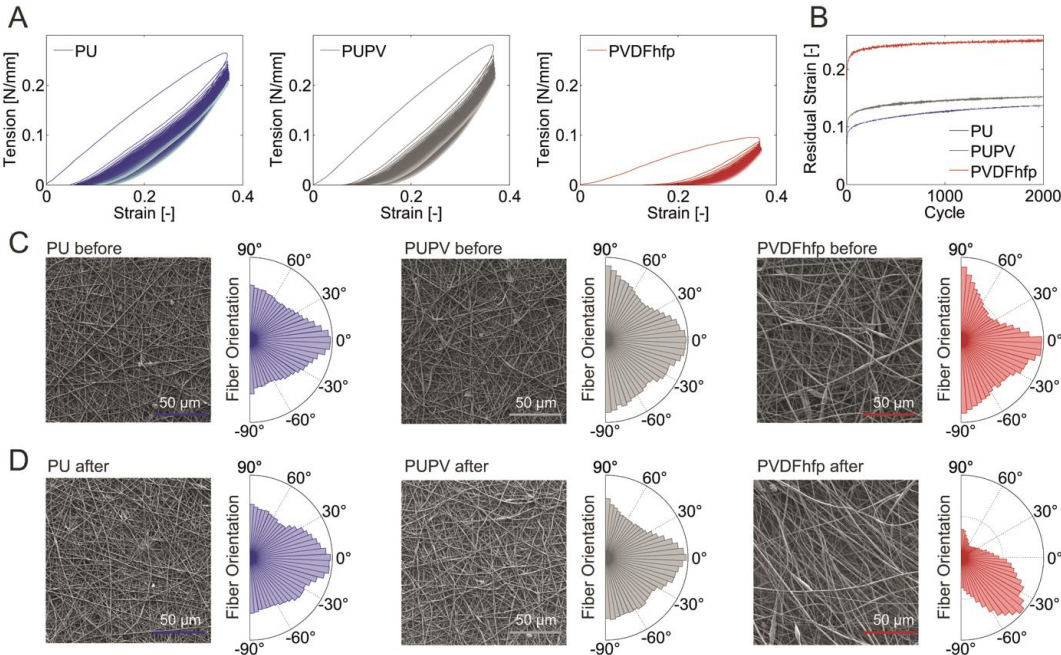


Figure 5.3: Mechanical characterization

A) Mechanical response of PU, PUPV, and PVDFhfp membranes under cyclic strip-biaxial loading. B) Plot of residual strain after each strip-biaxial loading cycle to compare the cumulative inelastic deformations in the tested membranes. C+D) SEM images of the electrospun membrane surfaces before and after the cyclic test. For each image, fiber orientation was analyzed and results summarized in the plots next to the SEM images with 0° describing the orientation in the horizontal axis.

For application in a PVAD, the electrospun interface needs to withstand mechanical loading in a cyclic fashion. Since the membrane deformation within such a device is multiaxial, cyclic strip-biaxial loading tests allow the mechanical characterization that is representative for the *in situ* mechanical load. Theoretically, the maximum applied strain should not exceed 15 % strain since this is the maximum value the endothelium is exposed to in the human body (Wittek *et al* 2016). Above this threshold, damage to the functional endothelium might occur. Strip-biaxial tests were performed to a maximum of 30 % strain to exclude potential material damage in the final application, where locally higher peak values of strain might occur. All tests were run with a loading frequency of 1 Hz, representing potential conditions in a PVAD, for 2000 cycles. The results of the cyclic mechanical tests are depicted in Figure 5.3, including the residual strain as a measure for the intrinsic amount of plastic deformation that accumulates over the cyclic loadings (Figure 5.3 B). While the PVDFhfp membrane experienced large amounts of plastic deformation already after the first cycles, PUPV displayed a similar performance to pure PU membranes. This indicates that the internal fiber structure of PU dictates the mechanical performance of the PUPV membrane. Repeating the measurement at elevated temperatures of 37°C in PBS, more closely mimicking conditions in the human body, resulted in almost the same results (Figure 5.9).

Part of the residual strain recorded for the PU/PUPV membranes is most likely derived from internal fiber reorganization processes within the scaffold and not directly related to plastic deformation of the fibers per se. At lower levels of strain, deformation mechanisms include fiber bending, relative fiber movement and inter-fiber bond damage (Chen *et al* 2016). It has been reported that the internal structural rigidity opposes the alignment of fibers within the membrane (Silberstein *et al* 2012). Above this threshold of strain, fibers within the scaffold start to align in direction of the applied force causing structural reorganization. This effect, however, is expected to emerge only at higher levels of strain alongside fiber bending and fiber layer delamination (Chen *et al* 2016).

To exclude large amounts of plastic deformation of the PU/PUPV membranes, the surface fiber orientation of the tested samples before and after the experiment was compared. As shown in Figure 5.3 D the PVDFhfp fibers were strongly reoriented

and aligned in the direction of the applied loading after 2000 cycles. In contrast, the other materials returned to their original state without any visible changes in their relative orientation.

In summary, mechanical tests could confirm that the PUPV membrane combines both the surface composition of PVDFhfp and the elastic properties of the PU material.

5.4.3 Effect of fiber surface composition on hemocompatibility

As designed for application in a blood-contacting device, the thrombogenic potential of fabricated PUPV membranes was investigated in comparison to bulk PU and PVDFhfp membranes.

The blood coagulation cascade represents a very complex and tightly balanced process. The first event upon contact of a biomaterial surface with blood is always the interaction with blood serum proteins such as albumin or fibrinogen (FG). FG is a key mediator for coagulation possessing a major binding motif for platelet adhesion and main building block of the blood clot. Therefore, in a first set of experiments, the initial adsorption of FG on the PUPV surface was investigated utilizing fluorophore conjugated FG and compared with membranes made out of bulk PU or PVDFhfp to obtain a qualitative measure of protein adsorption. As seen in the confocal laser scanning microscopy (CLSM) images of Figure 5.4 A higher amounts of fibrinogen were visible on the PU surface compared to both, PUPV and PVDFhfp, respectively. Subsequent quantification of the adsorbed FG fraction by extraction with SDS could confirm significantly higher levels of adsorption ($p < 0.001$) (Figure 5.4 B). Notably, FG adsorption was also tenfold higher on PUPV compared to pure PVDFhfp.

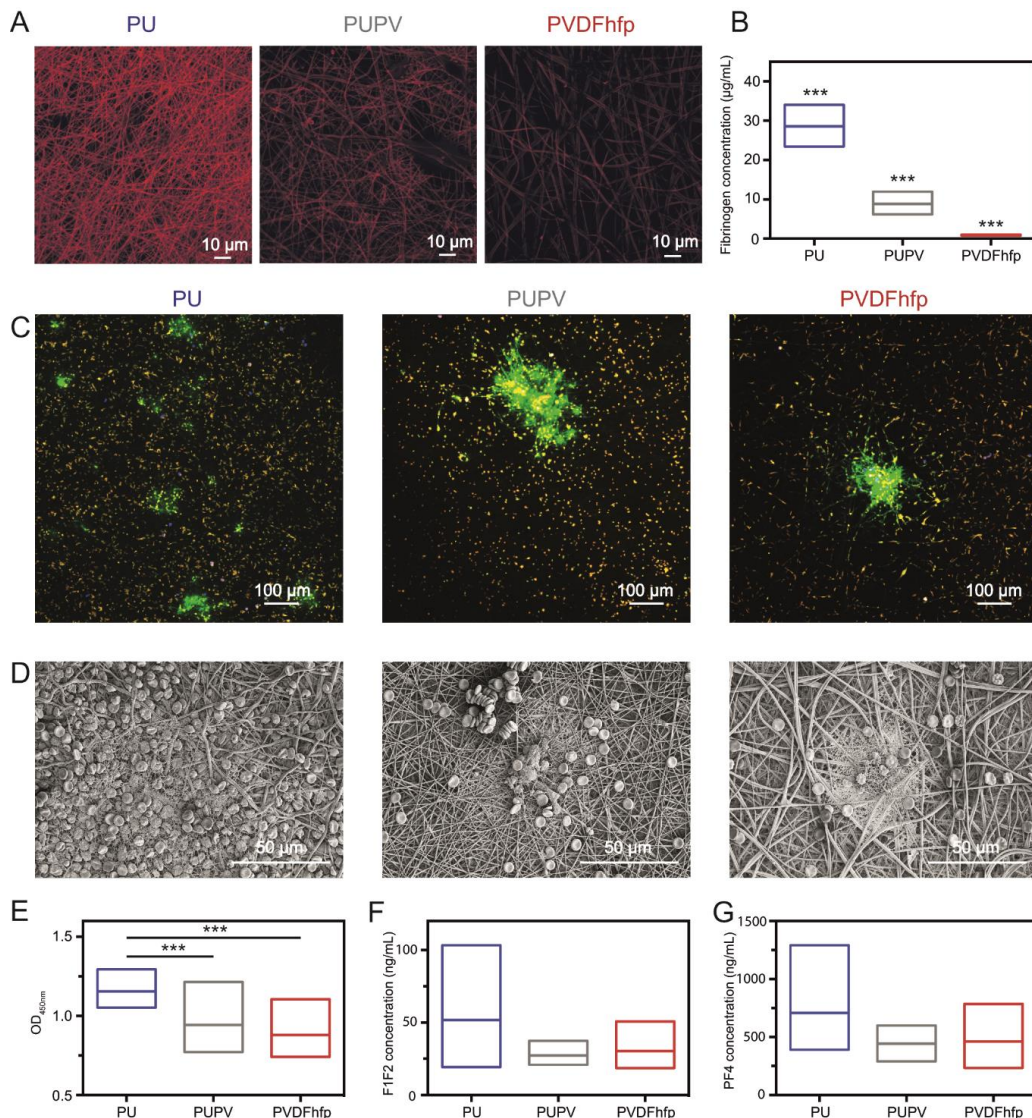


Figure 5.4: Membrane interactions with fibrinogen and blood

A) CLSM images of Alexa488-conjugated fibrinogen adsorbed on electrospun PU, PUPV, PVDFhfp membranes. B) Adsorbed concentrations of fibrinogen were quantified after extraction in SDS and measured by fluorescence spectroscopy. C) CLSM images of blot clot formation after incubation in whole blood. Samples were stained for fibrinogen (green) and actin of adherent platelets (orange). D) SEM images of PU, PUPV and PVDFhfp after incubation in human whole blood. E) Quantification of adherent platelets by means of LDH activity after incubation of the membranes in PRP. F+G) F1F2 and PF4 levels were measured in the supernatant after blood incubation via ELISA (* $p < 0.05$; ** $p < 0.01$; *** $p < 0.001$).

The low levels of adsorbed proteins on the fluorinated surfaces are in agreement with previous reports (Falde *et al* 2016) and could be caused by the C-F bonds, which hardly form any hydrogen bonds (Dunitz and Taylor 1997). Furthermore, at pH 7.4 FG possesses a negative net charge (isoelectric point, PI 5.5)(Bratek-Skicki *et al* 2013) and a strongly negative ζ -potential of the fluorinated surfaces PVDFhfp was measured inducing an additional repellent effect between the negatively charged surface and the protein. Low levels of protein adsorption are probably driven by hydrophobic interactions via the accessible -CH groups present on PVDFhfp. The higher amount of adsorbed FG on the PU surface compared to the fluorinated fiber surfaces might be attributed to stronger hydrophobic interactions of the polymer with FG and to lower electrostatic repulsion as the ζ -potential of PU was lower compared to PUPV or PVDFhfp (Thevenot *et al* 2008). The increased protein adsorption on PUPV compared to pure PVDFhfp could be explained by the slightly lower surface fluorine concentration on the PUPV membrane, caused by locally fluorine depleted areas leading to exposure to the PU core material. These observations match other reports on fluorine-enriched surfaces (Massa *et al* 2005) and complement previous results in more detail (Guex *et al* 2017).

In vivo, following the adsorption of serum proteins to the biomaterials surface, platelets adhere via the GPIIb/IIIa receptor to the adhesion motif located in the γ -chain of FG (Isenberg *et al* 1987). This event leads to (partial) activation of platelets, which in turn triggers the release of coagulation factors, e.g. platelet factor 4 (PF4), causing higher activation levels of platelets and the initiation/propagation of thrombus formation (Sperling *et al* 2009, Furie and Furie 2008).

Thus, membranes were incubated in platelet-rich plasma and the amount of adherent platelets was quantified via a lactate dehydrogenase assay (LDH). Significantly higher numbers of platelets were found on the PU membrane compared to both PUPV and PVDFhfp, which displayed similar numbers ($p < 0.001$) (Figure 5.4 E). Notably, the numbers of adherent platelets revealed the same trend as observed for the adsorbed concentrations of FG on the membranes, being highest for PU and lowest for PVDFhfp. These findings are in good agreement as FG includes the main platelet binding motif (Handa *et al* 2014). Thus, more FG could lead to higher numbers of binding motifs presented and consequently higher numbers of adherent platelets. Besides the chemical aspect, Milleret *et al.* revealed

a decreased amount of platelet adhesion and activation in dependence of fiber diameter and thus surface roughness of electrospun fiber meshes (Milleret *et al* 2012). Due to the nanosized fiber topography of the investigated membranes, the overall amount of adsorbed platelets was found to be on an equally low level. In fact, Ahmed *et al.* could even show a decrease in platelet numbers on electrospun surfaces in comparison to their solvent cast counterparts (Ahmed *et al* 2014).

Qualitative analysis of blood coagulation on the diverse fibrous membranes after incubation in freshly drawn human whole blood via CLSM and SEM revealed similar low levels of coagulation for all materials. On all surfaces, only few spots with thrombus formation were found. However, it seems that on both fluorinated surfaces, a less pronounced initiation of fibrin formation was observed (Figure 5.4 C+D) compared to the PU surface, which revealed slightly higher numbers of blood clots per area. When staining for the expression of CD62p, a marker for platelet activation (Handa *et al* 2014), no differences were observed between all investigated surfaces (data not shown). Analysis of biomarkers of the coagulation cascade in the blood supernatants after incubation did not reveal significant differences between the investigated groups. However, levels of prothrombin fragment 1 + 2 (F1F2) as well as PF4 were found to be slightly higher in blood exposed to the PU surface compared to PUPV or PVDFhfp (Figure 5.4 F+G).

Until now, only a few studies on the interaction of electrospun surfaces with human whole blood have been reported. It has been found that the material's topography of electrospun has the biggest influence on blood interactions on the molecular level, as well as in terms of platelet adhesion (Milleret *et al* 2012). Nonetheless, in our study we could show that changing the surface chemistry can have a significant effect on the amount of adsorbed platelets.

Taken together, from the set of investigated materials, membranes made of PU revealed the highest levels of protein adsorption, platelet adhesion and as a consequence blood clotting. However, the observed levels of blood-material interaction were rather low and according to literature, PU is already considered to exhibit a relatively low interaction with blood (Alves *et al* 2014). Remarkably, blending PU with PVDFhfp could further decrease the interactions of the

membrane with blood and proteins to a level comparable to PVDFhfp, demonstrating the potential of the PUPV blend for application in a PVAD.

5.4.4 Fabrication and characterization of PUPV-RTV

A process to fabricate a PVAD composite surface made of RTV decorated with electrospun PUPV nanofibers was developed after thorough characterization of the PUPV membrane. The process route of the fabrication of the novel surface is schematically illustrated in Figure 5.5 A.

In brief, a PTFE mold with defined depth of 400 μm was filled with the RTV precursor and the PUPV membrane was placed on top to allow for partial sink in of the membrane into the liquid silicone precursor. To prevent a full immersion of the fibers within the RTV substrate crosslinking was immediately performed by curing at 60°C. With this procedure, successful grafting of the two components was accomplished (Figure 5.5 E). The fibrous morphology, and thus the surface chemistry of the PUPV fibers, was maintained at the surface of the composite, perfectly shielding the RTV polymer at the backside of the membrane from interactions with the biological environment (Figure 5.5 E bottom).

Next, the response to cyclic deformation of the PUPV-RTV membrane was investigated as described above. During the cyclic test, it could be observed that the mechanical response of the composite membrane is governed by the stiffer PUPV network (Figure 5.5 B+C).

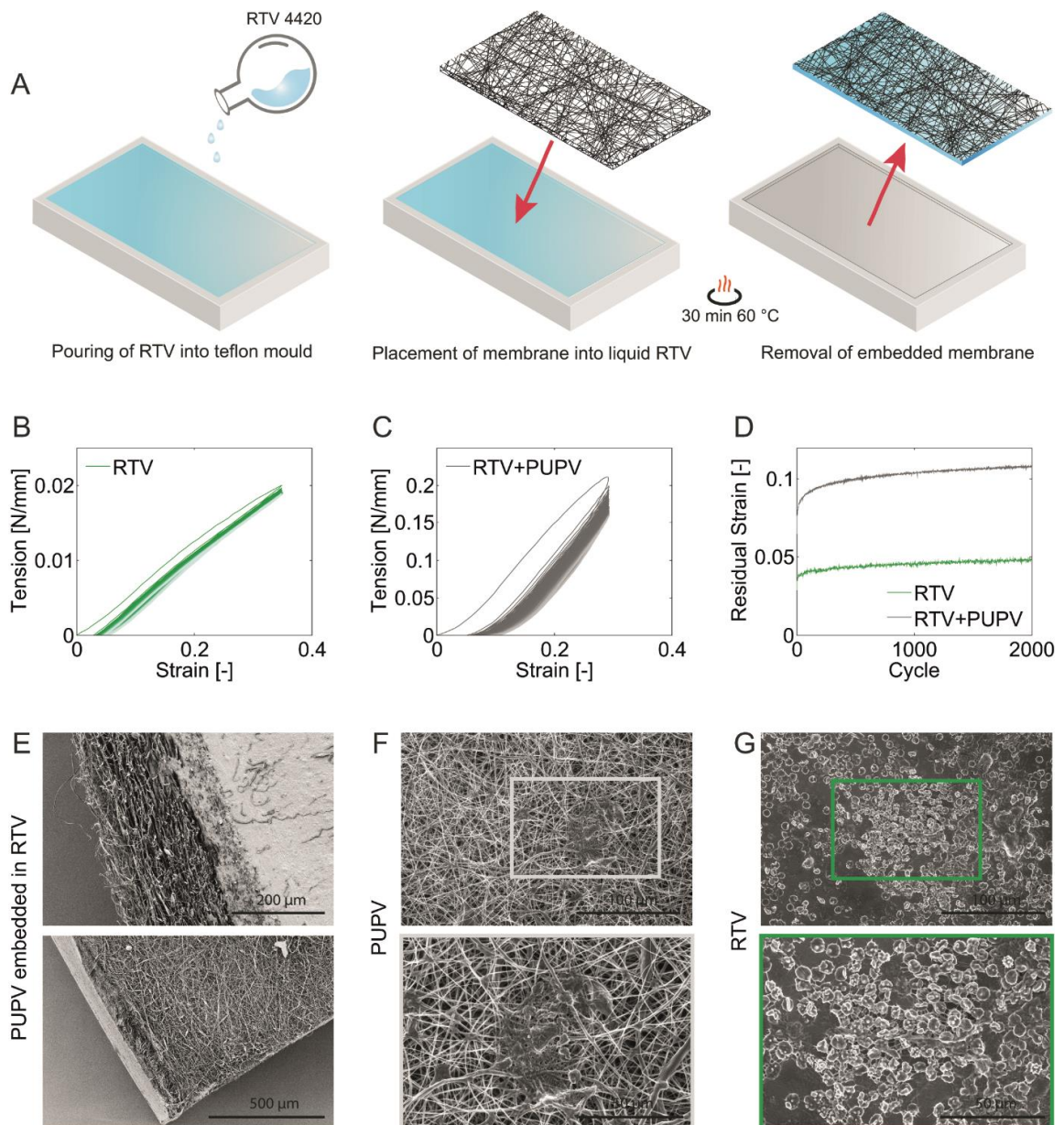


Figure 5.5: Fabrication and characterization of embedded fibers

A) Schematic illustration of the PUPV-RTV embedding procedure. B+C) Cyclic test of pure RTV film and the embedded PUPV-RTV composite for strip-biaxial loading. D) Plot of residual strain for both, RTV and the PUPV-RTV composite. E) Top view as well as cross section of an embedded PUPV membrane in RTV imaged via electron microscopy. F+G) An environmental SEM was used to image both the RTV as well as the embedded PUPV after blood incubation ($n = 3$).

The measured amount of residual gauge strain of the composite is thus greatly affected by the response of the electrospun PUPV membrane as displayed in Figure 5.5 D. Apart from that, an overall synergistic effect of the RTV silicone was observed in terms of elastic recovery of the composite system. After 2000 cycles, the amount of residual gauge strain was found to be lower compared to the isolated PUPV membrane (reduction of 4.4% strain). Notably, even though the mechanical properties of the bulk PUPV and RTV membranes are different, a stable bond at the interface between the silicone and the electrospun network was observed after the cyclic tests of the composite system. This result confirms the formation of a stable interconnection between the components and should verify potential application of the composite membrane for long-term performance.

Ultimately, to confirm the performance of the embedded PUPV membrane in contact with blood, bulk RTV was compared with the newly designed material. As shown in Figure 5.5 F, low levels of blood coagulation were observed for the composite PUPV-RTV membrane, i.e. only a few small clots were visible. On the contrary strong blood coagulation was observed on bulk RTV, where the surface was covered with a continuous fibrous layer of thrombus and adherent platelets (Figure 5.5 G). Notably, the performance of the embedded PUPV membrane in terms of thrombogenicity was very similar compared to the blank PUPV membrane, demonstrating that surface decoration of the RTV with a PUPV membrane drastically improves the hemocompatibility of the RTV substrate.

These results provide evidence that partial embedding of electrospun fibers into silicone, as shown for PUPV and RTV, is a straightforward concept to combine the properties of electrospun membranes and silicone into a new class of biofunctional and highly elastic membranes for application in a PVAD.

5.4.5 Surface endothelialization under flow

To ensure long-term bio- and hemocompatibility of the fabricated composite PUPV-RTV interface, rapid and stable endothelialization is key. Therefore, the PUPV-RTV surfaces were finally assessed in a recently developed bioreactor (Bachmann *et al* 2016) for their endothelialization potential. The employed setup (Figure 5.6 A) was designed to mimic similar flow conditions of maximum wall shear stress (WSS) as present within a PVAD *in vivo* (Bachmann *et al* 2016). This was achieved by combining the pulsatile deformation of the membrane, via application of pressure at the back of the RTV membrane, with constant fluid flow of medium on the cell-seeded surface of the PUPV membrane.

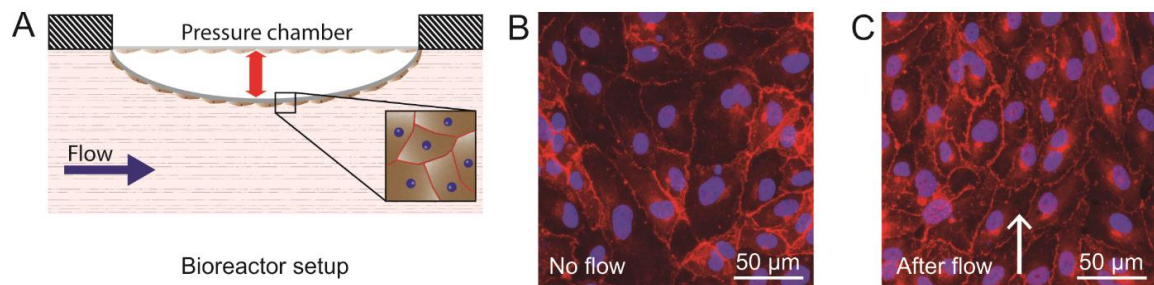


Figure 5.6: Bioreactor test

A) Illustration of bioreactor setup to apply both, shear stress as well as stretch to the ECs. B+C) CLSM images of endothelial cells cultured on the PUPV-RTV composite under static conditions and in the bioreactor. Cells were stained for VE Cadherin (red) as well as nuclei (blue).

To facilitate EC attachment to the surface, a thin layer of gelatin was crosslinked to the PUPV fibers, as usually utilized for EC culture on synthetic materials (Ai *et al* 2002). Subsequently, ECs were seeded on top of the surfaces and after 5 days of culture under static conditions without inflation of the membrane, formation of a confluent endothelium was observed on the surface (Figure 5.6 B).

The confluent ECs were then tested under conditions as previously established by Bachmann *et al* (Bachmann *et al* 2016). For culture in the bioreactor setup, 8% of strain at the apex of the inflated membrane were applied at a frequency of 1 Hz to the composite membranes, representing elevated physiological conditions as they

can occur within a PVAD due to disturbed flow inside the pump (Bachmann *et al* 2016) After 18 h of culture in the bioreactor under flow, the endothelium remained confluent without any detectable delamination of cells and started to align according to the flow conditions within the bioreactor. Furthermore, VE cadherin was strongly located at the cell-cell junctions and also more pronounced compared to the static control group (Figure 5.6 C). This indicates a stable intercellular attachment between the ECs. The herein utilized parameters of membrane deformation and fluid flow generated zones with supraphysiological WSS of about 5 Pa (Bachmann *et al* 2016), suggesting a high endothelialization potential of the PUPV-RTV composite. In contrast, Inoguchi *et al.* observed no expression of VE cadherin and substantial EC delamination on electrospun surfaces after 24 h under flow already at WSS values of 2 Pa (Inoguchi *et al* 2007).

These results provide evidence that the presented PUPV-RTV membranes are a promising biomaterial allowing for stable endothelialization even under the harsh conditions present in a pulsatile VAD. As a comparison, in large arteries in the human body WSS values range from about 1 - 3 Pa (Kroll *et al* 1996). To further mimic the native blood vessel architecture, e.g. by intercellular contact between smooth muscle cells (SMC) and ECs as well as the presence of extracellular matrix, in a future approach we envision a scaffold with SMCs encapsulated within the electrospun membrane in similar fashion to our previous study (Weidenbacher *et al* 2017).

5.5 Conclusion

In this study, a novel method to partially integrate nanofiber membranes, envisioned as an interface for PVAD surfaces was successfully developed. First of all, PUPV blend membranes were confirmed to successfully combine the beneficial properties of the PU component with the targeted repellent surface features of the PVDFhfp component. Remarkably, the composite of PUPV membranes and RTV yield a fibrous, fluorine enriched functional surface, possessing reduced protein adsorption and improved hemocompatibility, in comparison to bulk RTV films. The elastic properties of PUPV-RTV allow for long-term load bearing applications and the membranes exhibit a high potential for endothelialization, which was demonstrated by exposing ECs to WSS of 5 Pa in a bioreactor setup. Thus, we successfully demonstrated the potential of the highly elastic PUPV-RTV composites for application in PVADs. However, additional long-term studies will be necessary to critically assess these surfaces within a PVAD environment applied in large animal trials to further confirm the performance of these surfaces.

Finally, these results provide evidence that partial embedding of electrospun fibers into silicone, as shown for the example case of PUPV and RTV, is a straightforward concept for fabrication of novel composite (bio-)materials to be applied within the field of tissue engineering. Furthermore, the technique is not limited to tissue engineering but could also be utilized for any kind of application where a combination of an (in)organic fibrous membrane and a polymer backbone is desired. Examples for such functional composites could be textile applications (Turalija and Bechtold 2015), elastic sensors (Atalay *et al* 2017) or others, where functional membranes need mechanical support of a highly flexible component.

5.6 Acknowledgements

The authors would like to thank René Schneider for surface roughness measurements and Aldo Ferrari for providing the bioreactor equipment. This work is part of the Zurich Heart project of “Hochschulmedizin Zurich” (<http://www.hochschulmedizin.uzh.ch/en/projekte/zurichheart.html>).

5.7 Appendix

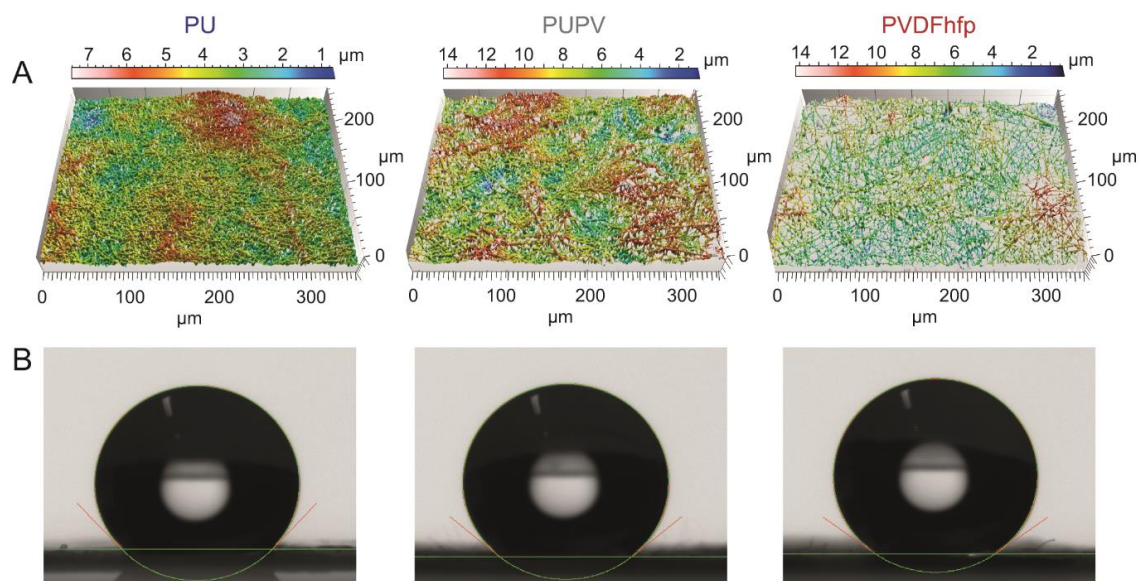


Figure 5.7: Surface characterization

Surface characterization of PU, PUPV and PVDFhfp. A) Confocal 3D optical surface metrology Surface roughness measurements. The color code corresponds to the height of the surface profile. B) Water contact angle measurements of the different surfaces showed similar drop shapes, revealing similar wetting behavior of PU, PUPV and PVDFhfp.

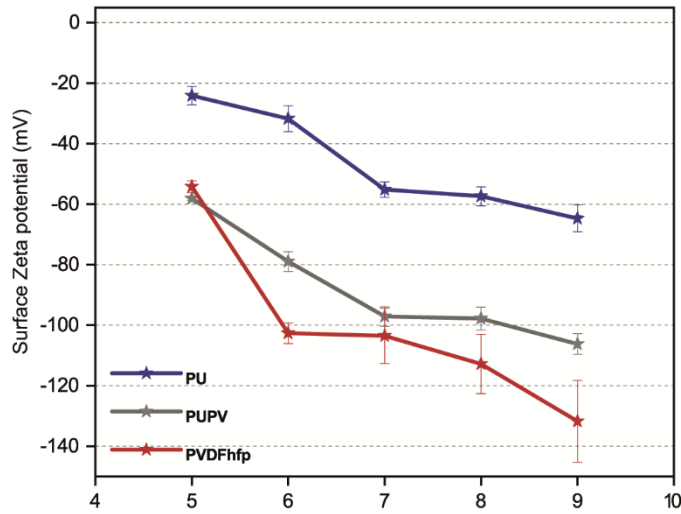


Figure 5.8: Zeta potential measurement

Surface zeta potential measurements. Surface charge of the different membranes as measured by a flow-through ζ -potential analyzer. For each material three samples were measured. Fluorinated surfaces revealed lower values of ζ -potentials throughout the whole pH range.

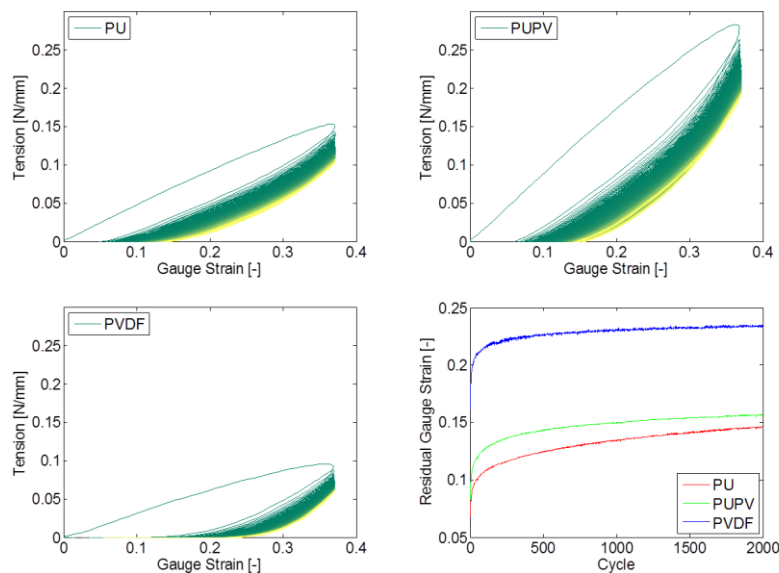


Figure 5.9: Mechanical characterization in PBS at 37°C

Mechanical testing of electrospun membranes in conditions mimicking the *in vivo* environment (immersed in PBS at 37°C): Mechanical response of PU, PUPV, and PVDFhfp membranes under cyclic strip-biaxial loading and corresponding cumulative residual strain after each loading cycle.

6 Biomimetic co-culture approach

Note: This chapter is under preparation for future submission. The presented results should give some preliminary insights into the concept of the study.

6.1 Abstract

In the human body, the endothelium provides an anticoagulant barrier between the sub-endothelial tissue and blood and is responsible for the regulation of immune and inflammatory reactions. Based on the complexity of the endothelium, the facilitation of completely endothelialized artificial surfaces is a challenging task. Despite the advances within the field of vascular tissue engineering, current options for a fully functional endothelial cell (EC) layer that maintains the function of the endothelium are still limited. The complexity of an engineered approaches lies in the fact that ECs are strongly affected by the surrounding environmental conditions like shear stress, as well as the underlying smooth muscle cells (SMC), which are present in the tunica media of the blood vessel. The interplay of both cell types is decisive for the vascular function.

Within this study, a tissue engineering based approach was utilized to generate an artificial fibrous substrate containing smooth muscle cells. This platform was used as a substrate for EC seeding to investigate the impact of the cellular interactions on the function of the endothelial cells.

6.2 Introduction

In the field of cardiovascular engineering access to synthetic materials to provide long-term functional solutions is still limited despite the clinical demand for vascular conduits or hemocompatible surfaces for cardiovascular implants (Zilla *et al* 2007). Recent strategies to increase the patency of synthetic materials include surface treatments or coatings to reduce the interaction with blood (de Mel *et al* 2012) or the introduction of anti-coagulative substances like heparin that are gradually released from the surface (Biran and Pond 2017). However, synthetic surfaces still might induce a certain level of foreign body reaction and inflammation, which can cause failure of the device (Tchantchaleishvili *et al* 2014). To design tissue engineered blood-contacting surfaces or vessels, which can be considered as hemocompatible, approaches aiming for fully endothelialized interfaces are almost inevitable. Therefore, the hierarchical structure of blood

vessels has to be taken into consideration to design advanced solutions to address the clinical demands (Song *et al* 2018).

Blood vessels are composed of three layers, namely the outer *tunica externa*, middle *tunica media* and inner *tunica intima*. The external layer is mostly made of loose connective tissue and fibroblasts while the media consists of aligned SMCs embedded in extracellular matrix of collagen I and proteoglycans, which are responsible for the maintenance of the vascular tone. On the inside a monolayer of adjacent ECs is adherent to the basement membrane (Medvedev *et al* 2006). The interactions and exchange between all these components and cells enable the complex functionality of the vasculature.

The vascular endothelium with its semi permeable nature is responsible for the maintenance of blood vessel homeostasis by regulating the blood flow, the transport of oxygen, nutrients and waste products via the vessel wall and the control of inflammatory as well as immune reactions (Michiels 2003, Sumpio *et al* 2002). To resist blood clotting, the antithrombotic function of the endothelium is sustained by secretion of nitric oxide, prostacyclin and tissue plasminogen activator (Mitchell and Niklason 2003). Alongside the secretion of active molecules, ECs express anticoagulants like heparin sulfate, ADPase and thrombomodulin on their cell membrane (Aird 2007).

Upon activation of the endothelium by e.g. bacterial endoxins, cytokines, thrombin or shear stress gradients, production of anticoagulant factors like tissue plasminogen activator and thrombomodulin, tissue factors such as van Willebrand factor (vWF), plasminogen activator inhibitor (PAI-1), thrombospondin and platelet activation factor (PAF) as well as cell adhesion molecules like VCAM-1 is upregulated (Truskey *et al* 1999, Stefopoulos *et al* 2017). During exposure to shear stress in particular, multiple transcription factors like AP-1, NF- κ B, Sp-1, or Egr-1 are directly involved in the gene expression profile to promote the survival of the endothelium (Michiels 2003).

When dysfunction of the endothelial cells occurs, the homeostatic function is lost. Usually this is related to EC injury or death, caused by e.g. shear stress, oxidative stress or metabolic stress that eventually leads to coronary artery diseases (CAD)

by atherosclerosis, congestive heart failure, inflammatory symptoms or other pathologies (Sumpio *et al* 2002, Pober *et al* 2009).

For tissue engineering approaches, the establishment of a long-term stable and functional endothelium is thus key for the success rate of cardiovascular transplants.

In fact, different strategies towards a fully covered luminal surface of artificial surfaces have been utilized. These include both, single cell-based approaches, as well as co-culture protocols that can be achieved either *in situ* post implantation, or prior to the graft implantation. To minimize the risk of graft rejection patient-derived autologous ECs are a potential cell source to enhance the outcome in a clinical setting (Al-Lamki *et al* 2008).

In situ single cell endothelialization was shown to be improved by e.g. chemical modifications or grafting EC specific peptides to the surface that attract host progenitor cells from the bloodstream (de Mel *et al* 2008). Besides the functionalization of surfaces, patterns that enable protection of ECs against the shear forces generated by the blood stream were developed (Stefopoulos *et al* 2017). By this, reinforcement of cell-cell as well as cell-substrate adhesion was enhanced to improve the long-term endothelialization.

Since the interplay of SMCs and ECs *in vivo* is pivotal for the function of the blood vessel, models more closely representing the architecture of native blood vessels, where SMCs and ECs are both present, are mandatory. The interactions between the two cell types include the control of cell phenotype, vessel wall maturation and cell survival (Ganesan *et al* 2017). Apart from that, SMCs orchestrate the EC response to flow as well as vessels injury (Balcells *et al* 2010, Hsiai 2008).

However, in most of the co-culture based approaches ECs and SMCs are in direct contact (Liu *et al* 2015b, Wu *et al* 2007), dissimilar from the *in vivo* situation, where the cells are separated by the basement membrane. In an combined approach of electrospinning and cell electrospraying, scaffolds loaded with cells can be fabricated (Stankus *et al* 2007, Weidenbacher *et al* 2017). This allows for a co-culture approach with locally separated cells similar to the *in vivo* architecture.

6.3 Materials and methods

6.3.1 Materials and reagents

All materials were purchased from Sigma Aldrich (Buchs, Switzerland), unless otherwise noted. All materials were used as received and without any further purification. Cell culture supplements and reagents were from Thermo Fisher Scientific (Waltham, USA) and used as received.

6.3.2 Cell culture substrates

To fabricate fibrous scaffolds to be used as a seeding platform for the cells, electrospinning of PU and PVDFhfp was carried out as described before to obtain blend fiber membranes (Guex *et al* 2017). Before seeding human umbilical vein endothelial cells (HUVEC) the surface was coated with a thin layer of gelatin to facilitate cellular attachment. In brief, the surface was initially adsorbed with 1.5 % (w/v) gelatin solution in DI water for 1 hour. Subsequently, excess gelatin was removed and gelatin crosslinked to the fibers for 15 min in a 2 % glutaraldehyde solution in water. The glutaraldehyde solution was then replaced with 70 % ethanol in phosphate buffered solution (PBS) for 30 min. After washing with PBS, the membranes were incubated over night in PBS containing 2 mM glycine, followed by a final washing step with PBS.

6.3.3 Cell culture

Primary human aortic smooth muscle cells (ATCC, Manassas, USA) were expanded in smooth muscle growth media supplemented with gentamicin/amphotericin-B, fetal calf serum, human fibroblast growth factor B, insulin and human epidermal growth factor (Lonza, Basel, Switzerland). For the collagen stimulation experiment, SMCs were seeded in 48-well plates and grown until confluency. HUVECs (Thermo Fisher Scientific, Waltham, USA) were cultured with phenol red free medium 200 supplemented with 2% (v/v) fetal bovine serum, hydrocortisone ($1\mu\text{g mL}^{-1}$), human epidermal growth factor (10 ng mL^{-1}), basic fibroblast growth factor (3 ng mL^{-1}) and

heparin ($10 \mu\text{g mL}^{-1}$) until 90 % confluency was reached. For cell seeding experiments, 5×10^4 cells cm^{-2} were seeded on the electrospun membranes for up to 7 days.

6.3.4 Immunofluorescence

To characterize the phenotype of cultured SMCs, the cells were first cultured for 3 days with either addition of ascorbic acid ($50 \mu\text{g mL}^{-1}$) or transforming growth factor β (TGF- β , 10 ng mL^{-1}). Subsequently, cells were fluorescently stained for the nuclei (1:1000 DAPI), actin skeleton (1:200, Alexa Fluor® 488, Thermo Fisher Scientific) and rabbit anti calponin (1:250, Thermo Fisher Scientific) primary antibodies over night at 4°C . After washing the samples 5 times in PBS samples were incubated with the secondary antibody anti-rabbit-Alexa Fluor® 555 (1:200, Thermo Fisher Scientific). Before imaging the cells on a confocal laser scanning microscope (LSM 780, Zeiss, Germany) the samples were washed again for 5 min with PBS.

HUVECS were also stained after the different incubation times for the nuclei (1:1000 DAPI) and rabbit anti VE-cadherin primary antibody (Vascular Endothelial Cadherin, 1:400, Cell Signaling Technology, Danvers, USA) overnight at 4°C . After washing for 5 min in PBS the secondary antibody anti-rabbit-Alexa Fluor® 633 (1:200, Thermo Fisher Scientific) was used and incubated for 1 hour at RT. Subsequent washing was done prior to imaging. All stainings were performed in PBS containing 4% BSA.

6.3.5 Collagen synthesis

To stimulate collagen synthesis of SMCs, $50 \mu\text{g mL}^{-1}$ ascorbic acid and $50 \mu\text{g mL}^{-1}$ fibronectin were added to the medium of the first group. The two other groups were cultured with two different concentrations (1x, 2x) of ficoll type 70 mixed with ficoll type 400 (1x 37.5 mg mL^{-1} F70 + 25 mg mL^{-1} F400; 2x 75 mg mL^{-1} F70 + 50 mg mL^{-1}) (Rashid *et al* 2014). Medium was exchanged every day. Collagen concentrations

synthesized after 4 days were measured by a Sircol assay (Biocolor, Carrickfergus, UK) according to the manufacturer's instructions.

Immunofluorescence stainings were also performed to observe the collagen synthesis of SMCs after up to 7 days. Therefore, cells were fixed for 1 hour in 4% paraformaldehyde and blocked in 4% BSA for 1 hour and permeabilized for 10 min in PBS containing 0.1% Triton-X, followed by a washing step with PBS (3x). Collagen type I was stained by a rabbit anti collagen I antibody (1:500, Thermo Fisher Scientific) for 6 hours. The samples were washed 3 times in PBS. Afterwards, cells were stained for the nuclei (1:1000 DAPI), actin skeleton (1:200, Alexa Fluor® 546, Thermo Fisher Scientific) and the secondary antibody anti-rabbit-Alexa Fluor® 488 (1:400, Thermo Fisher Scientific).

6.4 Results and discussion

The concept of this study is to investigate the response and functionality of ECs to different scaffold surfaces. As a control group, the ECs should be seeded on top of electrospun surfaces to observe the maturation of a confluent EC layer. This approach should be compared to a scaffold, which is infiltrated with SMCs that created their own collagenous ECM upon stimulation. As a last set of experiments, SMCs should be seeded on top of an electrospun membrane and ECs are seeded in direct contact on top of this structure. The different approaches are illustrated in Figure 6.1.

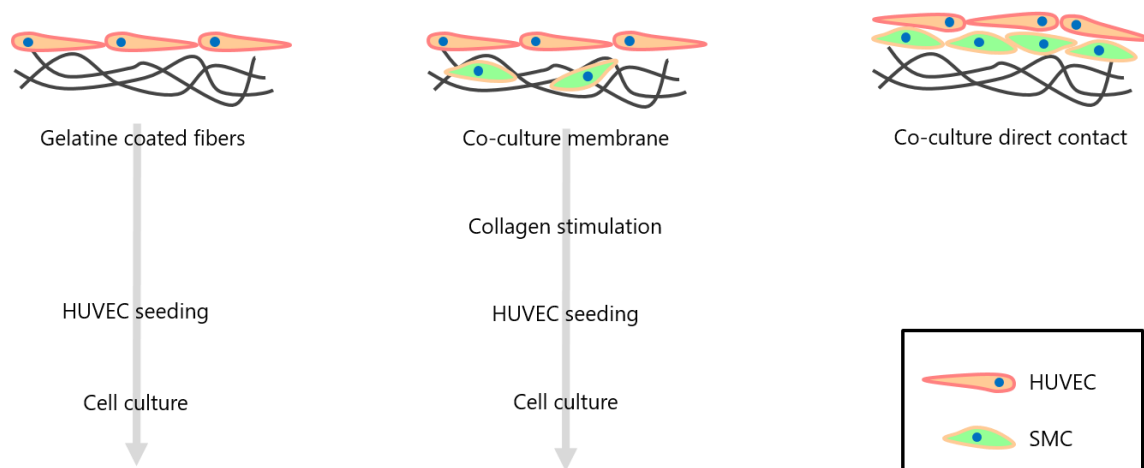


Figure 6.1: Cell seeding approaches

Different approaches of EC culture on different scaffold surfaces. The cells can either be cultured on blank electrospun surfaces, on top of a scaffold containing SMCs and a collagenous ECM, or in direct contact with SMC that are grown on top of the membrane.

6.4.1 Seeding of ECs on blend fiber membranes

Before applying the different cell seeding strategies the potential for stable endothelialization of the PUPV membranes had to be assessed. Therefore, HUVECs were seeded for up to 7 days on the gelatin coated membrane.

As seen in Figure 6.2 an almost confluent monolayer of ECs with only minor interruptions was obtained after 7 days of culture. Expression of VE cadherin was most pronounced at the margins of the cells. Based on the cellular morphology, it can be concluded, that the blank membranes with gelatin coating do facilitate cellular attachment and EC proliferation.

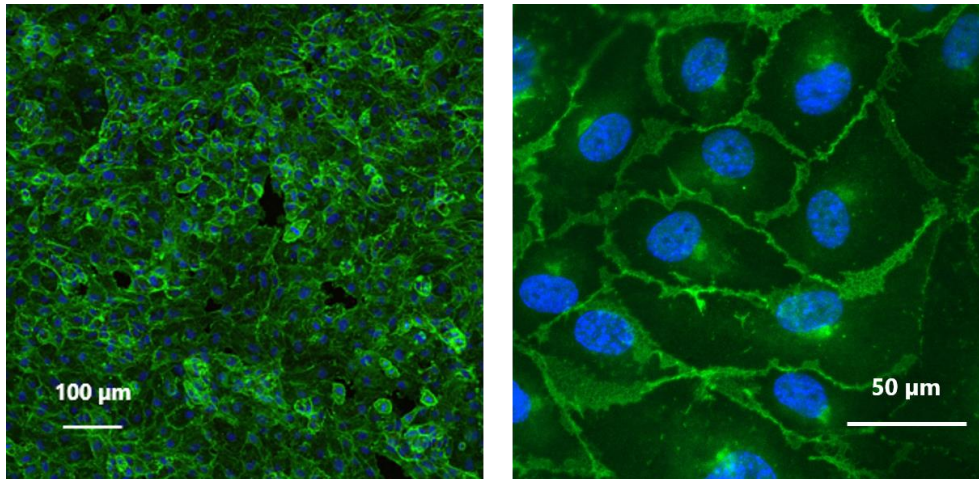


Figure 6.2: EC seeding

Fluorescence microscopy image of endothelial cells seeded on a PUPV membrane for 7 days. The cells are stained for their nuclei (blue) as well as VE cadherin (green). A confluent monolayer with only a few gaps in between can be observed.

6.4.2 Boosting collagen formation

One major aspect for stable surface attachment of ECs is the availability of surface binding sites. Even though cellular attachment can be obtained by coating the surface with gelatin, binding to ECM proteins like collagen more closely represents the *in vivo* situation. In their synthetic phenotype, SMCs constantly synthesize their own microenvironment, mostly made of collagenous ECM. Several studies to boost the secretion of the protein network have been described. These include the usage of ascorbic acid or macromolecular crowding agents to enhance the levels of synthesized ECM (Lareu *et al* 2007, Murad *et al* 1981).

SMCs were cultured in their normal growth medium and different additional supplements for up to 7 days. After one day only a little amount of collagen type I was found in the intracellular space (Figure 6.3). Most of the signal was found inside the cells. After seven days of culture, a higher amount of collagen type I was found for the cells treated with ascorbic acid/fibronectin as well as the low

concentration of ficoll. Surprisingly, the higher amount of ficoll added to the cell culture did not reveal an additional beneficial effect on the synthesis of collagen.

To quantify the amount of synthesized collagen, a Sircol assay was performed after four days of stimulation with the same agents. The results of the assay are displayed in Figure 6.4. The previously observed trend in terms of ECM production was confirmed. The highest amount of collagen was found when the cells were treated with the low concentration of ficoll, almost on a same level with the samples treated with the combined addition of ascorbic acid/fibronectin. Since it is known, that ascorbic acid specifically targets the synthesis of collagen without greatly affecting the synthesis of other proteins (Murad *et al* 1981), this stimulant might be even more beneficial for application in a biomimetic blood vessel structure.

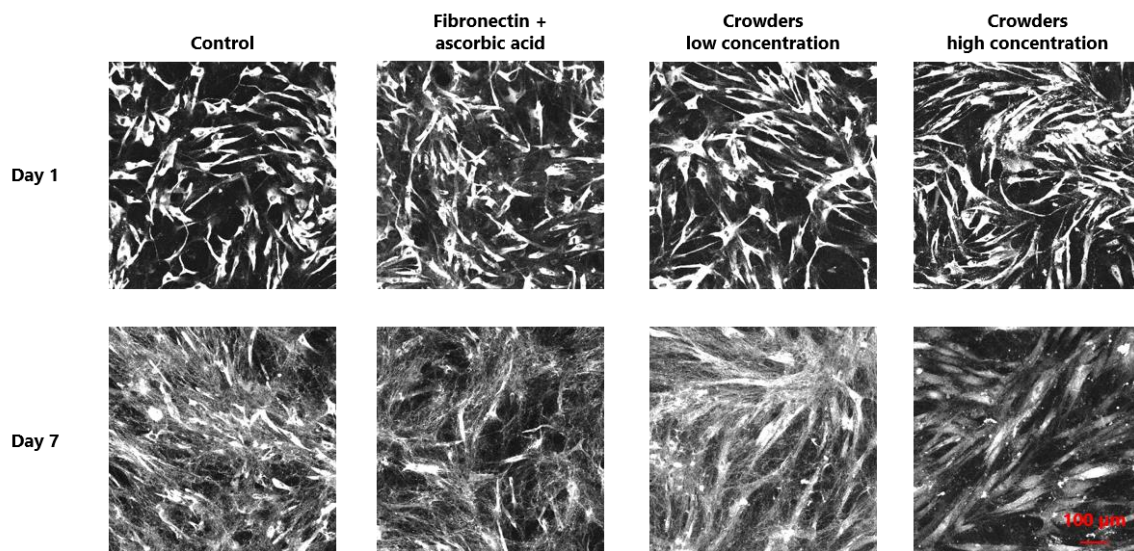


Figure 6.3: Collagen stimulation

Fluorescence microscopy images of collagen stained with a fluorescent dye specific for collagen type I (white). The effect of different concentrations of ficoll (crowders high and low concentration) and fibronectin + ascorbic acid was compared in terms of collagen synthesis by SMCs. All the investigated groups were imaged after 1 day and 7 days in culture, respectively.

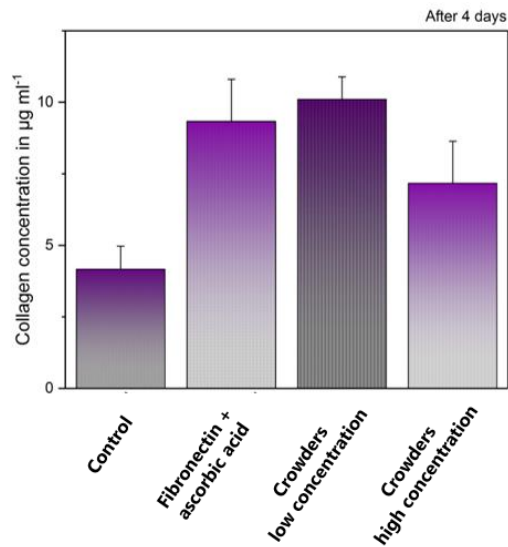


Figure 6.4: Collagen quantification

Quantification of synthesized collagen measured via a Sircol assay. SMCs were treated with different stimulants for 4 days before the measurement of the collagen content in cell culture well plates.

6.4.3 Control of SMC phenotype

After stimulation of the collagen synthesis, SMCs need to switch back their phenotype towards a quiescent state as present within a healthy blood vessel. A common marker for the quiescent phenotype is calponin, which is upregulated in resting contractile cells (Beamish *et al* 2010).

After successfully boosting the formation of a collagenous ECM by stimulation the synthetic phenotype with ascorbic acid in a previous step, the potential of switching the cells to a contractile phenotype was tested. As seen in Figure 6.5, the expression of calponin was highly different among the investigated groups. When cultured under normal control conditions, the cells express only low levels of calponin, indicating a rather synthetic phenotype. A similar expression pattern could be seen for the cells stimulated with ascorbic acid (previously discussed to

promote a synthetic phenotype). However, upon stimulation with TGF- β a strong upregulation of calponin expression was observed, revealing a shift towards the contractile phenotype. These results indicate the potential of controlling the SMC phenotype towards the targeted quiescent state (Beamish *et al* 2010).

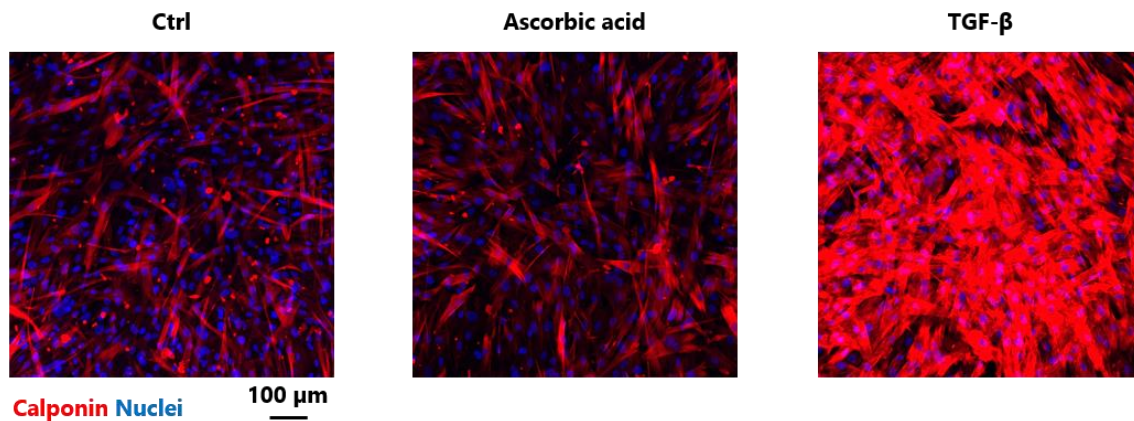


Figure 6.5: SMC phenotype control

Smooth muscle cells stained for their nuclei as well as calponin, a marker for the quiescent phenotype of SMCs. A control group is compared with cells stimulated with ascorbic acid and cell stimulated with TGF- β .

6.5 Conclusion

These preliminary results highlight the strong potential of controlling the cellular phenotype in the engineering of biomimetic scaffolds. First, it has been shown that SMCs can be stimulated with addition of different substances to secrete an extracellular environment. Especially the usage of ascorbic acid is of interest, based on the targeted stimulation of a collagenous matrix. This environment is strongly desirable to facilitate the attachment of ECs, which requires available binding sites to the matrix. To avoid the pathological condition of excessive ECM production, the phenotype of SMCs needs to be switched back to a quiescent and contractile state, as in native blood vessels. By treating the cells for three days with TGF- β , a transition towards this phenotype was successfully shown.

7 Appendix: Pore size fine-tuning

Note: Experiments within this chapter were mostly performed by Monika Malesa under supervision of L. Weidenbacher. Generated data was included in the master thesis of Monika Malesa.

7.1 Introduction

As introduced in chapter 2, porosity of electrospun membranes is an important parameter determining the potential of cell infiltration and migration. One of the approaches to enhance the porosity of electrospun membranes is the usage of a sacrificial polymer that is simultaneously electrospun/sprayed with the stable polymer phase. After the spinning process, the soluble polymer can be dissolved to increase the pore size and overall porosity of the scaffold. An example for such a two-component membrane can be seen in Figure 7.1. Water-soluble polymers such as polyethylene oxide (PEO) can be utilized since it can easily be processed via electrospinning in a variety of fiber diameters and electrospayed with different droplet sizes. The stable polymer used within this study was polyethylene terephthalate (PET). The potential use as a cell culture scaffold and thus suitability for medical applications was investigated. In fact, PET is utilized as graft material in vascular surgery since decades in a modified version under the brand name Dacron.

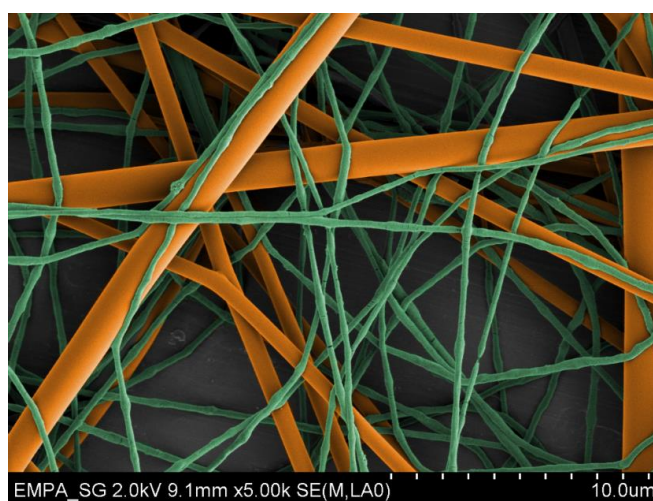


Figure 7.1: SEM image of electrospun membrane

SEM image of a membrane electrospun with two different polymeric phases. The orange fibers were electrospun from a polyethylene terephthalate (PET) solution, the fibers in green from polyethylene oxide (PEO).

7.2 Materials and methods

7.2.1 Materials and reagents

All materials were purchased from Sigma Aldrich (Buchs, Switzerland), unless otherwise noted. All materials were used as received and without any further purification. Cell culture supplements and reagents were from Thermo Fisher Scientific (Waltham, USA) and used as received.

7.2.2 Electrospinning and electrospraying

Electrospinning was performed on a custom-built device. Samples were collected on a planar stainless steel collector. To eject the polymer solution a syringe pump was used (World Precision Instruments, Sarasota, USA, model: Aladin 1000). The syringe was tipped with a 21G needle (B. Braun, Melsungen, Germany). For electrospinning, PET (ELANA PET SP. Z O. O., Poland) was dissolved in hexafluoroisopropanol (HFIP) at a concentration of 15 % w/v. The polymer was ejected at a flow rate of 20 $\mu\text{l min}^{-1}$ with a needle to collector distance of 20 cm. A positive voltage of 13 kV and a negative voltage of 3 kV were applied to the needle and collector, respectively. For the electrospinning/electrospraying of PEO dissolved in water, different molecular weights and process parameters were applied. The solution parameters and process settings can be found in Table 7.1.

Table 7.1: Solution parameters and spinning settings for PEO

PEO concentration [w/v]	3.5 %	4.5 %	6 %	70 %	75 %	80 %	85 %	90 %	100 %	120 %
Molecular weight [M _v]	10 ⁶		6x10 ⁵	2x10 ⁴						
Distance [cm]	25	26	24	15						
Flow rate [$\mu\text{l min}^{-1}$]	50	50	30	50						
Positive voltage	13	15	14	13						
Negative voltage	1									

7.2.3 Capillary flow porometry

To characterize the intrinsic pore size of the polymeric membranes after dissolution of PEO, capillary flow porometry was used (The POROLUX™ 1000, POROMETER nv, Belgium). For each membrane, triplicates were characterized to obtain the final results and compared to pure PET membranes.

7.2.4 Cell culture

A murine myoblast cell line (C2C12, ATCC, Manassas, USA) was used for the cell seeding experiments. Cells were expanded/cultivated in Dulbecco's modified Eagle Medium (DMEM) supplemented with 10% fetal calf serum (FCS) and 1% penicillin (5 mg ml⁻¹)/streptomycin (5 mg ml⁻¹)/neomycin (10 mg ml⁻¹) incubated at 37°C and 5% CO₂ before harvesting and seeding on the PET membranes.

7.2.5 Scanning electron microscopy

The electrospun membranes as well as sprayed particles were analyzed via scanning electron microscopy. Measurements were performed with an acceleration voltage of 2 kV and 10 mA current flow (Hitachi S-4800 (Hitachi High-Technologies, US, Illinois, USA). Samples were sputter coated with an 8 nm thick layer of gold-palladium.

The cell seeded samples were fixed in modified Karnovsky solution (4 % paraformaldehyde, 2.5 % glutaraldehyde) for 1 hour and dehydrated in an ascending ethanol series from 50 % to 100 % (30 – 60 minutes incubation for each concentration) and finally dried in hexamethyldisiloxane for 5 minutes before the sputtering process.

7.2.6 Fluorescence microscopy

C2C12 cells were stained for immunohistochemistry with fluorescent dyes for the nuclei (1:1000, DAPI) and actin (1:40, Alexa Fluor® 488 or 647 Phalloidin, Thermo Fisher Scientific). Prior to staining, samples were blocked (5 % goat serum, 1 % FCS in PBS). Staining was performed in PBS supplemented with 1.5 % w/v skimmed milk (Rapilait, Migros, Switzerland). All samples were subsequently imaged with a confocal laser scanning microscope (CLSM, LSM 780, Zeiss, Germany).

7.3 Results and discussion

7.3.1 Electrospinning/particle spraying

Molecular weight and solution concentrations highly affect the electrospinning process. If the solution viscosity is too low, electrospaying of polymer particles is likely to occur. By utilization of several different molecular weights and adjusting solution concentrations, different fiber diameters/droplet sizes of PEO were obtained. Images of the resulting morphologies can be seen in Figure 7.2. The average fiber diameter of the stable polymer PET was 1.18 μm . Polymer solutions prepared with higher molecular weight PEO allowed for electrospinning of fibers, whereas the different solutions of the low molecular weight PEO resulted in capsule spraying. Interestingly, it could be seen that the capsule diameter was increased from an average of 1.71 μm (70 % w/v) to 3.35 μm (120 % w/v). The increase of the capsule diameter can be explained by the ascending viscosity depending on the polymer concentration (Bock *et al* 2011).

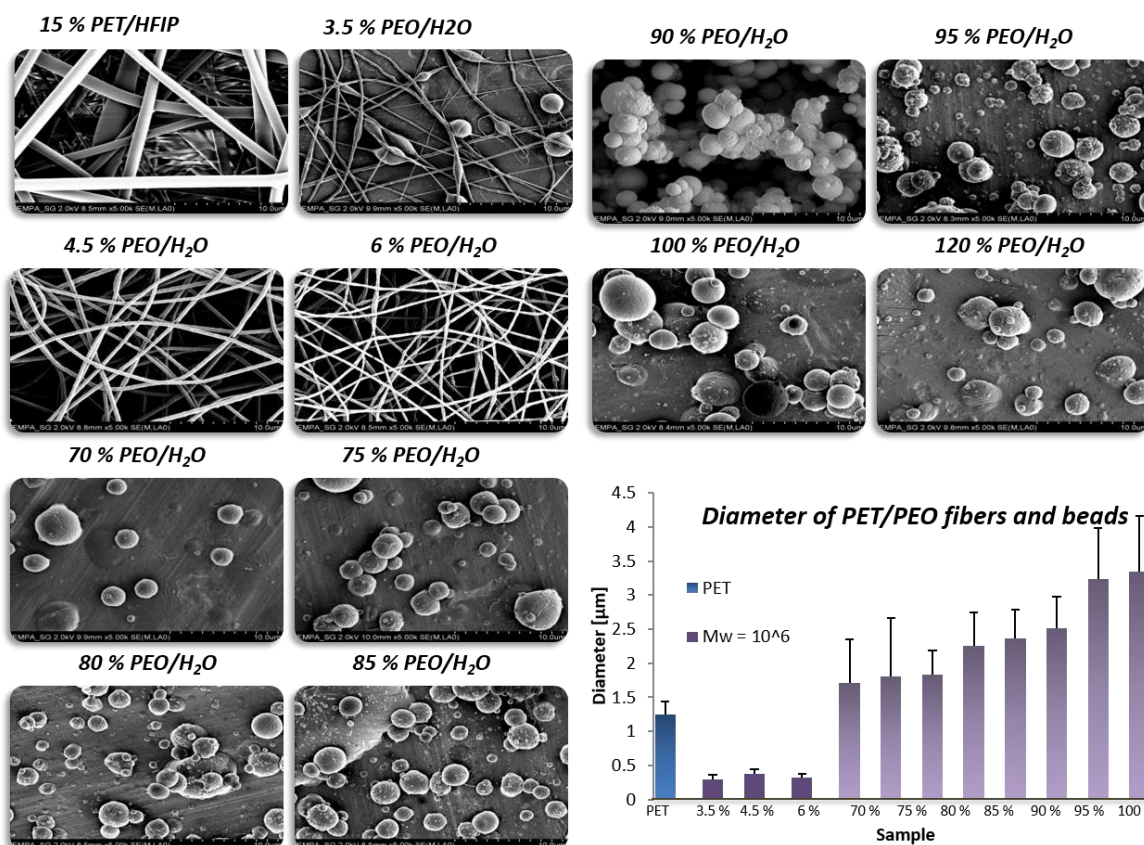


Figure 7.2: Electrospinning and particle spraying

SEM images of the stable electrospun PET fibers and sacrificial electrospun/electrosprayed PEO fibers or droplets respectively. The different solution concentrations and solvent system are depicted in the images. The average fiber diameter and droplet size of the different conditions are plotted in the graph in the bottom right.

7.3.2 Porosity measurements

In a simultaneous electrospinning/PEO particle spraying process, both polymers were collected on a rotating drum. To avoid interference of the polymer jets, both processes were done from opposing sides of the drum. The effect of selected sacrificial PEO fibers/beads (solutions of 4.5 % w/v, 70 % w/v and 120 % w/v) on the final pore size within the electrospun membranes was measured by capillary flow porometry. When the PET membrane was fabricated without a sacrificial component, the average pore size was found to be 2.7 µm. When spinning/spraying

PEO fibers and small particles (sprayed with the 70 % w/v solution) into the membrane the average pore size was slightly enhanced to values of 3.7 μm and 4.0 μm , respectively (Figure 7.3). The membranes, which were prepared with the 120 % w/v solution of PEO revealed the most pronounced increase in average pore size. An increase from 2.7 μm to 6.2 μm was measured. Interestingly, the increase almost perfectly matches with the average particle size, obtained with the spraying process of the PEO.

With the incorporation of a sacrificial component into the electrospun membranes, the potential of tuning the average pore size was successfully shown. However, it is unlikely that cellular infiltration will be observed with pore sizes of 6.2 μm . Wang et al. found that scaffolds with pore sizes of up to 10 μm were still too small to allow for cellular infiltration (Wang *et al* 2016). Yet, cellular infiltration might not only be affected by the average pore size, but also by the network stiffness and the amount of crosslinks between the fibers.

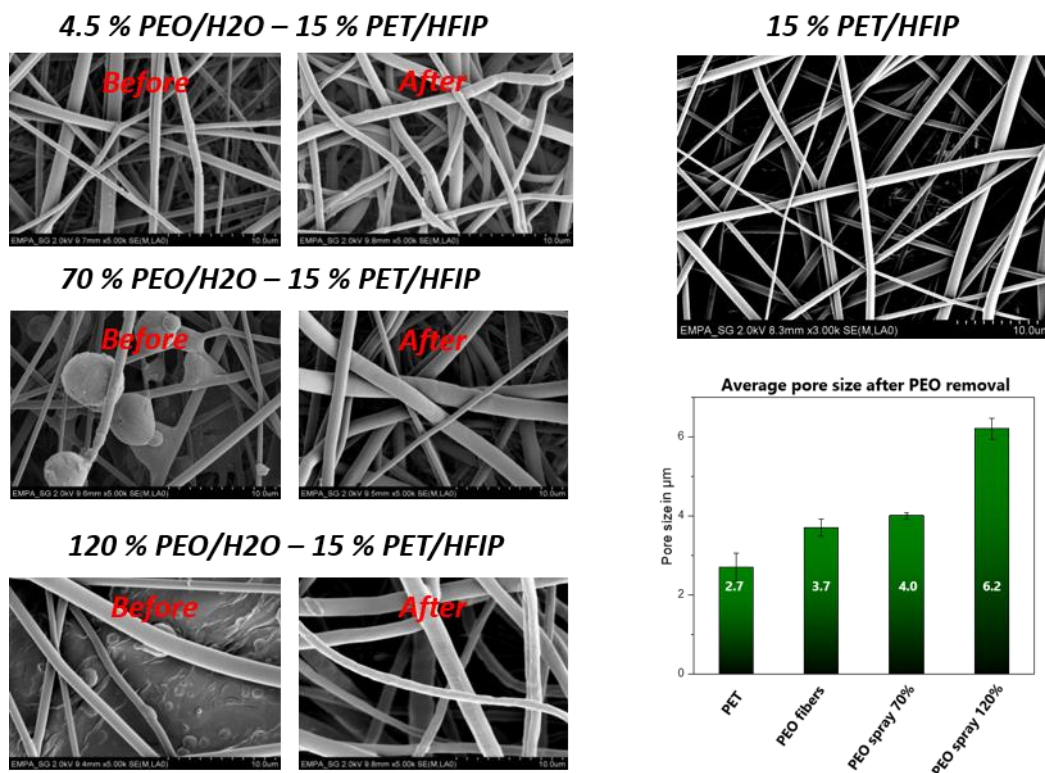


Figure 7.3: Porosity before and after PEO removal

SEM images of PET membranes simultaneously fabricated with electrospinning or electrospraying of PEO, respectively. The membranes were imaged before and after removal of the sacrificial PEO section. In the bottom right, the average pore size of the obtained membranes after the dissolution of PEO is plotted.

7.3.3 Cell culture

In a final set of experiments, the effect of enhanced membrane pore size on the culture of murine myoblasts was investigated. Therefore, PET membranes fabricated without sacrificial component as well as membranes prepared with PEO were compared. Fluorescence microscopy images did not reveal any visible differences in terms of cell attachment, or distribution. On both surfaces, the cells were well attached and spread after three days of culture (Figure 7.4).

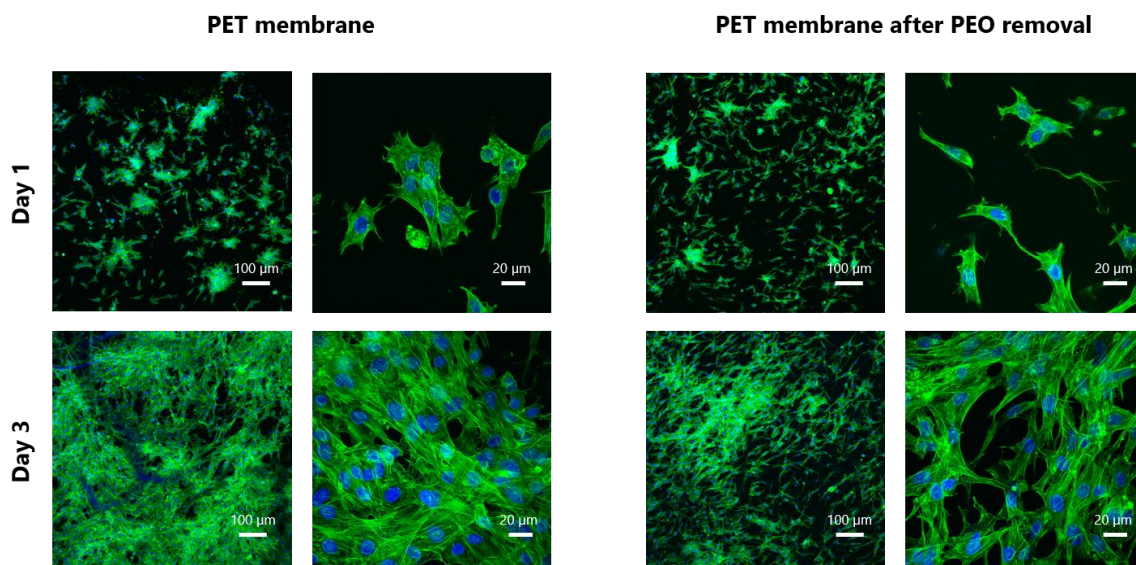


Figure 7.4: Fluorescence images of cells cultured on PET

CLSM images of PET membranes without and with usage of a sacrificial PEO phase. C2C12 myoblast cells were seeded on top of the membrane and stained after 1 and 3 days post seeding. Cells were stained for their nuclei (blue) and the actin skeleton (green).

Both membranes were imaged via electron microscopy after different time points (Figure 7.5). It could be seen that the cells homogeneously attach to the surface of the membranes. Adherent cells attach to the fibrous surface via pseudopodia that are formed, indicating that PET is a suitable scaffold material for cell culture. Closely investigating the pores of the network it was observed that some of the C2C12 cells started to infiltrate the scaffold and were attached to fibers in the lower sections of the membrane. This was only observed for the membranes with enhanced pore size, indicating a beneficial effect of the sacrificial component of the porogen on cellular infiltration.

It needs to be further confirmed, whether an additional increase in membrane pore size further promotes the infiltration of cells. Within the observed range of pore sizes of up to 6.2 μm, only a small amount of cells started to migrate into the superficial pores of the network. Membranes prepared with a sacrificial component were less interconnected than the membranes made of PET only, which might

enable the cells to push away single fibers from the scaffold to migrate to deeper areas of the surface. Boland *et al* described this hypothesis of cell migration into fibrous scaffolds, when cells were found to infiltrate into fibrous membranes with pore sizes lower than 10 μm (Boland *et al* 2004).

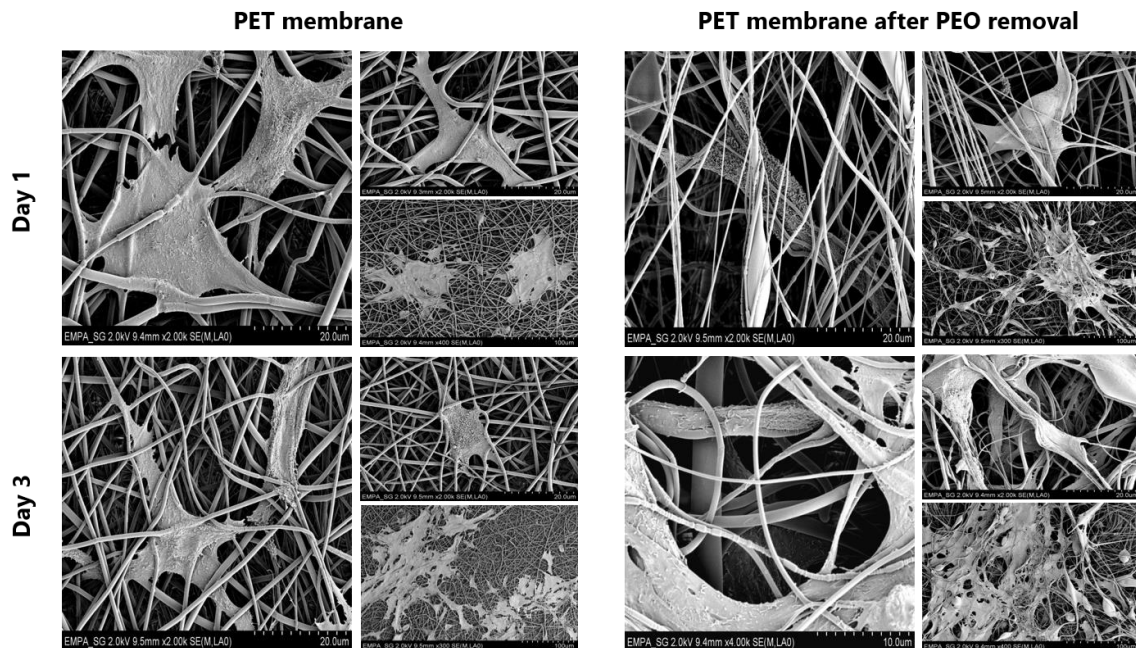


Figure 7.5: SEM images of cells cultured on PET

SEM images of C2C12 myoblasts grown on PET membranes without and with PEO sacrificial phase. Images were taken after 1 and 3 days in culture respectively. Cellular attachment to the fibrous scaffold can be observed. Some cells infiltrating the electrospun membrane that was fabricated with sacrificial PEO can be seen.

7.4 Conclusion

It can be concluded, that a simultaneous electrospinning/particle spraying process with a water-soluble polymer as sacrificial phase enables the fabrication of membranes with enhanced pore sizes. The increase in pore size is directly related to the particle size of the sacrificial PEO. A pore size increase of more than 100 % was achieved with PEO particles of an average size of 3.35 μm . For membranes with increased pore size, a small degree of cellular infiltration was observed. These results need to be further confirmed by fabrication of membranes with even larger pore sizes. These experiments should give additional information about the correlation of pore size and cell infiltration.

8.1 Summary and conclusion

Current issues related to lacking hemocompatibility of artificial surfaces within the field of medical device development were highlighted in the beginning of this thesis. Problems for patients having to rely on vascular prosthesis or cardiac assist devices such as PVADs often suffer from the consequences of adverse reactions of blood with the surface of the graft material. In many cases, the implanted devices or graft materials need to be explanted if the function of the implant is impaired. Apart from the drastic consequences for the patients, revision surgery displays a major cost factor for the health system globally. A major hurdle during the development of novel tailored surfaces is the difficulty to recreate the function of the endothelium as found in the human body, which does not only fulfill several biological functions but also provides the blood vessel with a permanent antithrombotic surface. Therefore, this gap needs to be closed with innovative solutions via biomimetic approaches. Merging the fields of material science, biology and tissue engineering can provide promising solutions to fabricate artificial surfaces that are not only fabricated from a polymeric component, but also selectively include viable cells in a three dimensional arrangement. This hierarchically architecture is envisioned to mimic the function of a native blood vessel in the human body. Even though the development of biomimetic engineering is just starting to enter the markets in selected fields, the topics discussed within this thesis provide information as well as useful thought for researches within the field of biomimetic engineering.

To generally assess the feasibility of introducing viable cells into a fibrous network fabricated via electrospinning, a first study was conducted to investigate the cellular response to the environmental conditions during the electrospinning process. Therefore, in a first set of experiments the utilization of a cell electrospaying process was investigated. Cells were sprayed in an electrostatic field with selected voltages and tested for cell viability and phenotype. Interestingly, the electric field had no negative impact on the viability of the cells. To further assess the cellular response within a three-dimensional construct a layer-by-layer approach of alternating electrospinning and cell electrospaying was

analyzed. It was shown that residual solvent present within and on top of the polymer fibers, had a huge impact on the viability of the cells. To overcome the issues related to residual solvents, a microfluidic cell encapsulation protocol was established to encapsulate the cells within gelatin. The idea was to create a temporal protective vehicle for the cells until the remaining solvents are washed out of the membrane. In fact, this procedure enabled a temporal protection of the cells when they were again simultaneously introduced into the membrane network by the electrospinning procedure. Further development of this scaffold fabrication process might facilitate a new generation of electrospun networks, which can be applied within several fields of tissue engineering.

The fabrication of electrospun blend fibers is an interesting approach to combine multiple materials properties within a single fiber. To investigate the phase separation of two polymers into a coaxial fiber, a study to thoroughly characterize the surface and structure of such a polymer blend fiber was carried out. Structural characterization revealed a coaxial fiber morphology. The surface of the fiber was highly enriched with the fluorinated polymeric components. Further proving the functionality of such a blend fiber, the surfaces of single polymer networks were compared to the surface of the blend fiber membrane in terms of protein adsorption. Due to the presence of the fluorinated polymer at the surface the amount of adsorbed proteins was substantially reduced. These intriguing results led to the decision to further investigate such blend fibers for potential application as a functional surface inside a blood pump. This concept of designing novel blend fibers might be applicable for other polymer systems as well.

Since the surfaces of medical devices should be made of a non-degradable polymer for long-term applications, and to avoid loosening of newly formed tissues or residues of degradable polymers, a potential material candidate for decorating silicone surfaces with electrospun membranes had to be found. Such a composite surface can potentially be applied for the design of a new generation of PVADs with improved hemocompatibility. The previously developed blend fibers revealed promising properties in terms of protein adsorption – a process, which is decisive

for the initiation of blood coagulation. Additional in-depth analysis of the blend fiber structure was conducted and their favorable protein repellent properties were confirmed. In a study of the materials in contact with human blood, it was observed that the previously reported low binding of proteins was also affecting the blood response. In fact, the blend fiber functionalized surface displayed a lower amount of blood coagulation compared to the blank silicone surface. Apart from the biological response due to the surface component, the blend fibers revealed a similar mechanical performance as found for raw polyurethane membranes. To further study the possibility of facilitating a functional layer of endothelial cells on top of the surface, a bioreactor setup was used to induce both, fluid flow as well as cyclic stretch on the ECs cultured on the surface of the composite structure. Tested conditions were similar as they might be on the inside of a PVAD. The cells remained attached and no loss of intracellular bindings was observed. These results were promising, since they further indicate that electrospun fiber surfaces possess the potential to create a biomimetic blood vessel-like surface.

In a native blood vessel, ECs are attached to the basal lamina, which mostly consists of different EMC components such as collagen type IV, laminin and perlecan. To fabricate a truly biomimetic surface, resembling the architecture of a blood vessel, SMCs need to be incorporated into the membrane and provide a collagenous ECM for the ECs to attach. Since the synthesis of collagen is highly dependent on the phenotype of SMCs, a first set of experiments was performed to control the phenotype of SMCs towards a synthetic phenotype during which higher amounts of collagen are generated. By this, the amount of newly formed collagen was enhanced. These preliminary experiments are a step into the right direction to stimulate a suitable environment for ECs that provides surface binding sites for the cells to attach.

8.2 Limitations of this work

Discussing 3D cell infiltrated structures, the question of nutrient supply always arises. One of the critical questions that has to be addressed when applying the process of combined electrospinning and cell electrospaying is how deep the cells can be embedded. Oxygen diffusion is most likely a limiting factor to maintain cellular viability. In the human body, capillaries supply the cells with oxygen and nutrients. It has been reported that any cells are located at least 150 μm from the nearest capillary (Rouwkema *et al* 2009). Within this study, cells were mostly located directly underneath a few layers of polymer fibers, so the question of embedding depth remains to be answered. It is quite likely that the physical properties of the membrane polymer, such as hydrophilicity and surface charge also have an impact on the transport properties via the scaffold. However, it was shown that the porosity as well as pore size of the membranes can be tuned to potentially steer the nutrient transport within the scaffold.

Apart from the supply with nutrients, the electrospaying results should also be repeated with different selected cell types, since the process might have an impact on cells from different origin. Within this study, the experiments were performed with a murine myoblast cell line to prove the concept, as well as with human SMCs. For both cell types, no damage to the cells and no changes in phenotypical gene expression profiles upon differentiation were detectable. However, this needs to be confirmed with more sensitive cell types such as primary cells. Based on literature, it can be assumed that the procedure should not affect different cell types since other reports, e.g. investigating the effect on human brain astrocytoma cells, primary cells or stem cells confirm the feasibility of this approach (Eddaoudi *et al* 2010, Poncelet *et al* 2012).

The blend fibers investigated in this study have proven to enhance the anti-thrombotic properties when compared to pure RTV silicon surfaces. Experiments to assess the response of blood were done for only two hours in Teflon molds on an orbital shaker. It might be necessary to provide more detailed information about

the long-term performance of the electrospun membranes in contact with blood under conditions found within a PVAD. However, due to the limited amount of anticoagulant that can be applied to the blood, longer incubation times are difficult to assess.

The same accounts for the mechanical response of the composite system with the embedded fibers. Cyclic tests were done for 2000 cycles to analyze the response in terms of plastic deformation. Even though no negative effect was observed, the duration of the test is by far not suitable to speculate on the lifetime of an elastic membrane interface within a PVAD. A long-term testing bench would be necessary to study the response for several million cycles.

To this end, both concepts of a combined electrospinning and cell electrospaying process as well as the stable embedding into the silicon surface should be combined. At this stage, a strategy to combine both has not been evaluated. Since the embedding procedure was carried out at elevated temperatures of 60°C the cells cannot be inside the scaffold at this stage, since they would undergo necrosis at such temperatures. A potential strategy is to embed the pure fibers into the RTV membrane and subsequently start with the electrospinning/cell electrospaying process to obtain a gradient structure. It can only be hypothesized that the amount of residual solvents within the fibers during the process is sufficient to facilitate a stable crosslink to the previously embedded membrane.

Novel tissue engineering approaches need to be evaluated in a clinical setting. At this stage, it is difficult to think of a suitable method to test the engineered structures *in vivo*. Since the idea is to use patient derived cells for the final application, it also needs to be considered that the engineering and maturation of the biomimetic surface needs time before it can be used for the desired application. Thus, the method would be limited to patients that can wait for the finalized product. Within the field of cardiovascular disease this time is quite often not given.

8.3 Outlook

Some of the presented approaches and technologies have only been discovered and/or investigated quite recently. The discovery of *in situ* formation of core shell fibers made from a blend polymer solution was shown for the combination of PU with PVDFhfp. The effect of phase separation was explained by the differences in solubility and surface tension. Even though this phenomenon has been dealt with in literature, it needs to be explored whether other properties of functional polymers can be combined. This might enable a whole new class of blend fibers with the potential of combining two or even more polymer specific functionalities.

A suitable material candidate for the surface decoration of silicon for application in a PVAD was found and a protocol to attach fibers to elastic surfaces as a general tool was developed. As a next step, this membrane material needs to be utilized for the incorporation of SMCs to obtain an engineered biomimetic tunica media. Finally, the SMCs need to be stimulated to synthesize their own ECM and thus provide a platform for EC adhesion. Ultimately, it would be interesting to analyze the response of an engineered blood vessel-like surface to blood. If a functional endothelium is presented to the blood interface, no signs of coagulation should be detectable. This envisioned biomimetic structure is suitable for *in vivo* experiments under suitable conditions (ISO 10993-4) (Seyfert *et al* 2002).

Even though some first steps towards a functional biomimetic surface coating that could potentially be used for a new generation of PVADs were done, there is still a lot of work ahead. This thesis provides first interesting insights and results that should be useful for the future design of biomimetic tissues in general and provide new ideas for the electrospinning process and respective communities.

Bibliography

- Abrishamkar A, Paradinas M, Bailo E, Rodriguez-Trujillo R, Pfattner R, Rossi R M, Ocal C, deMello A J, Amabilino D B and Puigmarti-Luis J 2016 Microfluidic Pneumatic Cages: A Novel Approach for In-chip Crystal Trapping, Manipulation and Controlled Chemical Treatment *J. Vis. Exp.* 3–9
- Affrossman S and Stamm M 1998 Topography and Surface Composition of Thin Films of Blends of Polystyrene with Brominated Polystyrenes: Effects of Varying the Degree of Bromination and Annealing *Macromolecules* **31** 6280–8
- Agarwal S, Wendorff J H and Greiner A 2008 Use of electrospinning technique for biomedical applications *Polymer* **49** 5603–21
- Ahmed F, Choudhury N R, Dutta N K, Brito E Abreu S, Zannettino A and Duncan E 2014 Interaction of platelets with poly(vinylidene fluoride-co- hexafluoropropylene) electrospun surfaces *Biomacromolecules* **15** 744–55
- Ahn Y C, Park S K, Kim G T, Hwang Y J, Lee C G, Shin H S and Lee J K 2006 Development of high efficiency nanofilters made of nanofibers *Curr. Appl. Phys.* **6** 1030–5
- Ai H, Mills D K, Jonathan A S and Jones S A 2002 Gelatin-Glutaraldehyde cross-linking on silicone rubber to increase endothelial cell adhesion and growth *Vitr. Cell. Dev. Biol. - Anim.* **38** 487–92
- Aird W C 2008 Endothelium in health and disease *Pharmacol. Reports* **60** 139–43
- Aird W C 2007 Phenotypic heterogeneity of the endothelium: I. Structure, function, and mechanisms *Circ. Res.* **100** 158–73
- Al-Lamki R S, Bradley J R and Pober J S 2008 Endothelial cells in allograft rejection *Transplantation* **86** 1340–8
- Alves P, Cardoso R, Correia T R, Antunes B P, Correia I J and Ferreira P 2014 Surface modification of polyurethane films by plasma and ultraviolet light to improve haemocompatibility for artificial heart valves *Colloids Surfaces B Biointerfaces* **113** 25–32
- Angulakshmi N and Stephan A M 2014 Electrospun trilayer polymeric membranes as separator for lithium-ion batteries *Electrochim. Acta* **127** 167–72
- Atalay A, Sanchez V, Atalay O, Vogt D M, Haufe F, Wood R J and Walsh C J 2017 Batch Fabrication of Customizable Silicone-Textile Composite Capacitive Strain Sensors for Human Motion Tracking *Adv. Mater. Technol.* **2** 1–8

- Aussawasathien D, Dong J-H and Dai L 2005 Electrospun polymer nanofiber sensors *Synth. Met.* **154** 37–40
- Babensee J, Babensee J E, Anderson J, McIntire L, Anderson J M, Mikos A, Mcintire L V and Mikos A G 1998 Host response to tissue engineered devices *Adv. Drug Deliv. Rev.* **33** 111–39
- Babu R, Gill R and Farrar D 2004 Biostability of thoralon left ventricular assist device blood pumping sacs after long-term clinical use *ASAIO J.* **50** 479–84
- Bachmann B J, Bernardi L, Loosli C, Marschewski J, Perrini M, Ehrbar M, Ermanni P, Poulikakos D, Ferrari A and Mazza E 2016 A novel bioreactor system for the assessment of endothelialization on deformable surfaces *Sci. Rep.* **6** 1–15
- Baker B M, Shah R P, Silverstein A M, Esterhai J L, Burdick J A and Mauck R L 2012 Sacrificial nanofibrous composites provide instruction without impediment and enable functional tissue formation *Proc. Natl. Acad. Sci.* **109** 14176–81
- Baker S C, Rohman G, Southgate J and Cameron N R 2009 The relationship between the mechanical properties and cell behaviour on PLGA and PCL scaffolds for bladder tissue engineering *Biomaterials* **30** 1321–8
- Balcells M, Martorell J, Olivé C, Santacana M, Chitalia V, Cardoso A A and Edelman E R 2010 Smooth muscle cells orchestrate the endothelial cell response to flow and injury *Circulation* **121** 2192–9
- Balint R, Cassidy N J and Cartmell S H 2013 Electrical Stimulation: A Novel Tool for Tissue Engineering *Tissue Eng. Part B Rev.* **19** 48–57
- Bartolovic K, Mongkoldhumrongkul N, Waddington S N, Jayasinghe S N and Howe S J 2010 The differentiation and engraftment potential of mouse hematopoietic stem cells is maintained after bio-electrospray *Analyst* **135** 157–64
- Bartzoka V, McDermott M R and Brook M A 1999 Protein - Silicone Interactions *Adv. Mater.* **11** 257–9
- Beachley V, Serpe A, Hepfer G R and Wen X 2013 Surface Functionalization of Electrospun Polyurethane Scaffolds Using Blended Polymer Solutions *J. Biomater. Tissue Eng.* **3** 472–8
- Beamish J A, He P, Kottke-Marchant K and Marchant R E 2010 Molecular Regulation of Contractile Smooth Muscle Cell Phenotype: Implications for Vascular Tissue Engineering *Tissue Eng. Part B Rev.* **16** 467–91
- Bendixen N, Losert S, Adlhart C, Lattuada M and Ulrich A 2014 Membrane – particle interactions in an asymmetric flow field flow fractionation channel studied with titanium dioxide nanoparticles *J. Chromatogr. A* **1334** 92–100

- Bergmeister H, Seyidova N, Schreiber C, Strobl M, Grasl C, Walter I, Messner B, Baudis S, Fröhlich S, Marchetti-Deschmann M, Griesser M, Di Franco M, Krssak M, Liska R and Schima H 2015 Biodegradable, thermoplastic polyurethane grafts for small diameter vascular replacements *Acta Biomater.* **11** 104–13
- Bernardi L, Hopf R, Sibilio D, Ferrari A, Ehret A E and Mazza E 2017 On the cyclic deformation behavior, fracture properties and cytotoxicity of silicone-based elastomers for biomedical applications *Polym. Test.* **60** 117–23
- Bezuidenhout D, Williams D F and Zilla P 2015 Polymeric heart valves for surgical implantation, catheter-based technologies and heart assist devices *Biomaterials* **36** 6–25
- Biran R and Pond D 2017 Heparin coatings for improving blood compatibility of medical devices *Adv. Drug Deliv. Rev.* **112** 12–23
- De Bock K, Georgiadou M and Carmeliet P 2013 Role of endothelial cell metabolism in vessel sprouting *Cell Metab.* **18** 634–47
- Bock N, Woodruff M A, Hutmacher D W and Dargaville T R 2011 Electrospraying, a reproducible method for production of polymeric microspheres for biomedical applications *Polymers (Basel)*, **3** 131–49
- Bogtitzki M, Frese T, Steinhart M, Greiner A, Wendorff J H, Schaper A and Hellwig M 2001 Preparation of Fibers with nanoscaled morphologies: electrospinning of Polymer Blends *Polym. Eng. Sci.* **41** 982–9
- Boland E D, Matthews J A, Pawlowski K J, Simpson D G, Wnek G E and Bowlin G L 2004 Electrospinning collagen and elastin: preliminary vascular tissue engineering *Front. Biosci.* **9** 1422–32
- Bratek-Skicki A, Zeliszewska P, Adamczyk Z and Cieśla M 2013 Human fibrinogen monolayers on latex particles: Role of ionic strength *Langmuir* **29** 3700–10
- Brisbois E J, Major T C, Goudie M J, Bartlett R H, Meyerhoff M E and Handa H 2016 Improved hemocompatibility of silicone rubber extracorporeal tubing via solvent swelling-impregnation of S-nitroso-N-acetylpenicillamine (SNAP) and evaluation in rabbit thrombogenicity model *Acta Biomater.* **37** 111–9
- Brouzes E, Medkova M, Savenelli N, Marran D, Twardowski M, Hutchison J B, Rothberg J M, Link D R, Perrimon N and Samuels M L 2009 Droplet microfluidic technology for single-cell high-throughput screening *PNAS* **106** 14195–200
- Buja L M and Schoen F J 2015 *The Pathology of Cardiovascular Interventions and Devices for Coronary Artery Disease, Vascular Disease, Heart Failure, and Arrhythmias* ed L M Buja and J Butany (New York City (NY): Elsevier)

- Butcher E C and Picker L J 1996 Lymphocyte Homing and Homeostasis *Science* **272**je 60–6
- Carter N A, Jayasinghe S N and Mauri C 2011 Biosprayed spleen cells integrate and function in mouse models *Analyst* **136** 3434–7
- Castner D G and Ratner B D 2002 Biomedical surface science: Foundations to frontiers *Surf. Sci.* **500** 28–60
- Chen M, Le D Q S, Baatrup A, Nygaard J V., Hein S, Bjerre L, Kassem M, Zou X and Bünger C 2011 Self-assembled composite matrix in a hierarchical 3-D scaffold for bone tissue engineering *Acta Biomater.* **7** 2244–55
- Chen N, Koker M K A, Uzun S and Silberstein M N 2016 In-situ X-ray study of the deformation mechanisms of non-woven polypropylene *Int. J. Solids Struct.* **97–98** 200–8
- Chen Y and Kim H 2009 Preparation of superhydrophobic membranes by electrospinning of fluorinated silane functionalized poly(vinylidene fluoride) *Appl. Surf. Sci.* **255** 7073–7
- Cheung Z L, Ng K M, Weng L T, Chan C M and Li L 2006 Crystallization-driven migration of the low surface energy segment of a copolymer to the bulk *Polymer* **47** 3164–70
- Chiu W-C, Slepian M J and Bluestein D 2014 Thrombus Formation Patterns in the HeartMate II VAD-Clinical Observations Can Be Predicted by Numerical Simulations *ASAIO J.* **60** 237–40
- Choi W S, Joung Y K, Lee Y, Bae J W, Park H K, Park Y H, Park J C and Park K D 2016 Enhanced Patency and Endothelialization of Small-Caliber Vascular Grafts Fabricated by Coimmobilization of Heparin and Cell-Adhesive Peptides *ACS Appl. Mater. Interfaces* **8** 4336–46
- Claesson-Welsh L 2015 Vascular permeability - The essentials *Ups. J. Med. Sci.* **120** 135–43
- Clark M B, Burkhardt C A and Gardella J A 1989 *Macromolecules* **22** 4495–501
- Clark M B, Burkhardt C A and Gardella J A 1991 Surface studies of polymer blends. 4. An ESCA, IR, and DSC study of the effect of homopolymer molecular weight on crystallinity and miscibility of poly(ϵ -caprolactone)/poly(vinyl chloride) homopolymer blends *Macromolecules* **24** 799–805
- Clausell-Tormos J, Lieber D, Baret J-C, El-Harrak A, Miller O J, Frenz L, Blouwolff J, Humphry K J, Köster S, Duan H, Holtze C, Weitz D A, Griffiths A D and Merten C A 2008 Article Droplet-Based Microfluidic Platforms for the Encapsulation and Screening of Mammalian Cells and Multicellular Organisms *Chem. Biol.* **15** 427–37
- Costa L M M, Bretas R E S and Gregorio R 2010 Effect of Solution Concentration on the Electrospay/Electrospinning Transition and on the Crystalline Phase of PVDF *Mater. Sci. Appl.* **1** 247–52

- Croisier F, Atanasova G, Poumay Y and Jérôme C 2014 Polysaccharide-Coated PCL Nanofibers for Wound Dressing Applications *Adv. Healthc. Mater.* **3** 2032–9
- Cui Z, Hassankiadeh N T, Zhuang Y, Drioli E and Lee Y M 2015 Crystalline polymorphism in poly(vinylidene fluoride) membranes *Prog. Polym. Sci.* **51** 94–126
- Dagher Z, Ruderman N, Tornheim K and Ido Y 2001 Acute Regulation of Fatty Acid Oxidation and AMP-Activated Protein Kinase in Human Umbilical Vein Endothelial Cells *Circ. Res.* **88** 1276–82
- Dalton P D, Klinkhammer K, Salber J, Klee D and Möller M 2006 Direct in vitro electrospinning with polymer melts *Biomacromolecules* **7** 686–90
- Das S, Pati F, Choi Y J, Rijal G, Shim J H, Kim S W, Ray A R, Cho D W and Ghosh S 2015 Bioprintable, cell-laden silk fibroin-gelatin hydrogel supporting multilineage differentiation of stem cells for fabrication of three-dimensional tissue constructs *Acta Biomater.* **11** 233–46
- Deitzel J M, Kosik W, McKnight S H, Beck Tan N C, DeSimone J M and Crette S 2002 Electrospinning of polymer nanofibers with specific surface chemistry *Polymer* **43** 1025–9
- Deutsch M, Meinhart J, Zilla P, Howanietz N, Gorlitzer M, Froeschl A, Stuempflen A, Bezuidenhout D and Grabenwoeger M 2009 Long-term experience in autologous in vitro endothelialization of infrainguinal ePTFE grafts *J. Vasc. Surg.* **49** 352–62
- Dhandayuthapani B, Yoshida Y, Maekawa T and Kumar D S 2011 Polymeric scaffolds in tissue engineering application: A review *Int. J. Polym. Sci.* **2011**
- Ding N, Pacetti S D, Tang F W, Gada M and Roorda W 2009 XIENCE V™ stent design and rationale *J. Interv. Cardiol.* **22** 18–27
- Dittrich P S and Manz A 2006 Lab-on-a-chip: Microfluidics in drug discovery *Nat. Rev. Drug Discov.* **5** 210–8
- Duan B 2017 State-of-the-Art Review of 3D Bioprinting for Cardiovascular Tissue Engineering *Ann. Biomed. Eng.* **45** 195–209
- Dunitz J D and Taylor R 1997 Organic Fluorine Hardly Ever Accepts Hydrogen Bonds *Chem. Eur. J.* **3** 89–98
- Eckman P M and John R 2012 Bleeding and thrombosis in patients with continuous-flow ventricular assist devices *Circulation* **125** 3038–47
- Eddaoudi A, Townsend-Nicholson A, Timms J F, Schorge S and Jayasinghe S N 2010 Molecular characterisation of post-bio-electrosprayed human brain astrocytoma cells *Analyst* **135** 2600–12

- Eelen G, De Zeeuw P, Simons M and Carmeliet P 2015 Endothelial cell metabolism in normal and diseased vasculature *Circ. Res.* **116** 1231–44
- Ekaputra A K, Prestwich G D, Cool S M and Hutmacher D W 2008 Combining electrospun scaffolds with electrosprayed hydrogels leads to three-dimensional cellularization of hybrid constructs *Biomacromolecules* **9** 2097–103
- Ercolani E, Del Gaudino C and Bianco A 2015 Vascular tissue engineering of small-diameter blood vessels: reviewing the electrospinning approach *J. Tissue Eng. Regen. Med.* **9** 861–88
- Falde E J, Yohe S T, Colson Y L and Grinstaff M W 2016 Superhydrophobic materials for biomedical applications *Biomaterials* **104** 87–103
- Féléto M 2011 *The Endothelium, Part1: Multiple functions of the endothelial cells-Focus on endothelium-derived vasoactive mediators* (San Rafael (CA): Morgan & Claypool Life Sciences)
- Feng D, Nagy J A, Dvorak H F and Dvorak A M 2002 Ultrastructural studies define soluble macromolecular, particulate, and cellular transendothelial cell pathways in venules, lymphatic vessels, and tumor-associated microvessels in man and animals *Microsc. Res. Tech.* **57** 289–326
- Fortunato G, Guex A G, Popa A M, Rossi R M and Hufenus R 2014 Molecular weight driven structure formation of PEG based e-spun polymer blend fibres *Polymer* **55** 3139–48
- Fuhrer R, Schumacher C M, Zeltner M and Stark W J 2013 Soft iron/silicon composite tubes for magnetic peristaltic pumping: Frequency-dependent pressure and volume flow *Adv. Funct. Mater.* **23** 3845–9
- Furie B and Furie B C 2008 Mechanisms of Thrombus Formation *N. Engl. J. Med.* **359** 938–49
- Galley H F and Webster N R 2004 Physiology of the endothelium *Br. J. Anaesth.* **93** 105–13
- Ganesan M K, Finsterwalder R, Leb H, Resch U, Neumüller K, de Martin R and Petzelbauer P 2017 Three-Dimensional Coculture Model to Analyze the Cross Talk Between Endothelial and Smooth Muscle Cells *Tissue Eng. Part C Methods* **23** 38–49
- Gaudreault N, Scriven D R L, Laher I and Moore E D W 2008 Subcellular characterization of glucose uptake in coronary endothelial cells *Microvasc. Res.* **75** 73–82
- Ge J, Si Y, Fu F, Wang J, Yang J, Cui L, Ding B, Yu J and Sun G 2013 Amphiphobic fluorinated polyurethane composite microfibrinous membranes with robust waterproof and breathable performances *RSC Adv.* **3** 2248–55

- Gitlin I, Carbeck J D and Whitesides G M 2006 Why are proteins charged? Networks of charge-charge interactions in proteins measured by charge ladders and capillary electrophoresis *Angew. Chemie - Int. Ed.* **45** 3022–60
- Griffin D R, Weaver W M, Scumpia P O, Di Carlo D and Segura T 2015 Accelerated wound healing by injectable microporous gel scaffolds assembled from annealed building blocks *Nat. Mater.* **14** 737–44
- Griffith L G and Swartz M A 2006 Capturing complex 3D tissue physiology in vitro *Nat. Rev. Mol. Cell Biol.* **7** 211–24
- Guex A G, Fortunato G, Hegemann D, Tevaearai H T and Giraud M-N 2013 General Protocol for the Culture of Cells on Plasma-Coated Electrospun Scaffolds *Methods Mol. Biol.* ed K Turksen (Totowa, NJ: Humana Press) pp 119–31
- Guex A G, Frobert A, Valentin J, Fortunato G, Hegemann D, Cook S, Carrel T P, Tevaearai H T and Giraud M N 2014 Plasma-functionalized electrospun matrix for biograft development and cardiac function stabilization *Acta Biomater.* **10** 2996–3006
- Guex A G, Kocher F M, Fortunato G, Körner E, Hegemann D, Carrel T P, Tevaearai H T and Giraud M N 2012a Fine-tuning of substrate architecture and surface chemistry promotes muscle tissue development *Acta Biomater.* **8** 1481–9
- Guex A G, Kocher F M, Fortunato G, Körner E, Hegemann D, Carrel T P, Tevaearai H T and Giraud M N 2012b Fine-tuning of substrate architecture and surface chemistry promotes muscle tissue development *Acta Biomater.* **8** 1481–9
- Guex A G, Weidenbacher L, Maniura-Weber K, Rossi R M and Fortunato G 2017 Hierarchical Self-Assembly of Poly(Urethane)/Poly(Vinylidene Fluoride-co-Hexafluoropropylene) Blends into Highly Hydrophobic Electrospun Fibers with Reduced Protein Adsorption Profiles *Macromol. Mater. Eng.* **302** 1–8
- Guo H F, Li Z S, Dong S W, Chen W J, Deng L, Wang Y F and Ying D J 2012 Piezoelectric PU/PVDF electrospun scaffolds for wound healing applications *Colloids Surfaces B Biointerfaces* **96** 29–36
- Handa H, Major T C, Brisbois E J, Amoako K A, Meyerhoff M E and Bartlett R H 2014 Hemocompatibility comparison of biomedical grade polymers using rabbit thrombogenicity model for preparing nonthrombogenic nitric oxide releasing surfaces *J. Mater. Chem. B* **2** 1059–67
- Hardman S J, Muhamad-Sarih N, Riggs H J, Thompson R L, Rigby J, Bergius W N A and Hutchings L R 2011 Electrospinning superhydrophobic fibers using surface segregating end-functionalized polymer additives *Macromolecules* **44** 6461–70

- Harjes U, Bensaad K and Harris A L 2012 Endothelial cell metabolism and implications for cancer therapy *Br. J. Cancer* **107** 1207–12
- Harter K, Levine M and Henderson S 2015 Anticoagulation Drug Therapy: A Review *West. J. Emerg. Med.* **16** 11–7
- Hasan A, Memic A, Annabi N, Hossain M, Paul A, Dokmeci M R, Dehghani F and Khademhosseini A 2014 Electrospun scaffolds for tissue engineering of vascular grafts *Acta Biomater.* **10** 11–25
- Hasebe T, Yohena S, Kamijo Y, Okazaki Y, Hotta A, Takahashi K and Suzuki T 2007 Fluorine doping into diamond-like carbon coatings inhibits protein adsorption and platelet activation *J. Biomed. Mater. Res. Part A* **83A** 1192–9
- Heo Y, Shin Y M, Lee Y Bin, Lim Y M and Shin H 2015 Effect of immobilized collagen type IV on biological properties of endothelial cells for the enhanced endothelialization of synthetic vascular graft materials *Colloids Surfaces B Biointerfaces* **134** 196–203
- Hernández R M, Orive G, Murua A and Pedraz J L 2010 Microcapsules and microcarriers for in situ cell delivery *Adv. Drug Deliv. Rev.* **62** 711–30
- Hillel A, Shah P and Elisseeff J 2007 *Hydrogels in cell encapsulation and tissue engineering in biomedical polymers* ed M Jenkins (Sawston (UK): Woodhead Publishing Limited)
- Van Hinsbergh V W M 2012 Endothelium - Role in regulation of coagulation and inflammation *Semin. Immunopathol.* **34** 93–106
- Hogg N and Berlin C 1995 Structure and function of adhesion receptors in leukocyte trafficking *Immunol. Today* **16** 327–30
- Hollister S J 2005 Porous scaffold design for tissue engineering *Nat. Mater.* **4** 518–24
- Hong J, Demello A J and Jayasinghe S N 2010 Bio-electrospraying and droplet-based microfluidics: Control of cell numbers within living residues *Biomed. Mater.* **5**
- Hopf R, Bernardi L, Menze J, Zündel M, Mazza E and Ehret A E 2016 Experimental and theoretical analyses of the age-dependent large-strain behavior of Sylgard 184 (10:1) silicone elastomer *J. Mech. Behav. Biomed. Mater.* **60** 425–37
- Hsiai T K 2008 Mechanical transduction coupling between endothelial and smooth muscle cells: role of hemodynamic forces *Am. J. Physiol. Cell Physiol.* **294** C695–C661
- Hutmacher D W 2000 Scaffolds in tissue engineering bone and cartilage *Biomaterials* **21** 2529–43

- Inoguchi H, Tanaka T, Maehara Y and Matsuda T 2007 The effect of gradually graded shear stress on the morphological integrity of a huvec-seeded compliant small-diameter vascular graft *Biomaterials* **28** 486–95
- Ippel B D and Dankers P Y W 2018 Introduction of Nature's Complexity in Engineered Blood-compatible Biomaterials *Adv. Healthc. Mater.* **7** 1–17
- Isenberg W M, McEver R P, Phillips D R, Shuman M A and Bainton D F 1987 The platelet fibrinogen receptor: An immunogold-surface replica study of agonist-induced ligand binding and receptor clustering *J. Cell Biol.* **104** 1655–63
- Jafari M, Paknejad Z, Rad M R, Motamedian S R, Eghbal M J, Nadjmi N and Khojasteh A 2017 Polymeric scaffolds in tissue engineering: a literature review *J. Biomed. Mater. Res. - Part B Appl. Biomater.* **105** 431–59
- Jahangir A R, McClung W G, Cornelius R M, McCloskey C B, Brash J L and Santerre J P 2002 Fluorinated surface-modifying macromolecules: Modulating adhesive protein and platelet interactions on a polyether-urethane *J. Biomed. Mater. Res.* **60** 135–47
- Jakovljevic D G, Yacoub M H, Schueler S, MacGowan G A, Velicki L, Seferovic P M, Hothi S, Tzeng B H, Brodie D A, Birks E and Tan L B 2017 Left Ventricular Assist Device as a Bridge to Recovery for Patients With Advanced Heart Failure *J. Am. Coll. Cardiol.* **69** 1924–33
- Janik H and Marzec M 2015 A review: Fabrication of porous polyurethane scaffolds *Mater. Sci. Eng. C* **48** 586–91
- Jennette J C and Stone J R 2014 *Diseases of Medium-Sized and Small Vessels* ed M S Willis, J W Homeister and J R Stone (New York City (NY): Elsevier)
- Ji S and Guvendiren M 2017 Recent Advances in Bioink Design for 3D Bioprinting of Tissues and Organs *Front. Bioeng. Biotechnol.* **5** 1–8
- St. John K R 2014 The use of polyurethane materials in the surgery of the spine: A review *Spine J.* **14** 3038–47
- Jun H W and West J 2004 Development of a YIGSR-peptide-modified polyurethaneurea to enhance endothelialization *J. Biomater. Sci. Polym. Ed.* **15** 73–94
- Jun Y, Kang E, Chae S and Lee S-H 2014 Microfluidic spinning of micro- and nano-scale fibers for tissue engineering *Lab Chip* **14** 2146–60
- Kidoaki S, Kwon I K and Matsuda T 2005 Structural Features and Mechanical Properties of In Situ-Bonded Meshes of Segmented Polyurethane Electrospun from Mixed Solvents *J. Biomed. Mater. Res. Part B Appl. Biomater.* **76B** 219–29

- Kirklin J K, Naftel D C, Kormos R L, Stevenson L W, Pagani F D, Miller M A, Timothy Baldwin J and Young J B 2013 Fifth INTERMACS annual report: Risk factor analysis from more than 6,000 mechanical circulatory support patients *J. Hear. Lung Transplant.* **32** 141–56
- Kohn S, Nagy J A, Dvorak H F and Dvorak A M 1992 Pathways of macromolecular tracer transport across venules and small veins. Structural basis for the hyperpermeability of tumor blood vessels *Lab Invest.* **67** 596–607
- Krabatsch T, Schweiger M, Dandel M, Stepanenko A, Drews T, Potapov E, Pasic M, Weng Y G, Huebler M and Hetzer R 2011 Is bridge to recovery more likely with pulsatile left ventricular assist devices than with nonpulsatile-flow systems? *Ann. Thorac. Surg.* **91** 1335–41
- Krishnan R, Alexander M, Robles L, Foster C E and Lakey J R T 2014 Islet and stem cell encapsulation for clinical transplantation *Rev. Diabet. Stud.* **11** 84–101
- Kroll M H, Hellums D J, McIntire L V, Schafer A I and Moake J L 1996 Platelets and shear stress *Blood* **88** 1525–41
- Kumar V, Brewster L, Caves J and Chaikof E 2011 Tissue engineering of blood vessels: functional requirements, progress, and future challenges *Cardiovasc. Eng Technol* **2** 137–48
- Lalia B S, Guillen-Burrieza E, Arafat H A and Hashaikeh R 2013 Fabrication and characterization of polyvinylidene fluoride-co-hexafluoropropylene (PVDF-HFP) electrospun membranes for direct contact membrane distillation *J. Memb. Sci.* **428** 104–15
- Lamalice L, Le Boeuf F and Huot J 2007 Endothelial cell migration during angiogenesis *Circ. Res.* **100** 782–94
- Lareu R R, Subramhanya K H, Peng Y, Benny P, Chen C, Wang Z, Rajagopalan R and Raghunath M 2007 Collagen matrix deposition is dramatically enhanced in vitro when crowded with charged macromolecules: The biological relevance of the excluded volume effect *FEBS Lett.* **581** 2709–14
- Lee D-H, Jang M and Park J-K 2014 Rapid one-step purification of single-cells encapsulated in alginate microcapsules from oil to aqueous phase using a hydrophobic filter paper: Implications for single-cell experiments *Biotechnol. J.* **9** 1233–40
- Lee K, Lee B, Kim C, Kim H, Kim K and Nah C 2005 Stress-strain behavior of the electrospun thermoplastic polyurethane elastomer fiber mats *Macromol. Res.* **13** 441–5
- Legnani C, Ventura A, Terzaghi C, Borgo E and Albisetti W 2010 Anterior cruciate ligament reconstruction with synthetic grafts. A review of literature *Int. Orthop.* **34** 465–71

- Lei Y G, Cheung Z L, Ng K M, Li L, Weng L T and Chan C M 2003 Surface chemical and morphological properties of a blend containing semi-crystalline and amorphous polymers studied with ToF-SIMS, XPS and AFM *Polymer* **44** 3883–90
- Letnik I, Avrahami R, Rokem J S, Greiner A, Zussman E and Greenblatt C 2015 Living Composites of Electrospun Yeast Cells for Bioremediation and Ethanol Production *Biomacromolecules* **16** 3322–8
- Levick J R 1991 *An introduction to cardiovascular physiology* (Oxford (UK): Butterworth-Heinemann)
- Ley K, Laudanna C, Cybulsky M I and Nourshargh S 2007 Getting to the site of inflammation: The leukocyte adhesion cascade updated *Nat. Rev. Immunol.* **7** 678–89
- Li L, Chan C-M and Weng L-T 1998 The effects of specific interactions on the surface structure and composition of miscible blends of poly(vinyl alcohol) and poly(N-vinyl-2-pyrrolidone) *Polymer* **39** 2355–60
- Li M, Neoh K G, Kang E T, Lau T and Chiong E 2014a Surface modification of silicone with covalently immobilized and crosslinked agarose for potential application in the inhibition of infection and omental wrapping *Adv. Funct. Mater.* **24** 1631–43
- Li M, Neoh K G, Xu L Q, Wang R, Kang E T, Lau T, Olszyna D P and Chiong E 2012 Surface modification of silicone for biomedical applications requiring long-term antibacterial, antifouling, and hemocompatible properties *Langmuir* **28** 16408–22
- Li Y-F, Rubert M, Aslan H, Yu Y, Howard K A, Dong M, Besenbacher F and Chen M 2014b Ultraporous interweaving electrospun microfibers from PCL-PEO binary blends and their inflammatory responses *Nanoscale* **6** 3392
- Liao Y, Wang R and Fane A G 2014 Fabrication of Bioinspired Composite Nanofiber Membranes with Robust Superhydrophobicity for Direct Contact Membrane Distillation *Environ. Sci. Technol.* **48** 6335–41
- Lin G, Guo D, Xie G, Jia Q and Pan G 2015 In situ observation of colloidal particle behavior between two planar surfaces *Colloids Surfaces A Physicochem. Eng. Asp.* **482** 656–61
- Lin Q, Ding X, Qiu F, Song X, Fu G and Ji J 2010 In situ endothelialization of intravascular stents coated with an anti-CD34 antibody functionalized heparin-collagen multilayer *Biomaterials* **31** 4017–25
- Liu C Z, Xia Z D, Han Z W, Hulley P A, Triffitt J T and Czernuszka J T 2008 Novel 3D collagen scaffolds fabricated by indirect printing technique for tissue engineering *J. Biomed. Mater. Res. - Part B Appl. Biomater.* **85** 519–28

- Liu Q, Tian S, Zhao C, Chen X, Lei I, Wang Z and Ma P X 2015a Porous nanofibrous poly(l-lactic acid) scaffolds supporting cardiovascular progenitor cells for cardiac tissue engineering *Acta Biomater.* **26** 105–14
- Liu S, Jiang M, Chan C-M and Weng L-T 2001 Elimination of Surface Enrichment in Polymer Blends via Interpolymer Complexation *Macromolecules* **34** 3802–4
- Liu W Y, S T and Xia Y N 2012 Electrospun Nanofibers for Regenerative Medicine *Adv. Healthc. Mater.* **1** 10–25
- Liu X, Lin T, Fang J, Yao G, Zhao H, Dodson M and Wang X 2010 In vivo wound healing and antibacterial performances of electrospun nanofibre membranes *J. Biomed. Mater. Res. - Part A* **94** 499–508
- Liu Y, Lu J, Li H, Wei J and Li X 2015b Engineering blood vessels through micropatterned co-culture of vascular endothelial and smooth muscle cells on bilayered electrospun fibrous mats with pDNA inoculation *Acta Biomater.* **11** 114–25
- Louis S F and Zahradka P 2010 Vascular smooth muscle cell motility: From migration to invasion *Exp. Clin. Cardiol.* **15**
- Lu T, Li Y and Chen T 2013 Techniques for fabrication and construction of three-dimensional scaffolds for tissue engineering *Int. J. Nanomedicine* **8** 337–50
- Di Luca A, Szlazak K, Lorenzo-Moldero I, Ghebes C A, Lepedda A, Swieszkowski W, Van Blitterswijk C and Moroni L 2016 Influencing chondrogenic differentiation of human mesenchymal stromal cells in scaffolds displaying a structural gradient in pore size *Acta Biomater.* **36** 210–9
- Luscinskas F W, Ma S, Nusrat A, Parkos C A and Shaw S K 2002 The role of endothelial cell lateral junctions during leukocyte trafficking *Immunol. Rev.* **186** 57–67
- Ma P X 2004 Scaffolds for tissue fabrication *Mater. Today* **7** 30–40
- Maitz M F 2015 Applications of synthetic polymers in clinical medicine *Biosurface and Biotribology* **1** 161–76
- Marshall B T, Long M, Piper J W, Yago T, McEver R P and Zhu C 2003 Direct observation of catch bonds involving cell-adhesion molecules *Nature* **423** 190–3
- Martinez-Lemus L A 2012 The dynamic structure of arterioles *Basic Clin. Pharmacol. Toxicol.* **110** 5–11
- Martins P M, Ribeiro S, Ribeiro C, Sencadas V, Gomes A C, Gama F M and Lanceros-Méndez S 2013 Effect of poling state and morphology of piezoelectric poly(vinylidene fluoride) membranes for skeletal muscle tissue engineering *RSC Adv.* **3** 17938–44

- Massa T M, Yang M L, Ho J Y C, Brash J L and Santerre J P 2005 Fibrinogen surface distribution correlates to platelet adhesion pattern on fluorinated surface-modified polyetherurethane *Biomaterials* **26** 7367–76
- Mazutis L, Baret J C, Treacy P, Skhiri Y, Araghi A F, Ryckelynck M, Taly V and Griffiths A D 2009 Multi-step microfluidic droplet processing: Kinetic analysis of an in vitro translated enzyme *Lab Chip* **9** 2902–8
- Mazutis L, Gilbert J, Ung W L, Weitz D A, Griffiths A D and Heyman J A 2013 Single-cell analysis and sorting using droplet-based microfluidics *Nat. Protoc.* **8** 870–91
- McAllister T N, Maruszewski M, Garrido S A, Wystrychowski W, Dusserre N, Marini A, Zagalski K, Fiorillo A, Avila H, Manglano X, Antonelli J, Kocher A, Zembala M, Cierpka L, de la Fuente L M and L'Heureux N 2009 Effectiveness of haemodialysis access with an autologous tissue-engineered vascular graft: a multicentre cohort study *Lancet* **373** 1440–6
- Medvedev A E, Samsonov V I and Fomin V M 2006 Rational structure of blood vessels *J. Appl. Mech. Tech. Phys.* **47** 324–9
- Mei Y, Yao C and Li X 2014 A simple approach to constructing antibacterial and anti-biofouling nanofibrous membranes *Biofouling* **30** 313–22
- de Mel A, Cousins B G and Seifalian A M 2012 Surface modification of biomaterials: A quest for blood compatibility *Int. J. Biomater.* **2012** 1–8
- de Mel A, Jell G, Stevens M M and Seifalian A M 2008 Biofunctionalization of biomaterials for accelerated in situ endothelialization: A review *Biomacromolecules* **9** 2969–79
- Michiels C 2003 Endothelial cell functions *J. Cell. Physiol.* **196** 430–43
- Milleret V, Hefti T, Hall H, Vogel V and Eberli D 2012 Influence of the fiber diameter and surface roughness of electrospun vascular grafts on blood activation *Acta Biomater.* **8** 4349–56
- Ming W, Tian M, Van De Grampel R D, Melis F, Jia X, Loos J and Van Der Linde R 2002 Low surface energy polymeric films from solventless liquid oligoesters and partially fluorinated isocyanates *Macromolecules* **35** 6920–9
- Mitchell S L and Niklason L E 2003 Requirements for growing tissue-engineered vascular grafts *Cardiovasc. Pathol.* **12** 59–64
- Mollá S and Compañ V 2011 Polyvinyl alcohol nanofiber reinforced Nafion membranes for fuel cell applications *J. Memb. Sci.* **372** 191–200
- Moncada S and Higgs A 2006 *The Vascular Endothelium II* (Berlin: Springer)

- Motherwell J M, Anderson C R and Murfee W L 2018 Endothelial Cell Phenotypes are Maintained during Angiogenesis in Cultured Microvascular Networks *Sci. Rep.* **8** 1–11
- Muñoz-Chápuli R, Quesada A R and Medina M Á 2004 Angiogenesis and signal transduction in endothelial cells *Cell. Mol. Life Sci.* **61** 2224–43
- Murad S, Grove D, Lindberg K A, Reynolds G, Sivarajah A and Pinnell S R 1981 Regulation of collagen synthesis by ascorbic acid. *Proc. Natl. Acad. Sci.* **78** 2879–82
- Murphy C M, Haugh M G and O'Brien F J 2010 The effect of mean pore size on cell attachment, proliferation and migration in collagen-glycosaminoglycan scaffolds for bone tissue engineering *Biomaterials* **31** 461–6
- Nagy J A, Benjamin L, Zeng H, Dvorak A M and Dvorak H F 2008 Vascular permeability, vascular hyperpermeability and angiogenesis *Angiogenesis* **11** 109–19
- Nam J, Huang Y, Agarwal S and Lannutti J 2007 Improved Cellular Infiltration in Electrospun Fiber via Engineered Porosity *Tissue Eng.* **13** 2249–57
- Nam J, Huang Y, Agarwal S and Lannutti J 2008 Materials Selection and Residual Solvent Retention in Biodegradable Electrospun Fibers *J. Appl. Polym. Sci.* **107** 1547–54
- Nguyen K T and West J L 2002 Photopolymerizable hydrogels for tissue engineering applications *Biomaterials* **23** 4307–14
- Nonckreman C J, Fleith S, Rouxhet P G and Dupont-Gillain C C 2010 Competitive adsorption of fibrinogen and albumin and blood platelet adhesion on surfaces modified with nanoparticles and/or PEO *Colloids Surfaces B Biointerfaces* **77** 139–49
- Norotte C, Marga F S, Niklason L E and Forgacs G 2009 Scaffold-free vascular tissue engineering using bioprinting *Biomaterials* **30** 5910–7
- O'Brien F J 2011 Biomaterials & scaffolds for tissue engineering *Mater. Today* **14** 88–95
- O'Connor C M and Adams J U 2010 *Essentials of Cell Biology* (Cambridge (MA): NPG Education)
- O'Hagan D 2008 Understanding organofluorine chemistry. An introduction to the C–F bond *Chem. Soc. Rev.* **37** 308–19
- Owen M J and Smith P J 1994 Plasma treatment of polydimethylsiloxane *J. Adhes. Sci. Technol.* **8** 1063–75

- Paletta J R J, Mack F, Schenderlein H, Theisen C, Schmitt J, Wendorff J H, Agarwal S, Fuchs-Winkelmann S and Schofer M D 2011 Incorporation of osteoblasts (MG63) into 3D nanofibre matrices by simultaneous electrospinning and spraying in bone tissue engineering *Eur. Cells Mater.* **21** 384–95
- Park H, Bhalla R, Saigal R, Radisic M, Watson N, Langer R and Vunjak-Novakovic G 2008 Effects of electrical stimulation in C2C12 muscle constructs *J. Tissue Eng. Regen. Med.* **2** 279–87
- Park J H, Hong J M, Ju Y M, Jung J W, Kang H W, Lee S J, Yoo J J, Kim S W, Kim S H and Cho D W 2015 A novel tissue-engineered trachea with a mechanical behavior similar to native trachea *Biomaterials* **62** 106–15
- Park S J, Milano C A, Tatoes A J, Rogers J G, Adamson R M, Steidley D E, Ewald G A, Sundareswaran K S, Farrar D J and Slaughter M S 2012 Outcomes in advanced heart failure patients with left ventricular assist devices for destination therapy *Circ. Hear. Fail.* **5** 241–8
- Park S Y, Kim Y J and Kwak S-Y 2016 Versatile surface charge-mediated anti-fouling UF/MF membrane comprising charged hyperbranched polyglycerols (HPGs) and PVDF membranes *RSC Adv.* **6** 88959–66
- Pashneh-Tala S, MacNeil S and Claeysens F 2015 The Tissue-Engineered Vascular Graft—Past, Present, and Future *Tissue Eng. Part B Rev.* **22** 68–99
- Patel S U, Patel S U and Chase G G 2013 Electrospun superhydrophobic poly(vinylidene fluoride- co -hexafluoropropylene) fibrous membranes for the separation of dispersed water from ultralow sulfur diesel *Energy and Fuels* **27** 2458–64
- Pezzoli D, Cauli E, Chevallier P, Farè S and Mantovani D 2017 Biomimetic coating of cross-linked gelatin to improve mechanical and biological properties of electrospun PET: A promising approach for small caliber vascular graft applications *J. Biomed. Mater. Res. - Part A* **105** 2405–15
- Pober J S, Min W and Bradley J R 2009 Mechanisms of Endothelial Dysfunction, Injury, and Death *Annu. Rev. Pathol. Mech. Dis.* **4** 71–95
- Pollard T D, Earnshaw W C, Lippincott-Schwartz J and Johnson G T 2008 *Cell Biology* (New York City (NY): Elsevier)
- Poncelet D, de Vos P, Suter N and Jayasinghe S N 2012 Bio-electrospraying and cell electrospinning: Progress and opportunities for basic biology and clinical sciences *Adv. Healthc. Mater.* **1** 27–34
- Rajendran P, Rengarajan T, Thangavel J, Nishigaki Y, Sakthisekaran D, Sethi G and Nishigaki I 2013 The vascular endothelium and human diseases *Int. J. Biol. Sci.* **9** 1057–69

- Rashid R, Lim N S J, Chee S M L, Png S N, Wohland T and Raghunath M 2014 Novel Use for Polyvinylpyrrolidone as a Macromolecular Crowder for Enhanced Extracellular Matrix Deposition and Cell Proliferation *Tissue Eng. Part C Methods* **20** 994–1002
- Ravi S and Chaikof E 2010 Biomaterials for vascular tissue engineering *Regen. Med.* **5** 1–21
- Ricotti L, Polini A, Genchi G G, Ciofani G, Iandolo D, Vazão H, Mattoli V, Ferreira L, Mencias A and Pisignano D 2012 Proliferation and skeletal myotube formation capability of C2C12 and H9c2 cells on isotropic and anisotropic electrospun nanofibrous PHB scaffolds *Biomed. Mater.* **7** 1–11
- Roach P, Farrar D and Perry C C 2005 Interpretation of Protein Adsorption: Surface-Induced Conformational Changes Interpretation of Protein Adsorption: Surface-Induced Conformational Changes *J. Am. Chem. Soc.* **127** 8168–73
- Rocco K A, Maxfield M W, Best C A, Dean E W and Breuer C K 2014 *In Vivo* Applications of Electrospun Tissue-Engineered Vascular Grafts: A Review *Tissue Eng. Part B Rev.* **20** 628–40
- Rodríguez-San-Miguel D, Abrishamkar A, Navarro J A R, Rodríguez-Trujillo R, Amabilino D B, Mas-Ballesté R, Zamora F and Puigmartí-Luis J 2016 Crystalline fibres of a covalent organic framework through bottom-up microfluidic synthesis *Chem. Commun.* **52** 9212–5
- Rousseau S, Houle F, Landry J and Huot J 1997 p38 MAP kinase activation by vascular endothelial growth factor mediates actin reorganization and cell migration in human endothelial cells. *Oncogene* **15** 2169–77
- Rouwkema J, Koopman B F J M, Blitterswijk C A V, Dhert W J A and Malda J 2009 Supply of nutrients to cells in engineered tissues *Biotechnol. Genet. Eng. Rev.* **26** 163–78
- Russell C and Peters C 2008 Endothelial Cells, Angiogenesis and Vasculogenesis *Stemcell Technol.* 1–4
- Rutten M C M 1995 *Arterial wall mechanics and atherosclerosis* (Eindhoven)
- Saito T, Hasebe T, Yohena S, Matsuoka Y, Kamijo A, Takahashi K and Suzuki T 2005 Antithrombogenicity of fluorinated diamond-like carbon films *Diam. Relat. Mater.* **14** 1116–9
- Salmi M and Jalkanen S 2005 Cell-surface enzymes in control of leukocyte trafficking *Nat. Rev. Immunol.* **5** 760–71
- Sandoo A, Veldhuijzen van Zanten J J C S, Metsios G S, Carroll D and Kitas G D 2010 The Endothelium and Its Role in Regulating Vascular Tone *Open Cardiovasc. Med. J.* **4** 302–12

- Savoji H, Hadjizadeh A, Maire M, Aji A, Wertheimer M R and Lerouge S 2014 Electrospun Nanofiber Scaffolds and Plasma Polymerization: A Promising Combination Towards Complete, Stable Endothelial Lining for Vascular Grafts *Macromol. Biosci.* **14** 1084–95
- Schmid Daners M, Kaufmann F, Amacher R, Ochsner G, Wilhelm M J, Ferrari A, Mazza E, Poulidakos D, Meboldt M and Falk V 2017 Left Ventricular Assist Devices: Challenges Toward Sustaining Long-Term Patient Care *Ann. Biomed. Eng.* **45** 1836–51
- Schneider C A, Rasband W S and Eliceiri K W 2012 NIH Image to ImageJ: 25 years of image analysis *Nat. Methods* **9** 671–5
- Seib F P, Herklotz M, Burke K A, Maitz M F, Werner C and Kaplan D L 2014 Multifunctional silk-heparin biomaterials for vascular tissue engineering applications *Biomaterials* **35** 83–91
- Seil J T and Webster T J 2011 Spray deposition of live cells throughout the electrospinning process produces nanofibrous three-dimensional tissue scaffolds. *Int. J. Nanomedicine* **6** 1095–9
- Seyfert U T, Biehl V and Schenk J 2002 In vitro hemocompatibility testing of biomaterials according to the ISO 10993-4 *Biomol. Eng.* **19** 91–6
- Shaw S K, Bamba P S, Perkins B N and Luscinskas F W 2001 Real-Time Imaging of Vascular Endothelial-Cadherin During Leukocyte Transmigration Across Endothelium *J. Immunol.* **167** 2323–30
- Shoeb M and Fang M C 2013 Assessing Bleeding Risk in Patients Taking Anticoagulants *J. Thromb. Thrombolysis* **35** 312–9
- Silberstein M N, Pai C L, Rutledge G C and Boyce M C 2012 Elasticplastic behavior of non-woven fibrous mats *J. Mech. Phys. Solids* **60** 295–318
- Simonet M, Schneider O D, Neuenschwander P and Stark W J 2007 Ultraporous 3D polymer meshes by low-temperature electrospinning: Use of ice crystals as a removable void template *Polym. Eng. Sci.* **47** 2020–6
- Sionkowska A 2011 Current research on the blends of natural and synthetic polymers as new biomaterials: Review *Prog. Polym. Sci.* **36** 1254–76
- Song H H G, Rumma R T, Ozaki C K, Edelman E R and Chen C S 2018 Vascular Tissue Engineering: Progress, Challenges, and Clinical Promise *Cell Stem Cell* **22** 340–54
- Sperling C, Fischer M, Maitz M F and Werner C 2009 Blood coagulation on biomaterials requires the combination of distinct activation processes *Biomaterials* **30** 4447–56

- Stan R V, Tse D, Deharvengt S J, Smits N C, Xu Y, Luciano R, MCGarry C L, Buitendijk M, Nemani K V, Kobayashi T, Shipman S L, Moodie K L, Charles P, Ernst P A, Lee H, Suriawinata A A, Schned A R, Longnecker D S, Fiering S N, Noelle R J, Gimi B, Nicholas W and Carrière C 2013 The diaphragms of fenestrated endothelia – gatekeepers of vascular permeability and blood composition *Dev Cell.* **23** 1203–18
- Stankus J J, Guan J, Fujimoto K and Wagner W R 2006 Microintegrating smooth muscle cells into a biodegradable, elastomeric fiber matrix *Biomaterials* **27** 735–44
- Stankus J J, Soletti L, Fujimoto K, Hong Y, Vorp D A and Wagner W R 2007 Fabrication of cell microintegrated blood vessel constructs through electrohydrodynamic atomization *Biomaterials* **28** 2738–46
- Starling R C, Moazami N, Silvestry S C, Ewald G, Rogers J G, Milano C A, Rame J E, Acker M A, Blackstone E H, Ehrlinger J, Thuita L, Mountis M M, Soltesz E G, Lytle B W and Smedira N G 2014 Unexpected Abrupt Increase in Left Ventricular Assist Device Thrombosis *N. Engl. J. Med.* **370** 33–40
- Stefopoulos G, Giampietro C, Falk V, Poulikakos D and Ferrari A 2017 Facile endothelium protection from TNF- α inflammatory insult with surface topography *Biomaterials* **138** 131–41
- Steinhilber D, Rossow T, Wedepohl S, Paulus F, Seiffert S and Haag R 2013 A Microgel Construction Kit for Bioorthogonal Encapsulation and pH-Controlled Release of Living Cells *Angew. Chem. Int. Ed.* **52** 13538–43
- Sumpio B E, Riley T R and Dardik A 2002 Cell in focus: endothelial cell *Int. J. Biochem. Cell Biol.* **34** 1508–12
- Swathi R and Elliot L C 2010 Biomaterials for vascular tissue engineering *Regen. Med.* **5** 1–21
- Tan B W and Takeuchi S 2007 Monodisperse Alginate Hydrogel Microbeads for Cell Encapsulation *Adv. Mater.* **19** 2696–701
- Tchantchaleishvili V, Sagebin F, Ross R E, Hallinan W, Schwarz K Q and Massey H T 2014 Evaluation and treatment of pump thrombosis and hemolysis *Ann Cardiothorac Surg* **3** 490–5
- Telemeco T A, Ayres C, Bowlin G L, Wnek G E, Boland E D, Cohen N, Baumgarten C M, Mathews J and Simpson D G 2005 Regulation of cellular infiltration into tissue engineering scaffolds composed of submicron diameter fibrils produced by electrospinning *Acta Biomater.* **1** 377–85
- Theberge A B, Courtois F, Schaerli Y, Fischlechner M, Abell C, Hollfelder F and Huck W T S 2010 Microdroplets in microfluidics: An evolving platform for discoveries in chemistry and biology *Angew. Chemie - Int. Ed.* **49** 5846–68

- Thevenot P, Hu W and Tang L 2008 Surface chemistry influence implant biocompatibility *Curr. Top. Med. Chem.* **8** 270–80
- Thomas R R, Anton D R, Graham W F, Darmon M J and Stika K M 1998 Films Containing Reactive Mixtures of Perfluoroalkylethyl Methacrylate Copolymers and Fluorinated Isocyanates: Synthesis and Surface Properties *Macromolecules* **31** 4595–604
- Thompson C J, Chase G G, Yarin A L and Reneker D H 2007 Effects of parameters on nanofiber diameter determined from electrospinning model *Polymer* **48** 6913–22
- Trent J S 1984 Ruthenium tetroxide staining of polymers: new preparative methods for electron microscopy *Macromolecules* **17** 2930–1
- Truskey G A, Herrmann R A, Kait J and Barber K M 1999 Focal Increases in Vascular Cell Adhesion Molecule-1 and Intimal Macrophages at Atherosclerosis-Susceptible Sites in the Rabbit Aorta After Short-Term Cholesterol Feeding *Arterioscler. Thromb. Vasc. Biol.* **19** 393–401
- Turalija M and Bechtold T 2015 Printing of reactive silicones for surface modification of textile material *J. Appl. Polym. Sci.* **132** 1–8
- Uludag H, De Vos P and Tresco P A 2000 Technology of mammalian cell encapsulation *Adv. Drug Deliv. Rev.* **42** 29–64
- Valtola L, Koponen A, Karesoja M, Hietala S, Laukkanen A, Tenhu H and Denifl P 2009 Tailored surface properties of semi-fluorinated block copolymers by electrospinning *Polymer* **50** 3103–10
- Vandekeere S, Dewerchin M and Carmeliet P 2015 Angiogenesis Revisited: An Overlooked Role of Endothelial Cell Metabolism in Vessel Sprouting *Microcirculation* **22** 509–17
- Versace D L, Ramier J, Grande D, Andaloussi S A, Dubot P, Hobeika N, Malval J P, Lalevee J, Renard E and Langlois V 2013 Versatile Photochemical Surface Modification of Biopolyester Microfibrous Scaffolds with Photogenerated Silver Nanoparticles for Antibacterial Activity *Adv. Healthc. Mater.* **2** 1008–18
- Visted T, Furmanek T, Sakariassen P, Foegler W B, Sim K, Westphal H, Bjerkvig R and Lund-Johansen M 2003 Prospects for delivery of recombinant angiostatin by cell-encapsulation therapy. *Hum. Gene Ther.* **14** 1429–40
- Vlierberghe S Van, Dubrueel R and Schacht E 2011 Biopolymer-Based Hydrogels As Scaffolds for Tissue Engineering Applications: A Review *Biomacromolecules* **12** 1387–408
- Vroman L and Adams A L 1969 Findings with the recording ellipsometer suggesting rapid exchange of specific plasma proteins at liquid/solid interfaces *Surf. Sci.* **16** 438–46

- Wang X, Lou T, Zhao W, Song G, Li C and Cui G 2016 The effect of fiber size and pore size on cell proliferation and infiltration in PLLA scaffolds on bone tissue engineering *J. Biomater. Appl.* **30** 1545–51
- Weber N, Lee Y-S, Shanmugasundaram S, Jaffe M and Arinzeh T L 2010 Characterization and in vitro cytocompatibility of piezoelectric electrospun scaffolds *Acta Biomater.* **6** 3550–6
- Wei M, Kang B, Sung C and Mead J 2006 Core-sheath structure in electrospun nanofibers from polymer blends *Macromol. Mater. Eng.* **291** 1307–14
- Weidenbacher L, Abrishamkar A, Rottmar M, Guex A G, Maniura-Weber K, deMello A J, Ferguson S J, Rossi R M and Fortunato G 2017 Electrospaying of microfluidic encapsulated cells for the fabrication of cell-laden electrospun hybrid tissue constructs *Acta Biomater.* **64** 137–47
- Weigel T, Schinkel G and Lendlein A 2006 Design and preparation of polymeric scaffolds for tissue engineering *Expert Rev. Med. Devices* **3** 835–51
- Weinberg C B and Bell E 1986 A blood vessel model constructed from collagen and cultured vascular cells *Science* **231** 397–400
- Whyman G, Bormashenko E and Stein T 2008 The rigorous derivation of Young, Cassie–Baxter and Wenzel equations and the analysis of the contact angle hysteresis phenomenon *Chem. Phys. Lett.* **450** 355–9
- Williams R L, Wilson D J and Rhodes N P 2004 Stability of plasma-treated silicone rubber and its influence on the interfacial aspects of blood compatibility *Biomaterials* **25** 4659–73
- Wittek A, Karatolios K, Fritzen C P, Bereiter-Hahn J, Schieffer B, Moosdorf R, Vogt S and Blase C 2016 Cyclic three-dimensional wall motion of the human ascending and abdominal aorta characterized by time-resolved three-dimensional ultrasound speckle tracking *Biomech. Model. Mechanobiol.* **15** 1375–88
- Wnek G E and Bowlin G L 2008 *Encyclopedia of Biomaterials and Biomedical Engineering* (London (UK): Taylor Francis)
- Wu H C, Wang T W, Kang P L, Tsuang Y H, Sun J S and Lin F H 2007 Coculture of endothelial and smooth muscle cells on a collagen membrane in the development of a small-diameter vascular graft *Biomaterials* **28** 1385–92
- Wu K K and Thiagarajan P 1996 Role of Endothelium in Thrombosis and Hemostasis *Annu. Rev. Med.* **47** 315–31
- Wu W, Yuan G, He A and Han C C 2009 Surface Depletion of the Fluorine Content of Electrospun Fibers of Fluorinated Polyurethane *Langmuir* **25** 3178–83

- Xie X, Guidoin R, Nutley M and Zhang Z 2010 Fluoropassivation and gelatin sealing of polyester arterial prostheses to skip preclotting and constrain the chronic inflammatory response *J. Biomed. Mater. Res. - Part B Appl. Biomater.* **93** 497–509
- Yau J W, Teoh H and Verma S 2015 Endothelial cell control of thrombosis *BMC Cardiovasc. Disord.* **15** 1–11
- Ye Y-S, Rick J and Hwang B-J 2012 Water Soluble Polymers as Proton Exchange Membranes for Fuel Cells *Polymers (Basel).* **4** 913–63
- Yeo M G, Ha J H, Lee H J and Kim G H 2016 Fabrication of hASCs-laden structures using extrusion-based cell printing supplemented with an electric field *Acta Biomater.* **38** 33–43
- Yodmuang S, McNamara S L, Nover A B, Mandal B B, Agarwal M, Kelly T A N, Chao P H G, Hung C, Kaplan D L and Vunjak-Novakovic G 2015 Silk microfiber-reinforced silk hydrogel composites for functional cartilage tissue repair *Acta Biomater.* **11** 27–36
- Young C J, Poole-Warren L A and Martens P J 2012 Combining submerged electrospray and UV photopolymerization for production of synthetic hydrogel microspheres for cell encapsulation *Biotechnol. Bioeng.* **109** 1561–70
- Zeplin P H, Maksimovikj N C, Jordan M C, Nickel J, Lang G, Leimer A H, Römer L and Scheibel T 2014 Spider silk coatings as a bioshield to reduce periprosthetic fibrous capsule formation *Adv. Funct. Mater.* **24** 2658–66
- Zhan W, Shi X, Yu Q, Lyu Z, Cao L, Du H, Liu Q, Wang X, Chen G, Li D, Brash J L and Chen H 2015 Bioinspired Blood Compatible Surface Having Combined Fibrinolytic and Vascular Endothelium-Like Properties via a Sequential Coimmobilization Strategy *Adv. Funct. Mater.* **25** 5206–13
- Zhang L, Casey B, Galanakis D K, Marmorat C, Skoog S, Vorvolakos K, Simon M and Rafailovich M H 2017 The influence of surface chemistry on adsorbed fibrinogen conformation, orientation, fiber formation and platelet adhesion *Acta Biomater.* **54** 164–74
- Zhang W J, Liu W, Cui L and Cao Y 2007 Tissue engineering of blood vessel *J. Cell. Mol. Med.* **11** 945–57
- Zhang Y, Li X S, Guex A G, Liu S S, Müller E, Malini R I, Zhao H J, Rottmar M, Maniura-Weber K, Rossi R M and Spano F 2017 A compliant and biomimetic three-layered vascular graft for small blood vessels *Biofabrication* **9** 1–14
- Zhao S, Xu Z, Wang H, Reese B E, Gushchina L V., Jiang M, Agarwal P, Xu J, Zhang M, Shen R, Liu Z, Weisleder N and He X 2016 Bioengineering of injectable encapsulated aggregates of pluripotent stem cells for therapy of myocardial infarction *Nat. Commun.* **7** 1–12

- Zhou H, Wang H, Niu H, Gestos A and Lin T 2013 Robust, Self-Healing Superamphiphobic Fabrics Prepared by Two-Step Coating of Fluoro-Containing Polymer, Fluoroalkyl Silane, and Modified Silica Nanoparticles *Adv. Funct. Mater.* **23** 1664–70
- Zhu J and Marchant R E 2011 Design properties of hydrogel tissue-engineering scaffolds *Expert Rev. Med. Devices* **8** 607–26
- Zhu L J, Liu F, Yu X M, Gao A L and Xue L X 2015 Surface zwitterionization of hemocompatible poly(lactic acid) membranes for hemodiafiltration *J. Memb. Sci.* **475** 469–79
- Zilla P, Bezuidenhout D and Human P 2007 Prosthetic vascular grafts: Wrong models, wrong questions and no healing *Biomaterials* **28** 5009–27
- Zimmermann J, Reifler F A, Fortunato G, Gerhardt L-C and Seeger S 2008 A Simple, One-Step Approach to Durable and Robust Superhydrophobic Textiles *Adv. Funct. Mater.* **18** 3662–9
- Zucker M B and Vroman L 1969 Platelet Adhesion Induced by Fibrinogen Adsorbed onto Glass *Proc. Soc. Exp. Biol. Med.* **131** 318–20

Curriculum vitae

Lukas Weidenbacher

Born on the 19th of January 1989 in Stadtbergen, Germany

Education

- 2015 – 2018 **PhD student at Swiss Federal Laboratories for Materials Science and Technology St. Gallen/ Institute for Biomechanics ETH Zurich**
Supervisor: Dr. Giuseppino Fortunato/Prof. Dr. Stephen J Ferguson
Thesis: Development of a biomimetic surface for blood-contacting devices via electrospinning technologies
- 2012 – 2015 **Master of Science in Materials Science at Friedrich-Alexander Universität Erlangen-Nürnberg**
Majors: materials in medicine, corrosion
Thesis: „CVD diamond coatings against particle erosion“, project with ALSTOM France
- 2013 – 2013 **Semester abroad at Université Paris-Sud**
Majors: Matériaux
Courses: corrosion, metals, polymers, materials chemistry
- 2008 – 2011 **Bachelor of Science in Nanotechnology at Friedrich-Alexander Universität Erlangen-Nürnberg**
Majors: tissue engineering, surface technology
Thesis: „Ion doped bioactive glasses and ceramics for bone tissue engineering through ion exchange process“
- 1999 – 2008 **General qualification for university entrance at Holbein Gymnasium Augsburg**

Work experience

- 2014 – 2015 **Internship at Kantospital St. Gallen**
Institute of Immunobiology
- 2012 – 2014 **Research assistant at Friedrich-Alexander Universität Erlangen-Nürnberg**
Departement of materials science
- 2012 – 2013 **Voluntary work at „bonding“ student initiative**
- 2011 – 2012 **Internship at DeguDent in Hanau**
Department: development and application technology

Publications

- 2018 **Weidenbacher L**, Müller E, Guex A G, Zündel M, Schweizer P, Marina V, Adlhart C, Vejsadová L, Pauer R, Spiecker E, Maniura-Weber K, Ferguson S J, Rossi R M, Rottmar M, Fortunato G 2018 In Vitro Endothelialization of Surface Integrated Nanofiber Networks for Stretchable Blood Interfaces with Reduced Thrombogenicity *Submitted*
- 2018 Maurya A K, **Weidenbacher L**, Spano F, Fortunato G, Rossi RM, Frenz M, Domman A, Neels A, Sadeghpour A 2018 Structural Insights into Semicrystalline States of Electrospun Nanofibers: new possibilities for steering the functionality *To be submitted*
- 2017 **Weidenbacher L**, Abrishamkar A, Rottmar M, Guex A G, Maniura-Weber K, deMello A J, Ferguson S J, Rossi R M and Fortunato G 2017 Electrospraying of microfluidic encapsulated cells for the fabrication of cell-laden electrospun hybrid tissue constructs *Acta Biomater.* 64 137–47
- 2017 Guex A G, **Weidenbacher L**, Maniura-Weber K, Rossi R M and Fortunato G 2017 Hierarchical Self-Assembly of Poly(Urethane)/Poly(Vinylidene Fluoride-co-Hexafluoropropylene) Blends into Highly Hydrophobic Electrospun Fibers with Reduced Protein Adsorption Profiles *Macromol. Mater. Eng.* 302 1–8

- 2017 Hsu C-P, Hejazi Z, Armagan E, Zhao S, Schmid M, Zhang H, Guo H, **Weidenbacher L**, Rossi R M, Koebel M M, Boesel L F, Toncelli C 2017 Carbon dots and fluorescein: The ideal FRET pair for the fabrication of a precise and fully reversible ammonia sensor *Sens. Actuators B* 253 714–722

Conference presentations

- 2017 **Weidenbacher L**, Tissue Engineering am Beispiel Zurich Heart, 6th workshop of the Subitex research initiative, St. Gallen, Switzerland
- 2017 **Weidenbacher L**, Abrishamkhar A, Rottmar M, Guex A G, Maniura-Weber K, deMello A J, Ferguson S J, Rossi R M, Fortunato G, Dealing with solvent retention in electrospinning of cell-laden 3D biograft scaffolds, 28th Annual Meeting of the European Society for Biomaterials (ESB), Athens, Greece
- 2017 **Weidenbacher L**, Abrishamkhar A, Rottmar M, Guex A G, Maniura-Weber K, deMello A J, Ferguson S J, Rossi R M, Fortunato G, Combination of microfluidics and electrohydrodynamics as tools for the development of in situ cell-laden biografts, European chapter meeting of the Tissue Engineering and Regenerative Medicine International Society (Termis), Davos, Switzerland
- 2016 **Weidenbacher L**, Abrishamkhar A, Rottmar M, Maniura-Weber K, Rossi R M, Ferguson S J, Fortunato G, Cell encapsulation – Enabling technologies for in situ cell delivery for a multilayer hybrid membrane, Empa PhD Symposium, Dübendorf, Switzerland
- 2016 **Weidenbacher L**, Mertgen A-S, Rottmar M, Puigmarti J, Maniura-Weber K, Rossi R M, Fortunato G, Cell-laden electrospun hybrid membrane to mimic native blood barrier, 22nd Annual meeting Swiss Society for Biomaterials + Regenerative Medicine (SSB RM), Zurich, Switzerland
- 2015 **Weidenbacher L**, Rottmar M, Maniura-Weber K, Puigmarti J, Rossi R M, Fortunato G, Evaluation of non-degradable membranes for medical applications, Nanofibers, Applications and Related Technologies (NART) Conference, Liberec, Czech Republic

